WAVE BREAKING IN KDV EQUATIONS WITH HIGHER NONLINEARITY

UNIVERSITY OF BERGEN

Department of Mathematics

Master's thesis in applied and computational mathematics

Author: Sara Mundal Aase

June 1, 2023

Acknowledgements

I want to express my gratitude to my supervisor Henrik Kalisch, for all your guidance and support this year. I am truly grateful for your patience and willingness to help whenever needed. Further, I want to thank Olufemi Elijah Ige and my fellow student Kaja Elgåen for good discussions during this study.

I would also like to thank my fellow students during these five years at the university for making this journey such a good experience.

Finally, I want to thank my family and friends for their encouragement, love and support during this time.

Abstract

The undular bore is a wave propagating in shallow water, often resulting from tidal forces that cause a slight change in the wave heights. Favre (1935) did a physical experiment where an undular bore was created and he discovered that the leading wave was breaking when the ratio between the height of the wave above the initial water height and the initial water height exceeded 0.281. He referred to this ratio as the bore strength.

This study numerically simulated an undular bore in dimensions and physical assumptions approximating the experiment of Favre to find the threshold for breaking. The nonlinear, dispersive KdV equation and two extensions of the KdV equation, which we called the eKdV equation and the eeKdV equation, based on the work of Norevik and Kalisch (2022), were utilised to produce the undular bore solutions and the solitary wave solutions. Moreover, the eKdV equation was evaluated with an addition of a background shear flow to analyse if this could improve the result further. The aim was to find an equation that models the breaking of undular bores.

The convective breaking criterion was applied on the numerical simulations of the undular bore, where the equation gave a good approximation on undular bore breaking if the bore strength was close to the bore strength found by Favre (1935). The higher-order eKdV and eeKdV equations experienced breaking with a higher bore strength compared to the KdV equation, while the eKdV equation with background vorticity exhibited breaking with an even lower bore strength than the KdV equation. Unfortunately, none of the equations had a lower bore strength than the one achieved by Bjørnestad et al. (2021).

Contents

List of Figures

1 Introduction

The study of wave breaking is an essential subject in fluid dynamics. As highlighted by Lubin and Chanson (2017), it plays a crucial role in various aspects, like air-sea transfer of gas, energy and momentum, and many technical applications, like acoustic underwater communication. However, the nature of wave breaking is poorly misunderstood due to its multiple-scale nature and complicated factors (Wong et al., 2019). All flows involving a free surface can have wave breaking, which various factors like circulation, turbulence, and capillarity effects can cause. Consequently, a wide range of wave types and corresponding methods for their study exist. This report will focus on bores, more specifically, weakly undular bores. Filippini et al. (2019) states the significance of bores for the sustainable management of water resources in estuaries and understanding the human impact on ecosystems. Additionally, Lin et al. (2019) studied the undular bore on the slope bottom that is relevant in illustrating tsunami-like waves towards land. This is important due to the enormous damage tsunamis can cost.

A bore is a wave caused by a sudden increase in the water flow in a channel with shallow water. The rapid transition between the different water heights create a bore front, which can either remain stationary and form a hydraulic jump or propagate further and form a bore (Kundu et al., 2016, p. 379). As explained by Johnson (1997, pp. 374–375), the bore was modelled as a discontinuity, but in reality, there is often a narrow region where variations in flow properties are significant. The transition to a continuously breaking wave occurs within a region of highly turbulent flow. However, a river flow can, under certain circumstances, cause a flow change to be more gradual with almost no turbulence, leading to an almost smooth transition. This occurs when the change in water levels is relatively small. Such gradual transitions give rise to a phenomenon known as an undular bore. The bore front is followed by a train of undulating, solitary-formed waves, and it is therefore called an undular bore (Ali & Kalisch, 2010). Bores and hydraulic jumps are, in nature, commonly formed at the mouth of rivers, where tidal forces are at play and cause a gradual change in the flow levels. Examples are the Severn River in England, the Dordogne River in France and the Qiantang River in China.

Favre (1935), (cited in Bjørnestad et al., 2021), made a series of experiments on creating undular bores. In an open tank with a length of 75.58 m, a width of 0.42 m and a depth of 0.40 m, the experiment was designed to create undular bores with varying initial heights and observe them as they propagated through the tank to study whether the solitary formed waves either reached the end of the tank or if the waves would break. Favre performed 30 experiments with

three different initial depths, where the leading edge of the waves was photographed at different positions within the tank. He introduced the bore strength, $\frac{a_0}{h_0}$, where a_0 was the height of the initial bore above the water depth and h_0 was the undisturbed water depth, as shown in Figure 1.1.

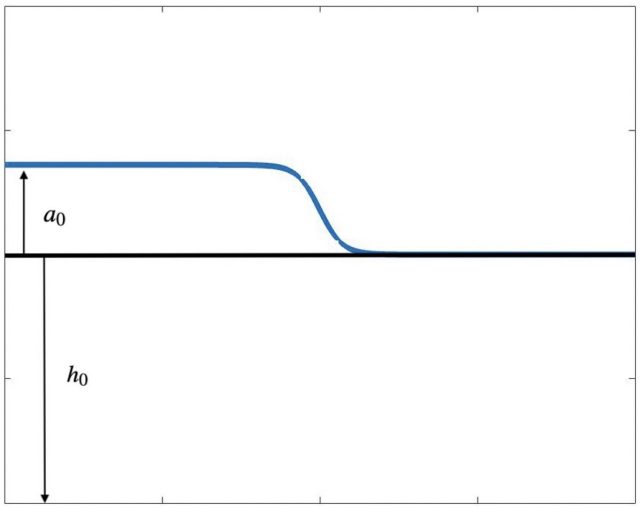

Figure 1.1: Illustration of the initial undular bore. a_0 is the height of the undular bore above the undisturbed water height h_0.

Favre (1935) discovered that with small bore strength the initial bore evolved into almost sinusoidal waves, but with higher bore strength the result was cnoidal waves. For experiment number 22 and 23, with an initial water depth of 0.1075 m and bore strengths of respectively 0.1395 and 0.2307, none of the waves experienced wave breaking when passing 64 meters. However, with bore strength of 0.281, experiment number 24 demonstrated spilling breaking after the wave had travelled a shorter distance. Hence, with the experimental result Favre concluded that the bore strength 0.281 was the threshold for undular bore breaking. The data from Favre's experiment is shown below in Figure 1.2. As the figure show, Favre noted the height of the leading wave at the point it broke. He discovered that the maximum height of the leading wave increased when the bore strength increased, reaching a peak at 2.06 times the initial height, corresponding to the bore strength 0.281. The figure illustrates that with bore strength higher than 0.281, the waves broke at a much lower height. Hence, the bore strength 0.281 gave the maximum possible wave height of the leading wave. The lowest bore strength that causes breaking is referred to as the critical bore strength in this report.

Previous studies have attempted to approximate wave breaking in Favre's experiment using various mathematical equations. Bjørkavåg and Kalisch (2011) made a numerical approximation using Boussinesq models and discovered wave breaking with a bore strength of 0.379. Brun and Kalisch (2018) explored wave breaking by approximating the wave with the Korteweg–De

Vries (KdV) equation, which resulted in wave breaking at a bore strength of 0.353. Bjørnestad et al. (2021) improved upon these results by including a constant background shear flow to the KdV equation. This modification resulted in wave breaking at a bore strength of 0.307, suggesting that the addition of constant background vorticity can impact the approximation of wave breaking.

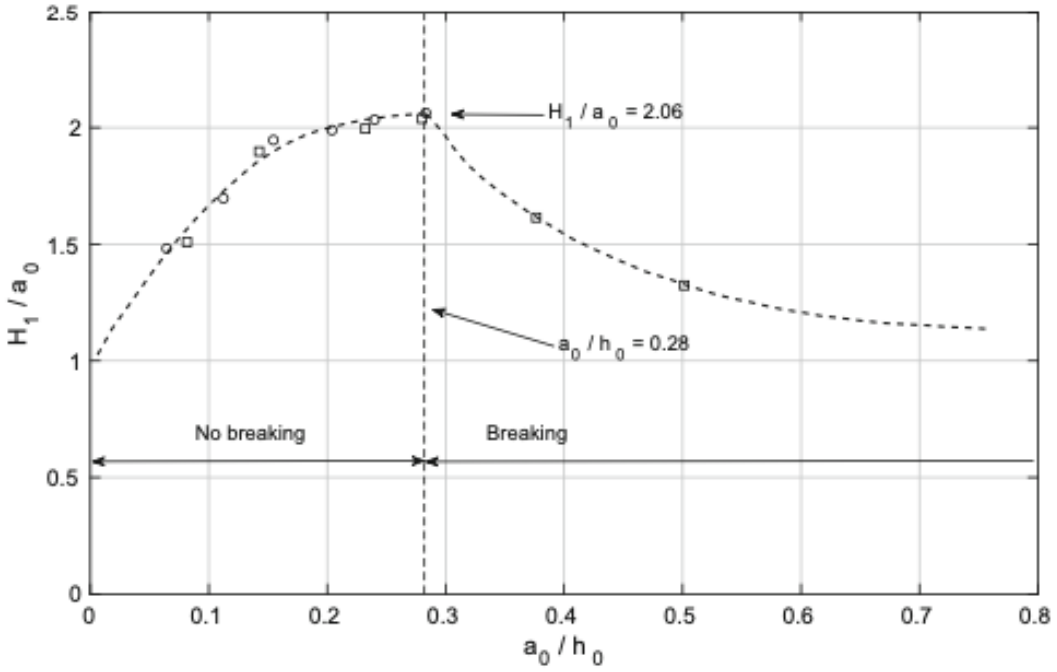

Figure 1.2: The dotted line show the relation between the initial relative height and the relative height of the leading wave of the undular bore. The figure is taken from Bjørkavåg and Kalisch (2011) who got the experimental data from Favre (1935).

In this study, I aimed to improve the numerical approximation of undular bore breaking. This was done using the eKdV equation and the eeKdV equation and compare the critical bore strength of the equations with the bore strength 0.281 from the experiments of Favre (1935). The assumption was that the critical bore strength of the eKdV equation and the eeKdV equation was closer to 0.281 than the previous results (Bjørkavåg and Kalisch, 2011; Brun and Kalisch, 2018; Bjørnestad et al., 2021). The motivation behind this study was that the figures from the experiments of Favre (1935) indicated that the wave's relative amplitude could be somewhat larger than the relative wavelength (Norevik & Kalisch, 2022). Based on this, I aimed to simulate the undular bore in Favre's experiment more precisely when using higher-order non-linear equations by extending the KdV equation to the eKdV equation and the eeKdV equation. In this study, the KdV equation was analysed as a foundation for comparison, even though similar analyses have been done before (Brun & Kalisch, 2018).

Also, since the results of Bjørnestad et al. (2021) achieved a smaller critical bore strength as

the threshold for wave breaking, I studied when a constant background shear flow was added to the eKdV equation. The motivation was that the inflow in Favre's experiment was added at the bottom of the water tank and I assumed that this inflow gave a constant vorticity in the water. Therefore, with the aim of improving the approximation of undular bore breaking, a higher-order equation with an incorporation of a constant shear flow was used. The assumption was that the eKdV equation with constant background vorticity would give a lower critical bore strength, which would be even closer to 0.281.

1.1 The solitary wave

The KdV equation is a relevant equation for solitary waves. Drazin and Johnson (1998) explains how the establishment of solitary waves happened. Before 1834, the existence of solitary waves was yet to be discovered. In that year, Russel (1844), cited in (Drazin & Johnson, 1998, pp. 7–8), observed a boat drawn by two horses on the Edinburgh-Glasgow canal. The boat suddenly stopped, causing the wave to accumulate in front of the boat and then roll forward in a solitary form. Russel followed the wave on a horseback for one or two miles while the wave kept its shape, but after some time, the height was gradually reduced, and at the end, it vanished in the windings of the channel. He named it the "great wave of translation". After this, Russel conducted physical experiments to recreate the solitary wave. He showed empirically that the amount of water in the wave was equal to the amount of water displaced and that the phase speed was obtained from

$$c^2 = g\,(h+a)\,,$$

meaning that the solitary wave was a gravity wave. The equation also denotes that higher waves have higher velocities. Further, Lord Rayleigh and Boussinesq deduced Russel's formula for c using the equation of motion for an inviscid, incompressible fluid and found the formula for the wave profile η. Finally, in 1895, Korteweg and de Vires completed an equation for the wave profile. The equation was the KdV equation.

The KdV equation exhibits two distinct types of wave solutions: the localised wave called the solitary wave and the periodic waves known as cnoidal waves. The solitary wave is characterised by its solitary nature and defined by being infinitely separated from any other wave. It represents a single travelling wave of a permanent form, maintaining a constant shape and moves with a steady velocity (Drazin & Johnson, 1998, p. 20).

Since it is known that the KdV equation has a solitary wave solution, I aimed to find the solitary wave solution of the eKdV equation and the eKdV equation with background shear flow and

then derive the maximum analytical height of the solitary waves. The solitary wave solution of the eKdV equation is already established. Still, I sought to derive the exact solution corresponding to the coefficients used in the eKdV equation in this study. Further studies have estimated the maximum height of solitary and periodical waves and found it to be close to $0.78h_0$ (Massel, 1996).

Furthermore, the solitary wave solution was also used in the numerical implementation since the numerical approximation of the solitary wave should converge towards the exact solution with the order of convergence corresponding to the numerical method. Therefore, knowing the exact solution was fundamental to our research as it verified our numerical scheme.

1.2 Outline of the report

Chapter 2: This chapter will provide an overview of the theoretical foundations on which the results were based. Initially, the physical system and basic water wave theory were derived and stated. This entails establishing the governing equations and the boundary conditions for the system. Further, the linear water wave theory for shallow water was derived, which served as a basis for developing the nonlinear theory of shallow water waves. The non-linear theory presents the non-linearity that had to be satisfied to present a breaking wave. Further, the Boussinesq system was established, balancing the non-linear and dispersive terms. Then, the KdV equation was derived from the Boussinesq system by assuming unidirectional waves. Finally, the convective wave-breaking criterion was established, based on the Froude number.

Chapter 3: In this chapter, the numerical methods are explained, where a finite difference scheme was used as a spatial approximation and a hybrid Crank-Nicolson/Adams-Bashfort scheme was used for the temporal approximation. These numerical methods were then applied to simulate the undular bore using the equations evaluated in this report.

Chapter 4: This chapter first presents the derivation of the solitary wave solution of the KdV equation, which was then used to verify the implementation of the numerical methods for the KdV equation. The implementation was then used to simulate the undular bore and calculate the corresponding horizontal particle velocity and the phase speed to establish the critical bore strength for the KdV equation.

Chapter 5: This chapter introduces the eKdV equation and the derivation of the equation. Then, the solitary wave solution was found, which was used to calculate the maximum height allowed for a natural surface wave. Next, the exact solitary wave solution was used to verify the

numerical approximation of the eKdV equation. Further, the critical bore strength was found for the eKdV equation.

Chapter 6: This chapter presents the eeKdV equation and shows the derivation leading to the equation. The exact solitary wave solution for the eeKdV equation has yet to be found, so the exact solution for the wave equation with an additional term was used to validate the implementation of the additional term. Then, the critical bore strength was found.

Chapter 7: The eKdV equation with a constant background shear flow was derived and introduced in this chapter. Then the exact solitary wave solution was found, which was further used to establish the maximum allowable height of the solitary wave for a natural wave. Additionally, the implementation of the equation was verified and the critical bore strength was found.

Chapter 8: At the end, the conclusion is presented.

2 Theory

This chapter presents the theory used as basis in this study, where the theory was primarily based on the work of Whitham (1974, pp. 431–466). Other sources are denoted when they were used.

2.1 Basic water wave equations and boundary conditions

We aimed to numerically approximate the experiment of Favre (1935) such that the physical system considered in this study was based on the actual experiment. A Cartesian coordinate system was used where the x-axis denoted the horizontal direction, the y-axis denoted the vertical direction and the wave propagated along the x-axis. Only two coordinates were used because the wave tank stretched out along the x-axis and we assumed that the tank was so narrow that we could neglect all transverse motion. The velocity coordinates were $\bar{u} = (u, v)$, which corresponded to $\bar{x} = (x, y)$ and the orthogonal unit vector $\bar{i}$ and $\bar{j}$ denoted the x and y direction. The undisturbed water dept at the bottom was set to $y = -h_0$, and the free surface of the wave was given by $y = \eta(x,t)$. This is illustrated in Figure 2.1.

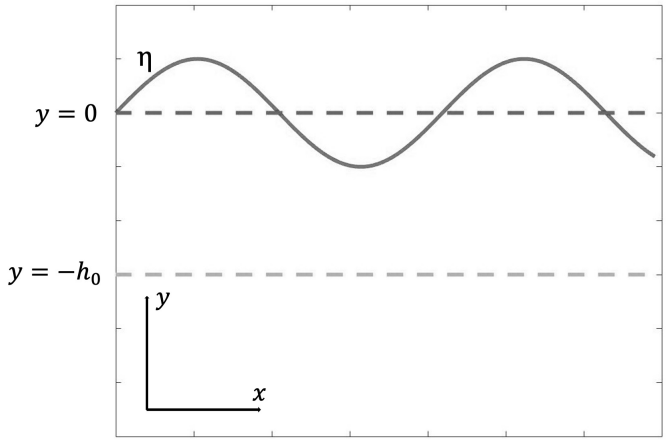

Figure 2.1: An illustration of the physical system considered in this study.

We considerd an inviscid, incompressible and irrotational fluid with constant gravitational flow. Hence, the fluid's viscosity equaled zero and the material density was constant within a fluid parcel such that it did not change with pressure (Kundu et al., 2016, p. 113). The frequency

was also assumed to be much higher than the Coriolis frequency, such that the waves were not affected by the rotation of the earth.

Two main equations for the water wave theory are the continuity equation and the Navier-Stokes equation (Kundu et al., 2016, pp. 116–130). The mass continuity equation is based on the principle that the mass of fluid particles is constant, meaning that tracked elements in a fluid do not disappear and new elements do not appear out of nothing. Hence, the integral of the fluid density is zero. From this, the equation for the mass conservation, the continuity equation, was derived, yielding

$$\frac{D\rho}{Dt} + \rho \nabla \cdot \bar{u} = 0,$$

where ρ denoted the density. Under the assumption of incompressible flow, the term $\frac{D\rho}{Dt}$ dropped out from the continuity equation, and it became

$$\nabla \cdot \bar{u} = 0. \tag{2.1}$$

The velocity potential was introduced as ϕ, satisfying $\bar{u} = \nabla\varphi$. Laplace's equation was then found when inserting the velocity potential into the continuity equation 2.1:

$$\nabla^2 \varphi = 0. \tag{2.2}$$

The conservation of fluid momentum formula is derived from Newton's second law of motion. Considering an infinitesimal fluid parcel and using Newton's second law, the Navier-Stokes momentum equation is obtained. The inviscid, incompressible Navier-Stokes equation, also named the Euler equation, is given by

$$\rho \frac{D\bar{u}}{Dt} + \nabla \bar{p} = \rho \bar{F},$$

where $\bar{p} = p(x,y,t)$ was the pressure and F were the external forces. It was assumed that the only external force were $\bar{F} = -\rho g \bar{j}$. Therefore, the inviscid, incompressible Navier Stokes equation could be written as

$$\frac{D\bar{u}}{Dt} = \frac{\partial \bar{u}}{\partial t} + (\bar{u} \cdot \nabla)\bar{u} = -\frac{1}{\rho}\nabla p - g\bar{j}.$$

The velocity potential was substituted into the previous equation and by using the vector identity, $(\bar{u} \cdot \nabla)\bar{u} = \nabla(\frac{1}{2}\bar{u}^2) + (\nabla \times \bar{u}) \times \bar{u}$, a rewriting yielded

$$\frac{\partial \nabla\varphi}{\partial t} + \nabla\left(\frac{1}{2}(\nabla\varphi)^2\right) + \omega \times \nabla\varphi = -\frac{1}{\rho}\nabla p - g\bar{j}.$$

Since the flow was assumed to be irrotational $\omega = 0$, where $\omega = \nabla \times \bar{u}$ was defined as the vorticity. Thus, the term $\omega \times \nabla\varphi$ vanished, i.e.

$$\frac{\partial \nabla\varphi}{\partial t} + \nabla\left(\frac{1}{2}(\nabla\varphi)^2\right) = -\frac{1}{\rho}\nabla p - g\bar{j}$$

The terms were rearranged and by integration over the spatial domain, the equation became

$$\frac{p - p_0}{\rho} = B(t) - \varphi_t - \frac{1}{2}(\nabla\varphi)^2 - gy,$$

where $B(t)$ was an arbitrary function resulting from the integration. By assuming a new potential φ', such that $\varphi' = \varphi - \int B(t)dt$, $B(t)$ was absorbed into φ and the inviscid and incompressible Navier-Stokes equation was then reduced to

$$\frac{p - p_0}{\rho} = -\varphi_t - \frac{1}{2}(\nabla\varphi)^2 - gy. \tag{2.3}$$

Two essential equations for water waves that satisfy the assumptions made on the fluid were established. Next, the boundary conditions had to be found. First, the kinematic boundary condition at the top of the wave was derived. A case of a body of water with air above it was considered, such that the interface between the water and the air could be described by $f(x,y,t) = 0$. At the free surface $y = \eta(x,t)$, such that the interface became

$$f(x,y,t) = \eta(x,t) - y. \tag{2.4}$$

At the interface, no water could cross it. Consequently, the kinematic boundary condition claimed no flow through the water's surface. For a particle $M(x(t), y(t))$ at the surface, it had to satisfy $f(M(t),t) = 0$ and $\frac{\partial}{\partial t}f(M(t),t) = 0$. Using the chain rule on the last equation gave

$$\frac{\partial}{\partial t}f + \frac{\partial}{\partial t}M\frac{\partial}{\partial M}f = 0. \tag{2.5}$$

$\frac{\partial}{\partial t}M$ equaled the velocity vector $\bar{u}$ of a particle at the surface and $\frac{\partial}{\partial M}f$ equaled the gradient of the surface 2.4, which equaled

$$\nabla f = (\eta_x, -1).$$

Substituting this and the velocity vector on form of the velocity potential into 2.5 yielded

$$\eta_t + (\varphi_x, \varphi_y) \cdot (\eta_x, -1)^T = 0.$$

The result was the kinematic boundary condition at the surface

$$\eta_t + \varphi_x \eta_x - \varphi_y = 0, \qquad y = \eta.$$

Next, the dynamic boundary condition was derived. Since the interface had no mass, the forces on each side had to be equal. If surface tension was neglected, the water and air pressure were the same. Additionally, motion in the air was neglected such that there were no surface disturbances. Therefore, the air pressure was approximated as an undisturbed and constant value, such that $p = p_0$, where p was pressure in the water and p_0 was the constant pressure in the air. Substituting this into 2.3 resulted in the dynamic boundary condition at the free surface

$$\varphi_t + \frac{1}{2}(\varphi_x^2 + \varphi_y^2) + g\eta = 0, \qquad y = \eta.$$

The interface between the water and the bottom could be described by $f(x,y) = y + h_0(x)$. Since there was no through flow at the bottom, the following had to hold for a particle $M(x,y,t)$ at the interface,

$$\frac{\partial}{\partial t} f + \frac{\partial}{\partial t} M \frac{\partial}{\partial M} f = 0.$$

This was equal to

$$f_t + \bar{u} \cdot \nabla f = (y + h_0(x))_t + (u, v) \cdot (h_{0x}, 1)^T = 0.$$

Because the bottom was solid, $\frac{\partial}{\partial t} f = 0$. Hence, substituting $\bar{u} = \nabla \varphi$ into the equation, the solid boundary condition at the bottom became

$$\varphi_y + \varphi_x h_{0x} = 0. \tag{2.6}$$

Two boundary conditions were needed at the free surface, one to determine the velocity potential and one to determine the water surface. In contrast, at the bottom, where $y = -h_0(x)$, the boundary was solid, and only one was needed. For the physical situation considered in the experiment of Favre (1935), the bottom was horizontally flat and constant, such that $h_{0x} = 0$. The boundary condition at the bottom was then

$$\varphi_y = 0, \qquad y = -h_0.$$

To sum up, the water wave problem with a free surface and constant flat bottom was

$$\varphi_{xx} + \varphi_{yy} = 0\,, \qquad -h_0 < y < \eta \tag{2.7}$$

$$\eta_t + \varphi_x \eta_x - \varphi_y = 0\,, \qquad y = \eta \tag{2.8}$$

$$\varphi_t + \frac{1}{2}(\varphi_x^2 + \varphi_y^2) + g\eta = 0\,, \qquad y = \eta \tag{2.9}$$

$$\varphi_y = 0\,, \qquad y = -h_0. \tag{2.10}$$

2.2 Linear theory for water waves

In this section, the linear water wave theory is presented. Later in the report, the linear equations will be used to advance to nonlinear theory. Since the free surface and the velocity were small quantities of shallow water initially at rest with small perturbations, we have assumed that the non-linear terms in free surface boundary conditions 2.8 and 2.9 could be neglected. The linear boundary conditions at the surface were then

$$\eta_t = \varphi_y, \qquad y = \eta \tag{2.11}$$

and

$$\varphi_t + g\eta = 0, \qquad y = \eta. \tag{2.12}$$

The boundary conditions at the free surface could be linearised further by expansion around $y = 0$, such that

$$\varphi_y|_{y=\eta} = \varphi_y|_{y=0} + \eta\,\varphi_y|_{y=0} \cdots$$

Neglecting the nonlinear terms due to the assumption of the variables being small, 2.11 became,

$$\eta_t = \varphi_y\,, \qquad y = 0.$$

The boundary condition 2.12 was differentiated with respect to time and $\eta_t = \varphi_y$ was used, resulting in the boundary condition

$$\varphi_{tt} + g\varphi_y = 0\,, \qquad y = 0.$$

Laplace's equation and the boundary condition at the bottom were linear, such that the linear

problem with a free surface and a solid flat bottom yielded

$$\varphi_{xx} + \varphi_{yy} = 0, \qquad -h_0 < y < 0 \tag{2.13}$$

$$\varphi_{tt} + g\varphi_y + = 0, \qquad y = 0 \tag{2.14}$$

$$\varphi_y = 0, \qquad y = -h_0 \tag{2.15}$$

The problem only depended on the velocity potential, not the free surface. Therefore, to solve for the surface,

$$\eta(x,t) = -\frac{1}{g}\varphi_t(x,0,t). \tag{2.16}$$

The water depth was assumed to be constant and the water waves propagated horizontally in an oscillatory motion in a sinusoidal traveling waveform. The waveform could therefore be represented by

$$\eta(x,t) = a\cos(kx - \omega t),$$

where a was the amplitude, λ the wavelength, $k = \frac{2\pi}{\lambda}$ the wave number telling the spatial frequency of the wave and $\omega = \frac{2\pi}{T}$ the time-frequency (Kundu et al., 2016, pp. 355–356). Because of the linear relationship between the waveform and the velocity potential, 2.16, we could assume that the form of the velocity potential was

$$\varphi = f(y)\sin(kx - \omega t).$$

The value of $f(y)$ was found by substituting the equation into 2.13, i.e.

$$f''(y) - k^2 f(y) = 0.$$

The general solution for $f(y)$ was given by $Ae^{ky} + Be^{-ky}$, such that the expression for the velocity potential became

$$\varphi = (Ae^{ky} + Be^{-ky})\sin(kx - \omega t).$$

Inserting the velocity potential into the boundary condition at the bottom, 2.15, we got that,

$$k(Ae^{-kh_0} - Be^{kh_0})\sin(kx - \omega t) = 0.$$

For this to hold,

$$B = Ae^{-2kh_0}.$$

We used the relationship $\eta_t = \phi_y$ at $y = 0$, and it yielded

$$-\omega a \sin(kx - \omega t) = k(A - B)\sin(kx - \omega t)$$

such that

$$k(A - B) = -\omega a$$

The two relationships between A and B determined that the following had to hold,

$$A = \frac{a\omega}{k(1 - e^{-2kh_0})} \qquad \text{and} \qquad B = \frac{a\omega e^{-2kh_0}}{k(1 - e^{-2kh_0})}.$$

Using that $\sinh(\xi) = \frac{1-e^{-2\xi}}{2e^{-\xi}}$ and $\cosh(\xi) = \frac{e^{-\xi}+e^{\xi}}{2}$ for a random variable ξ, the velocity potential could be expressed by

$$\varphi = \frac{a\omega}{k}\frac{\cosh(k(y + h_0)}{\sinh(kh_0)}\sin(kx - \omega t).$$

The equality 2.16 at $y = 0$ gave the linear dispersive relation

$$\omega^2 = gk \tanh kh_0. \tag{2.17}$$

The dispersive relation is the relationship between the wave's frequency and the wave number. Since the wave number was a function of the wavelength, the dispersive relation is a relationship between the frequency and the wavelength of the wave. The dispersion relation had two modes $\omega = \pm W(\kappa)$, where

$$W(k) = \sqrt{gk \tanh kh_0}.$$

Following, the phase speed of the surface waves, meaning the velocity of an individual wave component, was

$$c(k) = \frac{\omega}{k} = \sqrt{\frac{g}{k}\tanh kh}.$$

Hence, the phase speed was also dependent on the wave number.

2.3 Nonlinear theory for shallow water waves

In this section, the calculations will be specified towards equations for shallow water by including the nonlinear theory. For shallow water, $kh_0 \to 0$, such that the linear dispersion relation was approximated by $\omega^2 \sim gh_0k^2$ and the linear phase speed was approximated to be $c_0 \sim \sqrt{gh_0}$.

As we can see, the phase speed was independent of the wave number and, therefore, non-dispersive. For shallow water, the components in the vertical direction are small compared to the components in the horizontal direction. The earlier established inviscid and incompressible Navier-Stokes,

$$\frac{D\bar{u}}{Dt} = \frac{\partial \bar{u}}{\partial t} + (\bar{u} \cdot \nabla)\bar{u} = -\frac{1}{\rho}\nabla p - g\bar{j},$$

has vertical components that could be approximated by

$$-\frac{1}{\rho}\frac{\partial p}{\partial y} - g = 0.$$

Integration over the vertical domain of the previous equation resulted in an equation of the pressure,

$$p - p_0 = \rho g(\eta - y). \tag{2.18}$$

Inserting the equation for the pressure back into the inviscid and incompressible Navier-Stokes equation and use the assumption for the vertical components, yielded

$$\frac{\partial u}{\partial t} + u\frac{\partial u}{\partial x} + v\frac{\partial u}{\partial y} = -\frac{1}{\rho}\frac{\partial}{\partial x}(p_0 + \rho g\eta - \rho g y),$$

where both the initial pressure and the gravitational force were constant, and the result became

$$\frac{\partial u}{\partial t} + u\frac{\partial u}{\partial x} + v\frac{\partial u}{\partial y} = -g\frac{\partial \eta}{\partial x}.$$

As the equation show, the right-hand side was independent of y, while the left-hand side was the rate of change of u following a particle. If it is assumed that u was independent of y initially, it would always remain so, hence the term $v\frac{\partial u}{\partial y}$ had to be equal to zero and we ended up with the shallow water equation for the surface:

$$\frac{\partial u}{\partial t} + u\frac{\partial u}{\partial x} + g\frac{\partial \eta}{\partial x} = 0. \tag{2.19}$$

To find the shallow water equation for the velocity we began by taking the integral over the vertical domain of the Euler equation, 2.1,

$$\int_{-h_0}^{\eta} \nabla \cdot \bar{u} dy = 0.$$

Using Leibniz integral rule, this became

$$\frac{\partial}{\partial x}\int_{-h_0}^{\eta} u dy - [u]_{y=\eta}\frac{\partial \eta}{\partial x} - [u]_{y=-h_0}\frac{\partial h_0}{\partial x} + [v]_{y=-h_0}^{y=\eta} = 0.$$

The kinematic boundary conditions at the surface, 2.8, and the boundary condition at the flat bottom, 2.10, was inserted into the last term and the equation was then reduced to

$$\frac{\partial}{\partial x}\int_{-h_0}^{\eta} u dy + \frac{\partial \eta}{\partial t} = \frac{\partial}{\partial x}(\eta u + h_0 u) + \frac{\partial \eta}{\partial t} = 0.$$

Using that $h = \eta + h_0$, the equation became

$$\frac{\partial h}{\partial t} + \frac{\partial}{\partial x}(hu) = 0.$$

Together, this was the shallow water equations for the surface and the velocity:

$$\frac{\partial u}{\partial t} + u\frac{\partial u}{\partial x} + g\frac{\partial \eta}{\partial x} = 0,$$

$$\frac{\partial h}{\partial t} + \frac{\partial}{\partial x}(hu) = 0.$$

The approximation for the vertical components of the inviscid incompressible Navier-Stokes equation for shallow water had an order of error. This order of error was derived from the first term in the inviscid incompressible Navier-Stokes equation,

$$\frac{\partial \bar{u}}{\partial t} + (\bar{u}\cdot\nabla)\bar{u} = -\frac{1}{\rho}\nabla p - g\bar{j}.$$

When integrating the equation from $y = y$ to $y = \eta$, the nonlinear term and the horizontal velocity were approximately equal to zero. The remaining part was

$$\rho\int_{y}^{\eta} v_t dy = \rho v_t(\eta - y) \leq \rho v_t h_0.$$

The equality difference holds for small η, which is the case for shallow water. Hence, the error for approximating the pressure was $p \approx \rho v_t h_0$. The integral over the vertical domain from h_0 to η of the Laplace equation, 2.1, resulted in

$$v \approx -h_0 u_x$$

by the consideration that η was very small compared to h_0. The relative error for the assumptions made for the non-linear parts was then

$$-\frac{p_x}{\rho u_t} \approx -\frac{\rho h_0 v_{tx}}{\rho u_t} = \frac{h_0^2}{u_t}(u_{xxt}) \approx \frac{h_0^2}{l^2},$$

where l was the length scale of the wave in the horizontal direction. The last approximation

came from $u_{xx} \leq \frac{1}{l^2}$ since u_x could not be greater than the unit length of the wave. Later, this was expanded to incorporate dispersive terms.

The one-dimensional nonlinear shallow water wave equations were,

$$\begin{aligned} h_t + (uh)_x &= 0, \\ u_t + uu_x + gh_x &= 0. \end{aligned} \tag{2.20}$$

In matrix form it became,

$$\begin{bmatrix} h \\ u \end{bmatrix}_t + \begin{bmatrix} u & h \\ g & u \end{bmatrix} \begin{bmatrix} h \\ u \end{bmatrix}_x = \begin{bmatrix} 0 \\ 0 \end{bmatrix}. \tag{2.21}$$

The following calculations to find the Riemann invariants and the characteristics of the system were drawn upon the calculations of Gavrilyuk et al. (2017, pp. 1–4). The characteristic direction of the system was found as an eigenvalue of the middle matrix, which we named A. Using the characteristic equation, $\det(A - cI) = 0$, the eigenvalues were determined by,

$$\det(A - cI) = \det(\begin{bmatrix} u-c & h \\ g & u-c \end{bmatrix}) = (u-c)^2 - hg = 0,$$

and the characteristics of the system were $c^{\pm} = u \pm \sqrt{gh}$. For an eigenvector $\bar{I}$, the following condition had to hold for the characteristics,

$$\bar{I} \cdot ((\partial_t + c\partial_x)\bar{u}) = 0. \tag{2.22}$$

If there exist two scalar functions $r(\bar{u})$ and $\mu(\bar{u}, x, t)$ such that

$$\frac{\partial r}{\partial u_i} = \mu l_i, \qquad\qquad (i = 1, \ldots, n),$$

then the following equation was equivalent to 2.22,

$$(\partial_t + c\partial_x) r(\bar{u}) = -\mu \bar{I} \cdot \bar{b} = 0.$$

The vector $\bar{b}$ was the right-hand side in 2.21, consequently, it was a zero vector and the previous equation equaled zero. The term $r(\bar{u})$ was the Riemann invariant of the system and it was therefore constant along the system. The characteristics were inserted into the characteristic

equation to find the eigenvectors. The positive was

$$l^+ = \begin{bmatrix} \sqrt{h} \\ \sqrt{g} \end{bmatrix}.$$

This gave a system of equations for the Riemann invariants,

$$\frac{\partial r}{\partial h} = \mu\sqrt{g},$$

$$\frac{\partial r}{\partial u} = \mu\sqrt{h}.$$

The system could then be written as a first-order partial differential equation by excluding the integrating factor μ, such that

$$\frac{\partial r}{\partial u} - \sqrt{\frac{h}{g}}\frac{\partial r}{\partial h} = 0.$$

This was solved using the method of characteristics, i.e.

$$\frac{du}{1} = \frac{dh}{-\sqrt{\frac{h}{g}}} \quad \rightarrow \quad \frac{du}{dh} = -\sqrt{\frac{g}{h}} \quad \rightarrow \quad u = -\int \sqrt{\frac{g}{h}}dh \quad \rightarrow \quad u = -2\sqrt{gh} + B.$$

The Riemann invariant was a scalar function, hence $r = B = u + 2\sqrt{gh}$. The same procedure was utilised to find the other Riemann invariant. The conclusion was that for the one-dimensional shallow water equations, the characteristics were

$$c_1 = u + \sqrt{gh} \qquad \text{and} \qquad c_2 = u - \sqrt{gh}, \tag{2.23}$$

and the Riemann invariants were

$$r_1 = u + 2\sqrt{gh} \qquad \text{and} \qquad r_2 = u - 2\sqrt{gh}. \tag{2.24}$$

For a given point ξ, a wave moving into still water with height $h = h_0$ was given by

$$h = H(\xi), \qquad u = 2\sqrt{gH(\xi)} - 2\sqrt{gh_0} \qquad \text{and} \qquad x = \xi + (3\sqrt{gH(\xi)} - 2\sqrt{gh_0})t.$$

The second term was calculated from characteristics of the wave at $h = H(\xi)$ moving into the water with $h = h_0$. The last term was found by the use of equation $x = \xi + F(\xi)t$, calculated

from the equation for the characteristic velocity, $\frac{dx}{dt} = c$, where the function $F(\xi)$ was found by

$$F(\xi) = c(f(\xi)) = u(\xi,t) + \sqrt{gH(\xi)} = 2\sqrt{gH(\xi)} - 2\sqrt{gh_0} + \sqrt{gH(\xi)} = 3\sqrt{gH(\xi)} - 2\sqrt{gh_0}.$$

This wave, due to increase of elevation, must at a point break. Hence, at the breaking point a discontinuity would be created and a shock condition had to be satisfied. The conservative form of 2.20 was found to be

$$\begin{aligned} U^*[uh] + [u^2h + \frac{1}{2}gh^2] = 0, \\ -U^*[h] + [uh] = 0. \end{aligned}, \tag{2.25}$$

where U^* was the velocity of the shock. Shallow water theory predicts that all waves with an increase in elevation will at a point break, but observations show that this is not always the case. Bore conditions, 2.25, conserved mass and momentum across a bore, but what about the energy? From the system of equations for shallow water waves, 2.20, the conservation of energy across a bore could be expressed by

$$\left(\frac{1}{2}u^2h + \frac{1}{2}gh^2\right)_t + \left(\frac{1}{2}u^3h + ugh^2\right)_x = 0.$$

This expression was calculated from the integral over the area of the expression for the accumulation of energy plus the effusion of energy. The energy conservation equation could imply a third potential shock condition for the system, but only two were needed. Rayleigh proposed that energy was not conserved across the bore and that the loss was due to turbulence. Hence, the shock condition corresponding to the previous equation could not be used since it did not consider turbulence. From equation 2.25, the energy across a bore with two different heights h_1 and h_2, could be expressed as

$$\left[\frac{1}{2}u^3h + ugh^2\right]_1^2 - U^*\left[\frac{1}{2}u^2h + \frac{1}{2}gh^2\right]_1^2 < 0 \tag{2.26}$$

This hold for a bore when $h_2 > h_1$. The entropy required $E \leq 0$, causing the inequality sign. The energy across a bore is consequently decreasing. Based on Aavatsmark (2004), using the Rankine-Hugoniots equations on 2.25 would give the conservative solution of the velocity of the shock:

$$(h_2 - h_1)U^* = h_2u_2 - h_1u_1, \tag{2.27}$$

$$(h_2u_2 - h_1u_1)U^* = (h_2u_2^2 + \frac{1}{2}gh_2^2) - (h_1u_1^2 + \frac{1}{2}gh_1^2). \tag{2.28}$$

The velocity of the shock have to be equal in each equation, thus

$$U^* = \frac{h_2u_2 - h_1u_1}{(h_2 - h_1)} = \frac{(h_2u_2^2 + \frac{1}{2}gh_2^2) - (h_1u_1^2 + \frac{1}{2}gh_1^2)}{(h_2u_2 - h_1u_1)}.$$

Factorizing this gives,

$$u_2 = u_1 \pm \frac{h_2 - h_1}{h_2}\sqrt{\frac{gh_2(h_1 + h_2)}{2h_1}}.$$

Inserting the expression for u_2 back into 2.27 yielded the form of the velocity for the shock,

$$U^* = u_1 \pm \sqrt{\frac{gh_2(h_1 + h_2)}{2h_1}}$$

The derivation show the shock solutions when including energy loss across the bore due to turbulence, but in our study turbulence was not assumed.

2.4 The Boussinesq system

This section presents the derivation that led to the Boussinesq system, which, when considering unidirectional waves, lead to the KdV equation. The dispersive effects had to be incorporated into the nonlinear theory to find the Boussinesq system. For better understanding, this was first done with an intuitive procedure to show the incorporation of dispersion. We have proven that the linearised version of the equation had to satisfy the linear dispersive equation

$$\omega^2 = gk\tanh kh_0.$$

Using Taylor expansion around $k = 0$, the two first terms became

$$\omega^2 = c_0^2k^2 - \frac{1}{3}c_0^2h_0^2k^4.$$

The second term had to satisfy the linearised form of the dispersion as well. A linear equation for η that satisfied the previous dispersion relation was

$$\eta_{tt} - c_0^2\eta_{xx} - \frac{1}{3}c_0^2h_0^2\eta_{xxxx} = 0. \tag{2.29}$$

This was proved by substituting the term for the surface, $\eta = A\cos(kx - \omega t)$, into the equation

$$-\omega^2\eta + k^2c_0^2\eta - \frac{1}{3}k^4c_0^2h_0^2\eta = 0,$$

and solve for ω

$$\omega^2 = c_0^2 k^2 - \frac{1}{3} c_0^2 h_0^2 k^4.$$

Since the shallow water equations 2.20 were linearised to

$$\eta_{tt} - c_0^2 \eta_{xx} = 0,$$

adding the term $\nu \eta_{xxx}$ to the shallow water equations would make a system that could be linearised to 2.29. This would give a system of both nonlinear effects of relative order $\alpha = \frac{a}{h_0}$ and the dispersive effect of relative order $\beta = \frac{h_0^2}{l^2}$. The term was added to the linearised form of 2.20, it yielded

$$\eta_t + h_0 u_x = 0$$
$$u_t + g\eta_x + \nu \eta_{xxx} = 0$$

To find the value of ν, the first equation was differentiated w.r.t time and the second w.r.t space, and then solving for u_{xt}, it gave the linear equation

$$\eta_{tt} - c_0^2 \eta_{xx} - \nu h_0 \eta_{xxxx} = 0.$$

For this equation to be equal to 2.29, $\nu = \frac{1}{3} c_0^2 h_0$. The result was the nonlinear shallow water equations with dispersion,

$$h_t + (uh)_x = 0,$$
$$u_t + uu_x + gh_x + \frac{1}{3} c_0^2 h_0 h_{xxx} = 0.$$

It will reduce to 2.29 when $\frac{a}{h_0} \to 0$ and to 2.20 when $\frac{h_0^2}{l^2} \to 0$.

If we use the lowest approximation $\eta_{tt} - c_0^2 \eta_{xx} = 0$, such that $\eta_{xx} = \frac{1}{c_0^2} \eta_{tt}$, the correction term became $\frac{1}{3} c_0^2 h_0 h_{xxx} = \frac{1}{3} h_0 h_{xtt}$. The system of equations then yielded,

$$h_t + (uh)_x = 0,$$
$$u_t + uu_x + gh_x + \frac{1}{3} h_0 h_{xtt} = 0.$$

This system was linearised to the equation,

$$\eta_{tt} - c_0^2 \eta_{xx} - \frac{1}{3} h_0^2 \eta_{xxtt} = 0,$$

with corresponding dispersive relation

$$\omega^2 = \frac{c_0^2 k^2}{1 + \frac{1}{3}k^2 h_0^2}.$$

Boussinesq's equations include waves moving both left and right, but if we assumed unidirectional waves propagating to the right, we obtained the Korteweg-deVries equation with the dispersive relation,

$$\omega = c_0 k - \frac{1}{6} c_0 h_0^2 k^3$$

This dispersive relation corresponds to the equation

$$\eta_t + c_0 \eta_x + \frac{1}{6} c_0 h_0^2 \eta_{xxx} = 0. \tag{2.30}$$

As derived above, a wave moving to the right into undisturbed water has Riemann invariant,

$$u = 2\sqrt{g(h_0 + \eta)} - 2\sqrt{g h_0}.$$

Substitute $h = h_0 + \eta$ into the first equation in system 2.20, it yielded

$$(h_0 + \eta)_t + ((h_0 + \eta)u)_x = 0.$$

The equation for u was then substituted into the equation, i.e

$$\eta_t + (2\sqrt{g(h_0+\eta)} - 2\sqrt{g h_0})_x \eta + (2\sqrt{g(h_0+\eta)} - 2\sqrt{g h_0})\eta_x + (2\sqrt{g(h_0+\eta)} - 2\sqrt{g h_0})_x h_0 = 0,$$

resulting in

$$\eta_t + (3\sqrt{g(h_0+\eta)} - 2\sqrt{g h_0})\eta_x = 0$$

Adding the dispersive term in 2.30 to the equation, yielded

$$\eta_t + (3\sqrt{g(h_0+\eta)} - 2\sqrt{g h_0})\eta_x + \frac{1}{6} c_0 h_0^2 \eta_{xxx} = 0.$$

The Taylor expansion was used on the middle term and the approximation was derived to the first order of $\frac{a}{h_0}$,

$$3\sqrt{g(h_0+\eta)} - 2\sqrt{g h_0} \approx 3(\sqrt{g h_0} + \frac{g\eta}{2\sqrt{g h_0}}) - 2\sqrt{g h_0} = \sqrt{g h_0} + \frac{3}{2}\frac{g\eta}{\sqrt{g h_0}}.$$

Since $c_0 = \sqrt{gh_0}$, the equation became the KdV equation:

$$\eta_t + c_0(1 + \frac{3}{2}\frac{\eta}{h_0})\eta_x + \frac{1}{6}c_0 h_0^2 \eta_{xxx} = 0.$$

Next, a more formal explanation is presented to show the incorporation of the dispersion to the non-linear equations. As derived, for an incompressible and inviscid fluid, the Laplace equation had to hold,

$$\varphi_{xx} + \varphi_{YY} = 0, \qquad 0 < Y < h_0 + \eta,$$

with the boundary condition $\varphi_Y = 0$ on $Y = 0$. Here we have defined Y as the distance from the bottom to the free surface, where $Y = 0$ was at the bottom. Since the water was shallow, the velocity potential was approximately independent of Y and it was assumed that the asymptotic series below could represent it:

$$\varphi = \sum_0^\infty Y^n f_n(x,t).$$

This was substituted into the Laplace equation, i.e.

$$\sum_0^\infty Y^n \frac{d^2}{dx^2} f_n + \sum_0^\infty n(n-1)y^{n-2} f_n = 0.$$

The Laplace equation claimed that the following equations had to hold:

$$\begin{aligned}
\frac{d^2}{dx^2} f_0 + 2f_2 = 0 \qquad &\rightarrow \qquad f_2 = -\frac{1}{2}\frac{d^2}{dx^2} f_0 \\
y(\frac{d^2}{dx^2} f_1 + 6f_3) = 0 \qquad &\rightarrow \qquad f_3 = -\frac{1}{6}\frac{d^2}{dx^2} f_1 \\
y^2(\frac{d^2}{dx^2} f_2 + 12f_4) = 0 \qquad &\rightarrow \qquad f_4 = -\frac{1}{12}\frac{d^2}{dx^2} f_4 \\
&\vdots \qquad .
\end{aligned}$$

The boundary condition at the bottom required that:

$$\varphi_Y = \sum_0^\infty nY^{n-1} f_n(x,t) = f_1(x,t) + Y f_2(x,t) + O(Y^2) = 0 \qquad \rightarrow \qquad f_1(x,t) = 0.$$

As the pattern show, the even numbers of the function f_n were dependent on each other. Therefore, they were all dependent on f_0. The odd numbers also depended on each other, but the boundary condition at the bottom required $f_1 = 0$, consequently, the odd terms all equalled

zero. An expression for the velocity potential where $f = f_0$ was therefore

$$\varphi = \sum_0^\infty (-1)^m \frac{Y^{2m}}{2m!} \frac{\partial^{2m}}{\partial x^{2m}} f. \tag{2.31}$$

The free boundary conditions 2.8 and 2.9 were nonlinear and applied on $Y = h_0 + \eta$. The derivation became involved and the terms were therefore ordered by the relative amplitude $\alpha = \frac{a}{h_0}$ and the relative wave number $\beta = \frac{h_0^2}{l^2}$, where α and β were considered small and of approximately the same size. Further, to simplify and to represent the equations explicitly the different dominant lengths, the variables were non-dimensionalized as follow

$$\tilde{x} = \frac{x}{l}, \qquad \tilde{Y} = \frac{Y}{h_0}, \qquad \tilde{t} = \frac{c_0}{l} t, \qquad \tilde{\eta} = \frac{1}{a}\eta \qquad \text{and} \qquad \tilde{\varphi} = \frac{c_0}{gla}\varphi, \tag{2.32}$$

where the non-dimensional variables were noted with a tilde-sign. The non-dimensional differential operators were found by using the chain rule,

$$\begin{aligned}
\tfrac{\partial}{\partial \tilde{t}} &= \tfrac{\partial t}{\partial \tilde{t}} \tfrac{\partial}{\partial t} &&= \tfrac{l}{c_0} \tfrac{\partial}{\partial t}, \\
\tfrac{\partial}{\partial \tilde{x}} &= \tfrac{\partial x}{\partial \tilde{x}} \tfrac{\partial}{\partial x} &&= l \tfrac{\partial}{\partial x}, \\
\tfrac{\partial^2}{\partial \tilde{x}^2} &= l^2 \tfrac{\partial^2}{\partial x^2}, && \\
\tfrac{\partial}{\partial \tilde{Y}} &= \tfrac{\partial \tilde{Y}}{\partial Y} \tfrac{\partial}{\partial \tilde{Y}} &&= h_0 \tfrac{\partial}{\partial \tilde{Y}}, \\
\tfrac{\partial^2}{\partial \tilde{Y}^2} &= h_0^2 \tfrac{\partial^2}{\partial Y^2}. &&
\end{aligned} \tag{2.33}$$

The non-dimensional variables and operators were substituted into the Laplace equation 2.31, the boundary condition at bottom 2.10 and at the free boundary conditions 2.8 and 2.9 at the surface. The normalised problem was then

$$\beta \tilde{\varphi}_{xx} + \tilde{\varphi}_{YY} = 0, \qquad 0 < \tilde{Y} < 1 + \alpha\tilde{\eta}, \tag{2.34}$$

$$\tilde{\varphi}_y = 0, \qquad \tilde{Y} = 0, \tag{2.35}$$

$$\tilde{\eta}_t + \alpha\tilde{\varphi}_x\tilde{\eta}_x - \frac{1}{\beta}\tilde{\varphi}_Y = 0, \qquad \tilde{Y} = 1 + \alpha\tilde{\eta}, \tag{2.36}$$

$$\tilde{\eta} + \tilde{\varphi}_t + \frac{1}{2}\alpha\tilde{\varphi}_x^2 + \frac{1}{2}\frac{\alpha}{\beta}\tilde{\varphi}_Y^2 = 0, \qquad \tilde{Y} = 1 + \alpha\tilde{\eta}. \tag{2.37}$$

The asymptotic series for φ was inserted into 2.34 and 2.35. The same derivation as previously shown for the dimensional asymptotic equation was utilised and the non-dimensional

asymptotic expansion became

$$\tilde{\varphi} = \sum_{0}^{\infty} (-1)^m \frac{\tilde{Y}^{2m}}{2m!} \frac{\partial^{2m}}{\partial \tilde{x}^{2m}} \tilde{f} \beta^m = \tilde{f} - \beta \frac{\tilde{Y}^2}{2} \tilde{f}_{\tilde{x}\tilde{x}} + \beta^2 \frac{\tilde{Y}^4}{4!} \tilde{f}_{\tilde{x}\tilde{x}\tilde{x}\tilde{x}} + O(\beta^3).$$

The two first terms of the normalised asymptotic series were substituted into the boundary conditions 2.36 and 2.37. It yielded

$$\tilde{\eta}_t + [(1+\alpha\tilde{\eta})\tilde{f}_x]_x - [\frac{1}{6}(1+\alpha\tilde{\eta})^3 \tilde{f}_{xxxx} + \frac{1}{2}\alpha(1+\alpha\tilde{\eta})^2 \tilde{\eta}_x \tilde{f}_{xxx}]\beta + O(\beta^2) = 0,$$

$$\tilde{\eta} + \tilde{f}_t + \frac{1}{2}\alpha\tilde{f}_x^2 - \frac{1}{2}(1+\alpha\tilde{\eta})^2 [\tilde{f}_{xxt} + \alpha\tilde{f}_x\tilde{f}_{xxx} - \alpha\tilde{f}_{xx}^2]\beta + O(\beta^2) = 0.$$

Further, the notation $\tilde{w} = \tilde{f}_x$ was used. If the β orders were kept, but all of order $O(\alpha\beta, \beta^2)$ were assumed to be zero, the equations became

$$\begin{aligned} \tilde{\eta}_t + [(1+\alpha\tilde{\eta})\tilde{w}]_x - \tfrac{1}{6}\beta\tilde{w}_{xxx} = 0, \\ \tilde{w}_t + \alpha\tilde{w}\tilde{w}_x + \tilde{\eta}_x - \tfrac{1}{2}\beta\tilde{w}_{xxt} = 0. \end{aligned} \tag{2.38}$$

The system is the Boussinesq equations. Later in the report, it will be shown that these were used as a base when deriving the KdV equation, the eKdV equation, the eeKdV equation and the eKdV equation with background shear flow.

Other versions of the Boussinesq system are achievable. The velocity was given as the gradient of the velocity potential, $\bar{u} = \nabla\phi$, and the average velocity over the dept was found by integration over the vertical domain. Substituting this into the first terms in the asymptotic series

$$\tilde{\varphi}_x = \tilde{w} - \beta\frac{\tilde{Y}^2}{2}\tilde{w}_{xx} + O(\beta^2), \tag{2.39}$$

resulted in

$$\tilde{u}_{\text{mean}} = \tilde{w} - \frac{1}{6}\beta\tilde{w}_{xx} + O(\alpha\beta, \beta^2).$$

Rewriting the expression gave

$$\tilde{w} = (\frac{1}{1 - \frac{1}{6}\beta\partial_{xx}})\tilde{u}_{\text{mean}} + O(\alpha\beta, \beta^2).$$

Using the series $\frac{1}{1-x} = 1 + x + O(x^2)$, it yielded

$$\tilde{w} = \tilde{u}_{\text{mean}} + \frac{1}{6}\beta(\tilde{u}_{\text{mean}})_{xx} + O(\alpha\beta, \beta^2).$$

Setting the equation for $\tilde{w}$ into 2.38 resulted in

$$\tilde{\eta}_t + [(1+\alpha\tilde{\eta})\tilde{u}_{\text{mean}}]_x + O(\alpha\beta,\beta^2) = 0, \tag{2.40}$$

$$(\tilde{u}_{\text{mean}})_t + \alpha\tilde{u}_{\text{mean}}(\tilde{u}_{\text{mean}})_x + \tilde{\eta}_x - \frac{1}{3}\beta(\tilde{u}_{\text{mean}})_{xxt} + O(\alpha\beta,\beta^2) = 0. \tag{2.41}$$

From equation 2.40, the lowest order was

$$\tilde{u}_{\text{mean}} = -\tilde{\eta}_t.$$

The lowest order was substituted into 2.41 and it was assumed that higher orders were equal to zero. This gave the normalised Boussinesq's system in the form of the mean velocity,

$$\begin{aligned} \tilde{\eta}_t + [(1+\alpha\tilde{\eta})\tilde{u}_{\text{mean}}]_x + O(\alpha\beta,\beta^2) = 0 \\ \tilde{u} + \alpha\tilde{u}_{\text{mean}}(\tilde{u}_{\text{mean}})_x + \tilde{\eta}_x + \tfrac{1}{3}\beta\tilde{\eta}_{xtt} + O(\alpha\beta,\beta^2) = 0. \end{aligned} \tag{2.42}$$

2.5 The Korteweg–de Vries equation

The KdV-equation was derived from Boussinesq's equations by only considering waves moving to the right. The lowest order of 2.38 was,

$$\tilde{\eta}_t + \tilde{w}_x = 0,$$

$$\tilde{w}_t + \tilde{\eta}_x = 0.$$

This could be written in matrix form,

$$\begin{bmatrix} \tilde{\eta} \\ \tilde{w} \end{bmatrix}_t + \begin{bmatrix} 0 & 1 \\ 1 & 0 \end{bmatrix} \begin{bmatrix} \tilde{\eta} \\ \tilde{w} \end{bmatrix}_x = \begin{bmatrix} 0 \\ 0 \end{bmatrix}. \tag{2.43}$$

Using the characteristic equation $(A-\lambda I) = 0$ the eigenvalues were derived, yielding $\lambda_1 = 1$ and $\lambda_2 = -1$. The corresponding eigenvectors were then found, such that the diagonalised system became

$$A = P^{-1}\Lambda P = \frac{1}{2}\begin{bmatrix} 1 & 1 \\ -1 & 1 \end{bmatrix}\begin{bmatrix} 1 & 0 \\ 0 & -1 \end{bmatrix}\begin{bmatrix} 1 & -1 \\ 1 & 1 \end{bmatrix}.$$

By introducing the variables $(r,s) = P^{-1}(\tilde{\eta},\tilde{w})$, we had that $r = \frac{1}{2}(\tilde{\eta}+\tilde{w})$ and $s = \frac{1}{2}(-\tilde{\eta}+\tilde{w})$. The system 2.43 was then written on the diagonalized form and multiplied by P^{-1}, where

$$P{-}1 = \frac{1}{2}\begin{bmatrix} 1 & 1 \\ -1 & 1 \end{bmatrix}.$$

The result was

$$\begin{bmatrix} r_t \\ s_t \end{bmatrix}_t + \begin{bmatrix} 1 & 0 \\ 0 & -1 \end{bmatrix}\begin{bmatrix} r_x \\ s_x \end{bmatrix}_x = \begin{bmatrix} 0 \\ 0 \end{bmatrix},$$

where the solution of this was given on the form

$$r = r_0(x-t),$$
$$s = s_0(x+t).$$

From the definition of r and s, the constants were

$$r_0 = \frac{1}{2}(\tilde{\eta}_0+\tilde{w}_0),$$
$$s_0 = \frac{1}{2}(-\tilde{\eta}_0+\tilde{w}_0),$$

such that the solution to the system became

$$r = \frac{1}{2}\left[\tilde{\eta}_0(x-t)+\tilde{w}_0(x-t)\right],$$
$$s = \frac{1}{2}\left[-\tilde{\eta}_0(x+t)+\tilde{w}_0(x+t)\right].$$

Since $(r,s) = P^{-1}(\tilde{\eta},\tilde{w})$, the solution of $\tilde{\eta}$ and $\tilde{w}$ was found by $(\tilde{\eta},\tilde{w}) = P(r,s)$. Hence, the solution to the system of equations was

$$\tilde{\eta} = \frac{1}{2}\left[\tilde{\eta}_0(x-t)+\tilde{w}_0(x-t)+\tilde{\eta}_0(x+t)-\tilde{w}_0(x+t)\right],$$
$$\tilde{w} = \frac{1}{2}\left[\tilde{\eta}_0(x-t)+\tilde{w}_0(x-t)-\eta_0(x+t)+\tilde{w}_0(x+t)\right].$$

The KdV equation was found from this solution by considering waves moving to the right, such that the following holds

$$\tilde{w} = \tilde{\eta} \qquad \text{and} \qquad \tilde{\eta}_{\tilde{t}} + \tilde{\eta}_{\tilde{x}} = 0.$$

This was the solution of first order Boussinesq system, from this, we sought a solution of the KdV equation where the diffusion term and the nonlinear terms were balanced and on the form

$$\tilde{w} = \tilde{\eta} + \alpha A(\tilde{\eta}) + \beta B(\tilde{\eta}) + O(\alpha^2, \alpha\beta, \beta^2).$$

The variables A and B were functions of $\tilde{\eta}$ and its derivative, and they were found by substituting the equation for $\tilde{w}$ into the Boussinesq equations 2.38, such that

$$\begin{aligned} \tilde{\eta}_t + \tilde{\eta}_x + \alpha(A_x + 2\tilde{\eta}\,\tilde{\eta}_x) + \beta(B_x - \tfrac{1}{6}\tilde{\eta}_{xxx}) + O(\alpha^2 + \beta^2) = 0 \\ \tilde{\eta}_t + \tilde{\eta}_x + \alpha(A_t + \tilde{\eta}\,\tilde{\eta}_x) + \beta(B_t - \tfrac{1}{2}\tilde{\eta}_{xxt}) + O(\alpha^2 + \beta^2) = 0. \end{aligned} \tag{2.44}$$

Since $\tilde{\eta}_t = -\tilde{\eta}_x$, this was inserted into the equations, giving

$$\begin{aligned} \alpha(A_x + 2\tilde{\eta}\,\tilde{\eta}_x) + \beta(B_x - \tfrac{1}{6}\tilde{\eta}_{xxx}) + O(\alpha^2 + \beta^2) = 0, \\ \alpha(-A_x + \tilde{\eta}\,\tilde{\eta}_x) + \beta(-B_x + \tfrac{1}{2}\tilde{\eta}_{xxx}) + O(\alpha^2 + \beta^2) = 0. \end{aligned}$$

We assumed that the higher orders of α and β were equal to zero. The two equations are required to be consistent. Therefore, the first equations were set equal to the other equation and the result gave

$$\begin{aligned} \alpha\,(2A_x + \tilde{\eta}\,\tilde{\eta}_{\tilde{x}}) = 0 \quad &\rightarrow \quad A = -\frac{1}{4}\tilde{\eta}^2, \\ \beta\left(2B_x - \frac{2}{3}\tilde{\eta}_{\tilde{x}\tilde{x}\tilde{x}}\right) = 0 \quad &\rightarrow \quad B = \frac{1}{3}\tilde{\eta}_{\tilde{x}\tilde{x}}. \end{aligned}$$

The values of A and B were substituted into $\tilde{w}$, such that

$$\tilde{w} = \tilde{\eta} - \frac{1}{4}\alpha\tilde{\eta}^2 + \frac{1}{3}\beta\tilde{\eta}_{xx}. \tag{2.45}$$

Setting the variables of A and B into one of the equations in 2.44, the result gave the non-dimensional KdV equation

$$\tilde{\eta}_t + \tilde{\eta}_x + \alpha\frac{3}{2}\tilde{\eta}\,\tilde{\eta}_x + \beta\frac{1}{6}\tilde{\eta}_{xxx} = 0. \tag{2.46}$$

The KdV equation in dimensional form was found by substituting the dimensional variables into the equation, which gave

$$\eta_t + c_0\eta_x + \frac{3}{2}\frac{c_0}{h_0}\eta\,\eta_x + \frac{1}{6}c_0h_0^2\eta_{xxx} = 0.$$

We scaled the variables such that

$$x \to \frac{x}{h_0}, \qquad Y \to \frac{Y}{h_0}, \qquad t \to \frac{t}{\sqrt{\frac{h_0}{g}}} \qquad \text{and} \qquad \eta \to \frac{\eta}{h_0}. \tag{2.47}$$

Hence, h_0 was the unit of distance and $\sqrt{\frac{h_0}{g}}$ was the unit of time. In practice, this meant that we could set $g = 1$, $h_0 = 1$ and $c_0 = \sqrt{gh_0} = 1$ into the KdV equation. The result was the KdV equation

$$\eta_t + \eta_x + \frac{3}{2}\eta\eta_x + \frac{1}{6}\eta_{xxx} = 0. \tag{2.48}$$

2.6 The convective breaking criterion

At the end of the theory chapter, the breaking criterion we used to determine wave breaking had to be established. The convective breaking criterion is based on the Froude Number, Fr, which is a non-dimensional number defined as the ratio between the particle velocity of the wave and the square root of the gravity and the wavelength, given as $Fr = \frac{u}{\sqrt{gl}}$ (Kundu et al., 2016, pp. 378–379). As proven earlier, the phase velocity for shallow water was $c = \sqrt{gh}$ and the wavelength was proportional to the wave height. Hence, for shallow water, the Froude number is a relationship between the wave's particle velocity and phase speed:

$$Fr = \frac{u}{c}$$

If $F > 1$, the flow is supercritical, and if $F < 1$, it is subcritical. In the transition from subcritical flow to supercritical flow, a discontinuity occurs and a wave breaking is created.

In this study, the horizontal particle velocity was evaluated at the top of the front wave of the undular bore. If it was higher than the local phase speed, it was assumed that the wave would break. In the experiment of Favre (1935), when an undular bore was propagating into still water, the first wave was usually the greatest, and it would move approximately with the same speed as the bore front (Bjørkavåg & Kalisch, 2011). Hence, by testing when the horizontal particle velocity at the top of the front wave surpassed the local phase velocity, an approximation of when a shallow water wave was breaking was established. The convective breaking criterion was therefore given as

$$\frac{u}{c} \geq 1.$$

This study used the breaking criterion as the definition of wave breaking. In the article of

Hatland and Kalisch, 2019, the authors discussed the quality of the convective breaking criterion. Since it is based on theory, it can give a better agreement between theory and experiment. However, undular tidal bores have been observed with higher Froude numbers in physical experiments. For example, Lubin and Chanson (2017) stated that there are experiments where the Froude number equals 1.3 or 1.4 and breaking tidal bores have been observed with the Froude number from 1.4 to 1.6. Hence, the convective breaking criterion might lack agreement with the physical considerations in some situations. Furthermore, Senthilkumar and Kalisch (2019) discussed that the wave's steepness has also been used as an indicator for wave breaking.

3 Numerical methods

In this chapter, the numerical methods that were used to simulate the waves are presented. The numerical scheme consisted of finite differential spatial operators combined with a hybrid Crank-Nicolson/Adams-Bashfort method, based on the work of Skogestad and Kalisch (2009). The numerical scheme was used to find the equations' solitary wave and undular bore solutions. While the methods are presented here for the KdV equation, additional modifications were incorporated when implementing the eKdV equation, eeKdV equation and eKdV equation with background shear flow, as will be shown in their respective chapters.

The KdV equation was given as

$$\eta_t + \eta_x + \frac{3}{2}\eta\eta_x + \frac{1}{6}\eta_{xxx} = 0.$$

This study has analysed an undular bore propagating from left to right over an undisturbed depth, such that the initial condition was on the form of an initial undular bore given by the equation

$$\eta_0 = \frac{1}{2}\left[1 - \tanh\left(kx\right)\right],$$

where k was a parameter stating the steepness of the bore slope and it was always chosen to be $k = 1$. If the spatial domain was big enough, the surface elevation η in the far field upstream and downstream of the bore would approach respectively a_0 on the left end and zero on the right end, where a_0 was the initial height of the wave. The problem for the undular bore was therefore

$$\begin{aligned}
\eta_t + \eta_x + \frac{3}{2}\eta\eta_x + \frac{1}{6}\eta_{xxx} = 0,\ -h_0 < y < \eta, t > 0 \\
\eta(x,0) &= \eta_0(x), \\
\eta(-l,t) &= a_0, \\
\eta(l,t) &= 0, \\
\eta_x(l,t) &= 0.
\end{aligned}$$

Stated by Bona et al. (2003), this boundary value problem should be well-posed.

An auxiliary function ξ was introduced to enforce homogeneous boundary and initial condi-

tions for the problem, i.e.

$$\xi(x,t) = \eta(x,t) - \eta_0(x).$$

This simplified the problem and made the scheme usable for simulating the solitary wave solution without any changes. The auxiliary function was substituted into the problem such that it was on the form of ξ, i.e.

$$\begin{aligned}
\xi_t + \xi_x + \frac{3}{4}(\xi^2)_x + \frac{3}{2}(\eta_0\xi)_x + \frac{1}{6}\xi_{xxx} = -F,\ -h_0 < y < \eta, t > 0 \\
\xi(x,0) = 0, \\
\xi(-l,t) = 0 \\
\xi(l,t) = 0 \\
\xi_x(l,t) = 0,
\end{aligned}$$

where the forcing function was $F = \eta_{0x} + \frac{3}{2}\eta_0\eta_{0x} + \frac{1}{6}\eta_{xxx}$. The problem then had a homogeneous Dirichlet boundary condition at both ends and a homogeneous Neumann boundary condition at the right end. The solution of η was found by adding the initial undular bore to the solution of ξ. The spatial domain $[-l,l]$ was discretised by using a finite set of points $\{x_j\}_{j=0}^N \subset [-l,l]$. The first point in the set was $x_0 = -l$, the last point was $x_N = l$ and the distance between neighbouring points was given by $\delta x = \frac{2l}{N}$. The time domain was uniformly discretised by defining $t_n = n\delta t$, where t_0 was the initial time. The numerical approximation was defined by $v_j^n \approx \xi\left(x_j, t^n\right)$.

The first and the third spatial derivatives were approximated by the central difference schemes given by

$$\xi_x(x_j,t) \approx \frac{v_{j+1} - v_{j-1}}{2\delta x},$$

and

$$\xi_{xxx}(x_j,t) \approx \frac{v_{j+2} - 2v_{j+1} + 2v_{j-1} - v_{j-2}}{2\delta x^3}.$$

Due to the Dirichlet boundary conditions, the endpoints could be excluded from the calculations of the derivatives. The equations were therefore solved for $\{x_j\}_{j=1}^{N-1}$, and the scheme for the first derivative was valid at each point. The scheme for the third derivative could not solve for the values v_1 and v_{N-1}. Therefore a central difference scheme was utilised on the Neumann condition at $x = l$, giving $\frac{v_{N+1} - v_{N-1}}{2\Delta x} = 0$ and this allowed us to set $v_{N+1} = v_{N-1}$. Hence, the third derivative approximation at the grid point x_{N-1} was

$$\xi_{xxx}(x_{N-1},t) \approx \frac{v_{N-1} + 2v_{N-2} - v_{N-3}}{2\delta x^3}.$$

There was no Neumann condition at the point x_1, so a forward difference scheme was used to

approximate the third derivative. It was given by,

$$\xi_{xxx}(x_1,t) \approx \frac{-v_4+6v_3-12v_3+10v_1-3v_0}{2\delta x^3}.$$

To sum up, the results of the spatial differential matrices used to derive the KdV equation's first and third-order derivatives numerically were

$$D_1 = \frac{1}{2\Delta x}\begin{bmatrix} 0 & 1 & 0 & & \cdots & & 0 \\ -1 & 0 & 1 & 0 & & & \vdots \\ 0 & -1 & 0 & 1 & 0 & & \\ \vdots & & & \ddots & & & \\ 0 & \cdots & & & & 0 & 1 \\ 0 & \cdots & & & & -1 & 0 \end{bmatrix}$$

and

$$D_3 = \frac{1}{2\Delta x^3}\begin{bmatrix} 10 & -12 & 6 & -1 & 0 & \cdots & 0 & \\ 2 & 0 & -2 & 1 & 0 & & \vdots & \\ -1 & 2 & 0 & -2 & 1 & 0 & & \\ \vdots & -1 & 2 & & \ddots & & & \\ & & & \ddots & & & 0 & 1 \\ 0 & & & & & & 0 & -2 \\ 0 & \cdots & & & & -1 & 2 & 1 \end{bmatrix}.$$

To verify the differential matrices, they were tested on first and third-order derivative functions with the same boundary conditions, such that the schemes gave an exact solution. Hence, it was confirmed that the spatial differential matrices were correct before continuing. However, the convergence of the schemes are presented later, showing the accuracy of the operators.

To approximate the time iterations of the equations, the trapezoidal method, also known as the implicit Crank-Nicolson method, was utilised for the linear terms. The method is implicit, however, the evaluation was treated explicitly. The error of the method decays globally with

$O(h^2)$ (Iserles, 1996/2000, pp. 8–9). The method is presented as

$$\bar{y}_{n+1} = \bar{y}_n + \frac{1}{2}h\left[\bar{f}(t_n, \bar{y}_n) + \bar{f}(t_{n+1}, \bar{y}_{n+1})\right].$$

$\bar{y}_{n+1}$ is the vector with the solutions at the future time step, while $\bar{y}_n$ denotes the vector with the current solutions utilised to determine the next step. $\bar{f}$ corresponds to the vector containing the equation evaluated at the given position and time.

The explicit Adams-Bashforth method of order two was used to solve for the non-linear terms to gain a more efficient scheme (Skogestad & Kalisch, 2009). The Adams Bashforth method is a multistep method given as

$$\bar{y}_{n+2} = \bar{y}_{n+1} + h\left[\frac{3}{2}\bar{f}(t_{n+1}, y_{n+1}) - \frac{1}{2}\bar{f}(t_n, \bar{y}_n)\right].$$

Hence, two time steps were needed to find the next iteration. Since we used the second-order Adams-Bashforth method, the error of the approximation should be decreasing quadratically since the global error of the method decreases with $O(h^2)$ (Iserles, 1996/2000, pp. 20–21).

Even though the methods were both second-order, a combination of the method do not necessarily prevent a second-order convergence. However, the numerical result presented by Skogestad and Kalisch (2009) indicated that we should expect a second-order convergence with this scheme. With $v_j^n \approx \xi\left(x_j, t^n\right)$, the vector of values v^{n+1} was determined by the scheme

$$\frac{v^{n+1} - v^n}{\Delta t} = \frac{3}{2}\left[-\frac{3}{4}D_1(v^n)^2 - \frac{3}{2}D_1 v^n \eta_0\right] - \frac{1}{2}\left[-\frac{3}{4}D_1(v^{n-1})^2 - \frac{3}{2}D_1 v^{n-1}\eta_0\right]$$

$$+\frac{1}{2}\left[-D1(v^{n+1} + v^n) - \frac{1}{6}D1(v^{n+1} + v^n)\right] - F.$$

Due to the methods using two previous time steps, both v_0 and v_1 was defined before the iteration began. The first time step was the initial value of ξ given as a vector of zeros and the vector with the second time step was found by a forward Euler method combined with the Crank Nicholson method:

$$\frac{v^1 - v^0}{\Delta t} = -\frac{3}{4}D1(v^0)^2 - \frac{3}{2}v^0\eta_0 + \frac{1}{2}\left[-D1(v^1 + v^0) + \frac{1}{6}D1(v^1 + v^0)\right] - F.$$

The forward Euler method had a local truncation error of order two, so it would not cause any problems when used in one iteration (Skogestad & Kalisch, 2009).

This numerical scheme was used to implement all four equations considered in this study, with

some additional terms included for the eKdV equation, the eeKdV equation and the eKdV equation with background vorticity. The numerical implementations were verified for each equation and the convergence is presented in the corresponding chapters. Due to the duration to run the wave simulations, the numerical schemes grid size was $\delta x = 0.2$ and $\delta t = 0.01$ when implementing the undular bore. Skogestad and Kalisch (2009) have studied the stability of the numerical scheme, where the method for the linear parts was stable for all values of δt and δx and the scheme of the non-linear components was technically never stable, but for small enough δt the system would be as good as stable. Therefore, the implementations of the waves were tested with a smaller temporal grid size to check the stability of the numerical scheme. The authors define that the boundary conditions were exact up to machine precision when the spatial domain was big enough.

4 Wave breaking modelled by the KdV equation

As presented in chapter 2, the KdV equation is a model equation for surface waves of an inviscid and incompressible fluid. With α as the relative amplitude and the order of the nonlinear steepening effects and β as the relative wavelength and the order of the dispersive spreading, the KdV equation is an equation that balances the two parts such that they are of the same order. The solution of the undular bore simulated by the KdV equation lead to a formation of steady waves in the form of solitary waves, but since the KdV equation balances the non-linear components with the dispersive components, the numerical simulated undular bore would never break. Therefore, as stated by Brun and Kalisch (2018), the solution is only valid for certain amplitudes.

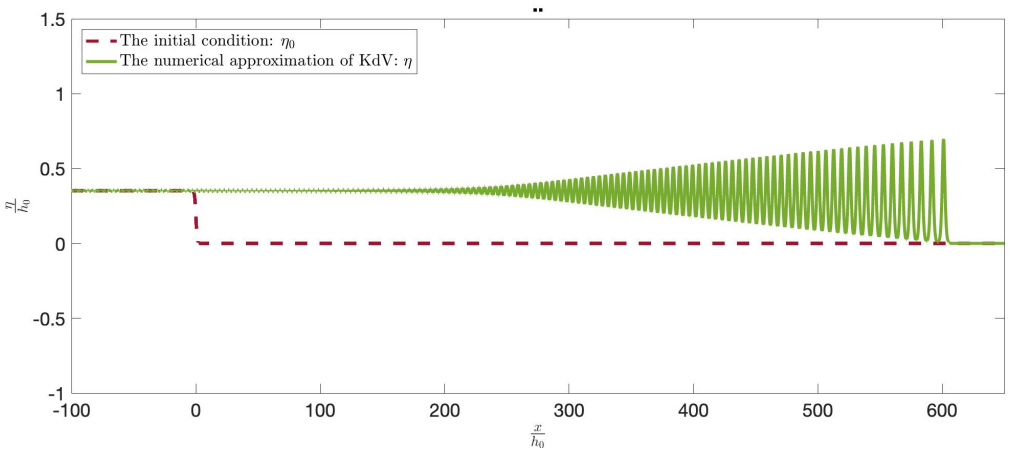

Figure 4.1: An undular bore modelled by the KdV equation with initial bore strength of 0.353. It propagated to the endpoint of 600 depths, where the height of the wave was 0.6992.

4.1 The solitary wave solution

This section presents the derivation of the solitary wave solution of the KdV equation. Derived from the work of Drazin and Johnson (1998, pp. 21–22), I started with the KdV equation

$$\eta_t + \eta_x + \frac{3}{2}\eta\eta_x + \frac{1}{6}\eta_{xxx} = 0.$$

The travelling wave solution was given by $\eta = f(\xi)$, where $\xi = x - ct$ and c was the constant phase speed of the wave. The solution was substituted into the KdV equation, yielding

$$(-c+1)f' + \frac{3}{2}ff' + \frac{1}{6}f''' = 0.$$

The equations were integrated once.

$$(-c+1)f + \frac{3}{4}f^2 + \frac{1}{6}f'' = A.$$

Using f' as the integrating factor, the equation was integrated once more, which resulted in

$$\frac{1}{2}(-c+1)f^2 + \frac{1}{4}f^3 + \frac{1}{12}\left(f'\right)^2 = Af + B.$$

Since a solitary wave is infinitely separated from other waves, the boundary conditions yielded that f, f' and $f'' \to 0$ when $\xi \to \pm\infty$, causing A and B to become zero. Then,

$$\left(f'\right)^2 = f^2\left(6(c-1) - 3f\right).$$

The integrated form of this resulted in

$$\int \frac{df}{f\sqrt{6(c-1)-3f}} = \pm\int d\xi.$$

By substituting the expression $f(\theta) = 2(c-1)\,\mathrm{sech}^2(\theta)$ into the equation, I got

$$\int \frac{-2\tanh(\theta)}{\sqrt{6\,(c-1)\left(1-\mathrm{sech}^2(\theta)\right)}}d\theta = \pm\int d\xi.$$

Using that $\tanh(\theta) = \pm\sqrt{1-\mathrm{sech}^2(\theta)}$, gave the integral

$$\int \frac{-2}{\sqrt{6\,(c-1)}}d\theta = \pm\int d\xi.$$

This had the solution $\theta = \frac{\sqrt{6(c-1)}}{2}\xi$. Using $c = \frac{H}{2} + 1$ gave $\theta = \frac{\sqrt{3H}}{2}(x - ct - x_0)$. Hence, the solitary wave solution of the KdV equation was derived to be,

$$f(x,t) = H\,\mathrm{sech}^2\left(\frac{\sqrt{3H}}{2}(x - ct - x_0)\right).$$

The choice of $\pm$ did not matter since this was an even function.

4.2 Code validation

The numerical methods presented in chapter 3 were utilised to numerically estimate the KdV equation and run simulations of an undular bore. To verify the implementation of the KdV equation, the result of the approximation was tested towards the exact solitary wave solution. As mentioned, from the results of Skogestad and Kalisch (2009) a second-order convergence was expected. With the initial condition

$$\eta_0 = H \operatorname{sech}^2 \left[\frac{\sqrt{3H}}{2}(x) \right],$$

the numerical solution should converge towards the exact solution

$$\eta(x,t) = H \operatorname{sech}^2 \left[\frac{\sqrt{3H}}{2}(x - cT) \right].$$

where $c = \frac{H}{2} + 1$.With $H = 1$, the spatial convergence is presented in table 4.1 where the temporal grid size was $\delta t = 0.001$ and the final time was $T = 1$. The error at each time step was defined by using the L^2 norm.

Table 4.1: The spatial convergence rate of the numerical approximation of the KdV.

δx	L^2-norm	Convergence rate $\left(\frac{\log \frac{e_1}{e_2}}{\log \frac{\delta x_1}{\delta x_2}} \right)$
0.16	0.01382	-
0.08	0.00342	2.015
0.04	0.00085	2.008
0.02	0.00021	2.017
0.01	0.00005	2.070
0.005	0.00001	2.322

The results of the temporal convergence are presented in table 4.2 where the spatial grid size was $\delta x = 0.01$ and the final time was $T = 1$.

Table 4.2: The temporal convergence rate of the numerical approximation of the KdV.

δt	L^2-norm	Convergence rate $\left(\frac{\log \frac{e_1}{e_2}}{\log \frac{\delta t_1}{\delta t_2}}\right)$
2^{-2}	0.18968	-
2^{-3}	0.04594	2.046
2^{-4}	0.01097	2.066
2^{-5}	0.00274	2.001
2^{-6}	0.00067	2.032

As the result in the tables show, the numerical solution converged towards the exact solution with a 2. order convergence of time and space. Thus, I was confident that the numerical implementation was accurate.

4.3 Numerical convective breaking criterion for KdV

To determine the critical bore strength of the KdV equation, it was necessary to establish the breaking criterion. In chapter 2, the derivation of the equation for the non-dimensional horizontal component $\tilde{w}$ corresponding to the KdV equation was shown, equation 2.45. To find the expression for the horizontal particle velocity, $\tilde{w}$ was substituted into the non-dimensional horizontal velocity equation 2.39, i.e.

$$\tilde{\varphi}_x = \tilde{\eta} - \frac{1}{4}\alpha\tilde{\eta}^2 + \beta\left(\frac{1}{3} - \frac{\tilde{Y}^2}{2}\right)\tilde{\eta}_{xx} + O(\alpha^2, \alpha\beta, \beta^2).$$

It was assumed that the higher orders of α and β were equal to zero. The horizontal particle velocity was transformed into dimensional form by substituting the dimensional variables in 2.32 into the expression, such that

$$\varphi_x = \frac{g}{c_0}\eta - \frac{g}{c_0 h}\frac{1}{4}\eta^2 + h_0^2\left(\frac{1}{3} - \frac{Y^2}{2h_0^2}\right)\eta_{xx}.$$

When all the variables were scaled by 2.47, the undisturbed depth h_0 was taken as a unit of distance and $\sqrt{\frac{h_0}{g}}$ as a unit of time, such that

$$\varphi_x = \eta - \frac{1}{4}\eta^2 + \left(\frac{1}{3} - \frac{Y^2}{2}\right)\eta_{xx}.$$

To find the strength of the bore when the leading wave broke, the breaking criterion was utilised for the numerical approximation of the horizontal particle velocity and the phase speed. Hence, the velocities were found at each numerical iteration as the undular bore propagated along the horizontal axis. Given that the numerical solution of the KdV equation was $\eta(x_j, t_n) = \eta_j^n$, the numerical horizontal particle velocity was found by

$$u_j^n = \eta_j^n - \frac{1}{4}\left(\eta_j^n\right)^2 + \left(\frac{1}{3} - \frac{(Y_j^n)^2}{2}\right)\frac{\eta_{j-1}^n - 2\eta_j^n + \eta_{j+1}^n}{\delta x^2},$$

where a second-order central-difference scheme was used to approximate the second-order spatial derivative. I was interested in the horizontal particle velocity at the crest of the front wave, therefore with $\eta_{\text{front}}^n = \eta(x_{\text{front}}, t^n)$, where x_{front} was the horizontal position of the top of the front wave, the numerical horizontal particle velocity at the top of the front wave became

$$U^n = \eta_{\text{front}}^n - \frac{1}{4}(\eta_{\text{front}}^n)^2 + \left(\frac{1}{3} - \frac{(1+\eta_{\text{front}}^n)^2}{2}\right)\frac{\eta_{\text{front+1}}^n - 2\eta_{\text{front}}^n + \eta_{\text{front+1}}^n}{dx^2},$$

where U is the velocity at the top of the wave. The phase velocity of the undular bore was found using a first-order central difference scheme. Since the location of the top of the leading wave was defined by x_{front}, the following method was used for the approximation,

$$c_n = \frac{x_{\text{front}}^n - x_{\text{front}}^{n-1}}{\delta t}.$$

4.4 Numerical results on the breaking of undular bores

This section presents the result of the breaking of the undular bore simulated by the KdV equation. The numerical horizontal velocity at the top of the leading wave and the phase speed found in the previous section were used to see when the breaking criterion was reached.

Favre (1935) ran many experiments before he found at experiment number 24 that the bore strength of 0.281 caused the leading wave to exhibit breaking. Experiments no.22 and no.23 had bores with a slightly smaller initial height above the undisturbed water, and the crest of the

waves was photographed at approximately 64 meters without breaking, while no.24 did break during this distance. Thus, this length was adopted for numerical testing. Since the undisturbed depth h_0 was taken as a unit of distance and $\sqrt{\frac{h_0}{g}}$ as a unit of time, the values had to be scalded to use the unit in meters and seconds. The length of 64 meters, with the undisturbed water height of 0.1075 m, corresponded to 595.35 depths. Therefore, 600 times the depth was used as the endpoint for the wave during the numerical testing. Hence, if the wave satisfied the breaking criterion before reaching 600, I concluded that the wave was breaking.

When applying the breaking criterion, the phase speed was challenging due to the significant oscillations resulting from the first-order finite difference scheme. A higher-order difference scheme was tested to avoid this, but it did not yield an improved result. Since the spatial grid size was smaller than the temporal grid size, x^n_{front} would not switch position at every implementation, and when it first moved, the jump was relatively large, resulting in a non-smooth graph. An effort was made to decrease the spatial grid size, but this resulted in an excessively long simulation duration. The conclusion was that the best approximation was to take the mean value of every 500 points of the horizontal position of the front wave, x^n_{front}, as the front wave propagated during the simulation. The simulations showed that the undular bores used a maximum of $500\sqrt{\frac{h_0}{g}} \approx 52$ sec to reach 600 depths. With $\delta t = 0.01$, 500 points were about 0.52 sec, so each part of mean values of x_n equals around 1% of the total x_n. Worth mentioning is that this approach corresponds with the physical experiment conducted by Favre, where obtaining an accurate determination of the physical phase speed could be challenging. Hence, taking the mean value of every 500 x^n_{front} gave an approximation of the phase speed that I was comfortable with.

Brun and Kalisch (2018) concluded that the wave modelled by the KdV equation broke when the bore strength was 0.353. Hence, this was tested to determine if the results agreed. Figure 4.2 show the result of the horizontal particle velocity at the top of the front wave and the phase speed for the bore strength 0.353. Since the horizontal particle velocity passed the phase velocity, I concluded that the leading wave was breaking.

The bore strength of 0.352 was also tested to see if there was a lower value where the leading wave was breaking. Figure 4.3 below show that the horizontal particle velocity never exceeded the phase speed before the wave reached 600 depths.

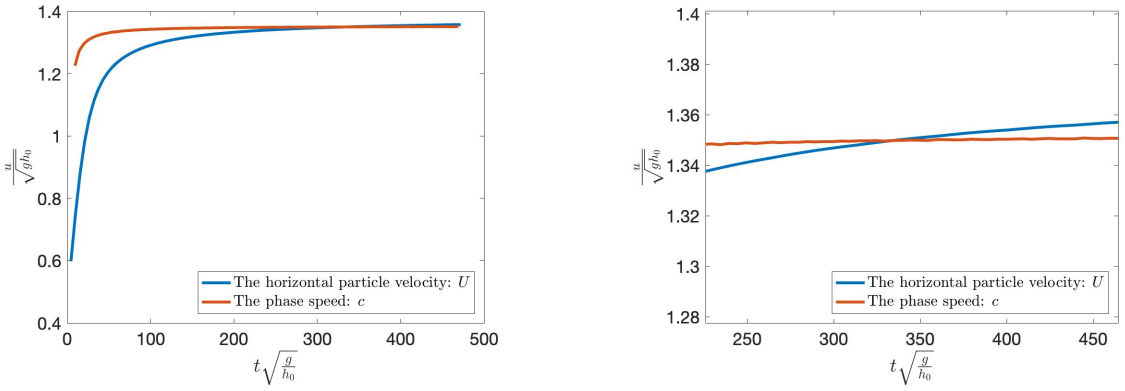

(a) **(b)**

Figure 4.2: The horizontal particle velocity, coloured in blue, and the phase speed, coloured in red, when the bore strength was 0.353. Panel (b) provides a closer view of panel (a).

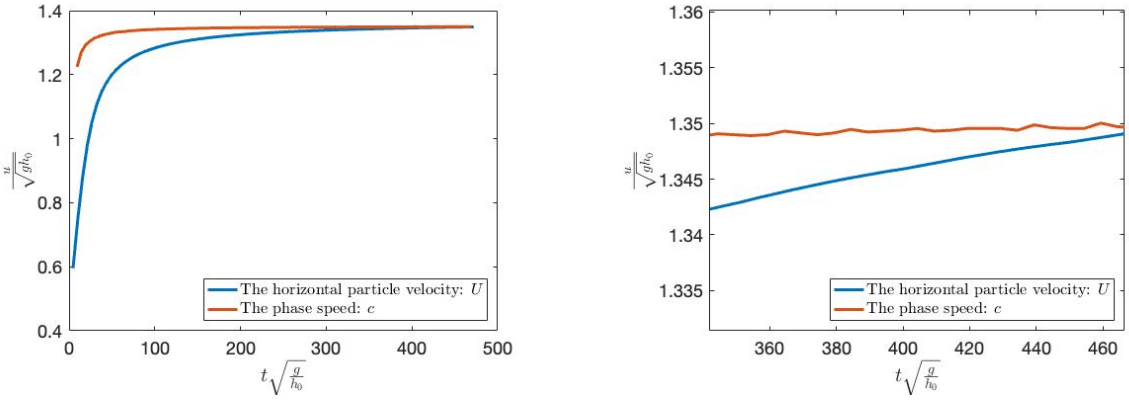

(a) **(b)**

Figure 4.3: The horizontal particle velocity, coloured in blue, and the phase speed, coloured in red, when the bore strength was 0.352. Panel (b) provides a closer view of panel (a).

4.5 Discussion

The result show that the undular bore simulated by the KdV equation was breaking for a bore strength 0.353, which agreed with the result found by Brun and Kalisch (2018). However, as figure 4.3b illustrates, the horizontal velocity potential was close to cross the phase speed at the end with bore strength 0.352. Hence, the leading wave would break if the horizontal domain was longer.

Brun and Kalisch (2018) derived the maximum analytical height of the solitary wave solution of the KdV equation and found it to be 0.6879. The authors discovered that the maximum analytical height of the solitary wave was smaller than the height of the leading wave of the numerical simulated undular bore with a critical bore strength of 0.535. Therefore, an asymp-

totic bore strength was derived from the numerical results, assuming that a lower bore strength was achievable when the time evaluation was large. The authors found that the asymptotic bore strength of 0.328 would lead to breaking. This, again, indicated that for an extended horizontal domain and time evaluation, the threshold for breaking would be for a lower bore strength. Even though, in the current study the purpose was to approximate the experiment of Favre (1935) and therefore, if the leading wave did not break before reaching 600 depths, I considered it not to break.

5 Wave breaking modelled by the the extended KdV equation

This chapter evaluates wave breaking of a wave modelled by the extended KdV equation, denoted the eKdV equation. The eKdV equation, also called the Gardner equation, is well known and early derivations on the equation were done by Benney (1966) and Lee (1974).

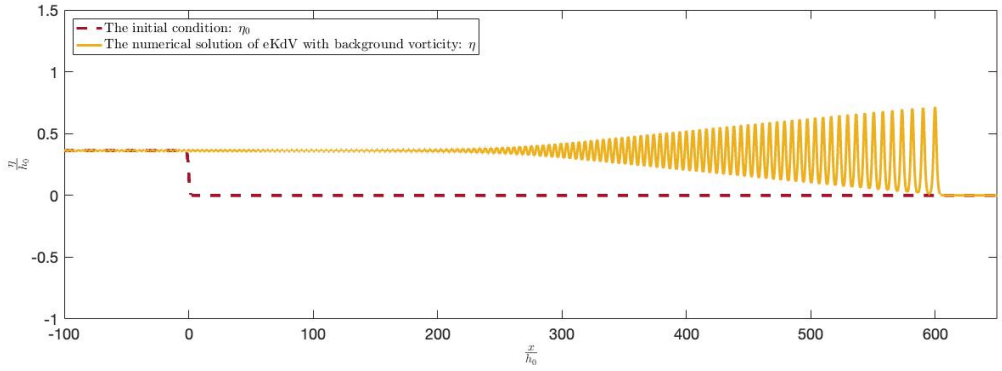

Figure 5.1: The undular bore was simulated by the eKdV equation with bore strength 0.363, where the leading wave was at 600 depths and had a height of 0.7183.

5.1 Derivation of the eKdV equation

This section will present the derivation of the eKdV equation. It was found by including higher powers of α to the regular KdV equation, which was done under the assumption that $\alpha^2 \approx \beta$, meaning that the squared non-linear term was on the same order as the dispersive term. This assumption was made because situations may arise where the relative wavelength is larger than the relative amplitude. Norevik and Kalisch (2022) illustrated the waves in the experiment of Favre (1935) and the figures indicated that the wavelength could be slightly larger than the amplitude. Therefore, it was interesting to analyse if the breaking criterion for the eKdV equation was reached for a smaller value of the bore strength than for the KdV equation.

The procedure to find the eKdV equation was based on the work of Whitham (1974) presented in chapter 2 when finding the KdV equation. However, to include the second-order non-linear

term, I sought a solution where $\tilde{w}$ was on the form

$$\tilde{w} = \tilde{\eta} + \alpha A(\tilde{\eta}) + \beta B(\tilde{\eta}) + \alpha^2 C(\tilde{\eta}) + O(\alpha^3, \alpha\beta, \beta^2),$$

such that variables A, B and C were functions of $\tilde{\eta}$ and its derivative. It was assumed that the higher orders of α and β equaled zero. The expression for $\tilde{w}$ was then substituted into the non-dimensional Boussinesq equations 2.38, and the result were the system of equations,

$$\tilde{\eta}_{\tilde{t}} + \left(\tilde{\eta} + \alpha A + \beta B + \alpha^2 C\right)_{\tilde{x}} + \alpha\left(\tilde{\eta}(\tilde{\eta} + \alpha A + \beta B + \alpha^2 C)\right)_{\tilde{x}} - \frac{1}{6}\beta\left(\tilde{\eta} + \alpha A + \beta B + \alpha^2 C\right)_{\tilde{x}\tilde{x}\tilde{x}} = 0,$$

$$\left(\tilde{\eta} + \alpha A + \beta B + \alpha^2 C\right)_{\tilde{t}} + \tilde{\eta}_{\tilde{x}} + \alpha\left(\tilde{\eta} + \alpha A + \beta B + \alpha^2 C\right)(\tilde{\eta} + \alpha A + \beta B + \alpha^2 C)_{\tilde{x}} + - \frac{1}{2}\beta\left(\tilde{\eta} + \alpha A + \beta B + \alpha^2 C\right)_{\tilde{x}\tilde{x}\tilde{t}} = 0.$$

The equations were required to be equal and then the terms in front of α, α^2 and β had to be identical. With the use of $\tilde{\eta}_{\tilde{t}} = -\tilde{\eta}_{\tilde{x}}$ the coefficients A and B were derived, and as presented below, they were the same as for the regular KdV equation:

$$\alpha\left(A_{\tilde{x}} + \left(\tilde{\eta}^2\right)_{\tilde{x}}\right) = \alpha\left(A_{\tilde{t}} + \frac{1}{2}\left(\tilde{\eta}^2\right)_{\tilde{x}}\right) \qquad \rightarrow \qquad A = -\frac{1}{4}\tilde{\eta}^2,$$

$$\beta\left(B_{\tilde{x}} - \frac{1}{6}\tilde{\eta}_{\tilde{x}\tilde{x}\tilde{x}}\right) = \beta\left(B_{\tilde{t}} - \frac{1}{2}\tilde{\eta}_{\tilde{x}\tilde{x}\tilde{t}}\right) \qquad \rightarrow \qquad B = \frac{1}{3}\tilde{\eta}_{\tilde{x}\tilde{x}}.$$

The coefficients A and B were then substituted back into the equations. The equations were sorted after order and set to equal each other. The terms in front of β would cancel or result in orders assumed to be zero. Hence, only terms with α and α^2 were left and the equation yielded

$$\alpha\left(-\frac{1}{2}\tilde{\eta}\,\tilde{\eta}_{\tilde{x}} + 2\tilde{\eta}\,\tilde{\eta}_{\tilde{x}}\right) + \alpha^2\left(C_x - \frac{3}{4}\tilde{\eta}^2\tilde{\eta}_{\tilde{x}}\right) = \alpha\left(-\frac{1}{2}\tilde{\eta}\,\tilde{\eta}_{\tilde{t}} + \tilde{\eta}\,\tilde{\eta}_{\tilde{x}}\right) + \alpha^2\left(C_t - \frac{1}{4}\tilde{\eta}^2\tilde{\eta}_x - \frac{1}{2}\tilde{\eta}^2\tilde{\eta}_{\tilde{x}}\right).$$

To find the coefficient C, the next term of the KdV equation had to be included in the derivation relation such that

$$\tilde{\eta}_{\tilde{t}} = -\tilde{\eta}_{\tilde{x}} - \frac{3}{2}\alpha\tilde{\eta}\,\tilde{\eta}_{\tilde{x}}.$$

An additional α^2 term was then created. By removing all orders except α^2 the equation became

$$\alpha^2\left(C_x - \frac{3}{4}\tilde{\eta}^2\tilde{\eta}_{\tilde{x}}\right) = \alpha\left(\frac{3}{4}\alpha\tilde{\eta}^2\tilde{\eta}_{\tilde{x}}\right) + \alpha^2\left(-C_x - \frac{3}{4}\tilde{\eta}^2\tilde{\eta}_{\tilde{x}}\right).$$

Simplifying the terms yielded

$$\alpha^2\left(2C_{\tilde{x}}-\frac{3}{4}\tilde{\eta}^2\tilde{\eta}_{\tilde{x}}\right)=0 \qquad \rightarrow \qquad C=\frac{1}{8}\tilde{\eta}^3.$$

Substituting A, B and C into the equation for $\tilde{w}$ resulted in

$$\tilde{w}=\tilde{\eta}+\frac{1}{3}\beta\tilde{\eta}_{\tilde{x}\tilde{x}}-\frac{1}{4}\alpha\tilde{\eta}^2+\frac{1}{8}\alpha^2\tilde{\eta}^3.$$

The coefficients were substituted into one of the Boussinesq equations and it resulted in the non-dimensional eKdV-equation

$$\tilde{\eta}_{\tilde{t}}+\tilde{\eta}_{\tilde{x}}+\frac{3}{2}\alpha\tilde{\eta}\,\tilde{\eta}_{\tilde{x}}-\frac{3}{8}\alpha^2\tilde{\eta}^2\tilde{\eta}_{\tilde{x}}+\frac{1}{6}\beta\tilde{\eta}_{\tilde{x}\tilde{x}\tilde{x}}=0. \tag{5.1}$$

The eKdV equation was transformed to dimensional form by substituting the dimensional variables 2.32 into the equation, such that

$$\frac{1}{c_0}\eta_t+\eta_x+\frac{3}{2}\frac{1}{h_0}\eta\,\eta_x-\frac{3}{8}\frac{1}{h_0^2}\eta^2\eta_x+\frac{1}{6}h_0^2\eta_{xxx}=0.$$

With scaling 2.47, this resulted in the eKdV equation with dimensional variables

$$\eta_t+\eta_x+\frac{3}{2}\eta\,\eta_x-\frac{3}{8}\eta^2\eta_x+\frac{1}{6}\eta_{xxx}=0. \tag{5.2}$$

5.2 The solitary wave solution

The extended KdV equation usually models internal waves of an ideal fluid, but it can also simulate shallow water waves. The equation has a solitary wave solution, where the amplitude can be both positive and negative. Kalisch and Nguyen (2010) stated that the equation

$$\tilde{\eta}_t+\tilde{\eta}\,\tilde{\eta}_x+\sigma\tilde{\eta}^2\tilde{\eta}_x+\tilde{\eta}_{xxx}=0, \tag{5.3}$$

has an exact solitary wave solution, given as $\eta(x,t)=\Phi(\zeta)$ where $\zeta=x-ct$, on the form

$$\Phi(\zeta)=\frac{A}{b+(1-b)\cosh^2(K\zeta)} \tag{5.4}$$

where

$$A = \frac{-1+\sqrt{1+6c\sigma}}{\sigma}, \qquad K = \frac{\sqrt{c}}{2} \qquad \text{and} \qquad b = -\frac{\sigma A^2}{6c}.$$

By substituting the exact solitary wave solution into 5.3, the following equation holds,

$$-c\Phi^{'} + \Phi\Phi^{'} + \sigma\Phi^2\Phi^{'} + \Phi^{'''} = 0, \tag{5.5}$$

where $\Phi^{'} = \frac{d\Phi}{d\zeta}$. The eKdV equation evaluated in this study had other coefficients than the equation evaluated by Kalisch and Nguyen (2010). Therefore, the solitary wave solution 5.4 had to be scaled to align with the formulation considered in this analysis. It was assumed a solution on the form $\eta = \lambda\Phi_(\mu x - \nu t)$, where λ, μ, and ν were constants and the values had to be determined such that they satisfied the solution of this studies eKdV equation. To find the values, $\eta = \lambda\Phi_(\mu x - \nu t)$ was substituted into the eKdV equation 5.2, which yielded

$$\lambda(-\nu+\mu)\Phi^{'} + \frac{3}{2}\lambda^2\mu\Phi\Phi^{'} - \frac{3}{8}\lambda^3\mu\Phi^2\Phi^{'} + \frac{1}{6}\lambda\mu^3\Phi^{'''} = 0. \tag{5.6}$$

Since it was known that Φ satisfies the equation 5.5, this was used to find to correct values of λ, μ and ν. By using λ, μ and ν to scale 5.6 such that it became equal to 5.5, I knew that also 5.6 would be satisfied by the solitary wave solution 5.4. Hence, this gave the system of equations

$$\lambda(-\nu+\mu) = -c, \qquad \frac{3}{2}\lambda^2\mu = 1, \qquad -\frac{3}{8}\lambda^3\mu = \sigma \qquad \text{and} \qquad \frac{1}{6}\lambda\mu^3 = 1.$$

In equation 5.5, the variable σ was not stated, but it was a value that could be determined. Therefore, the values of λ, μ, and ν was calculated first and then σ was fixed to satisfy the values of λ, μ and ν. Solving the system of equations resulted in,

$$\lambda = \frac{2^{\frac{2}{5}}}{3^{\frac{4}{5}}}, \qquad \mu = 2^{\frac{1}{5}}3^{\frac{3}{5}}, \qquad \nu = \frac{3^{\frac{4}{5}}}{2^{\frac{2}{5}}}c + 2^{\frac{1}{5}}3^{\frac{3}{5}} \qquad \text{and} \qquad \sigma = -\frac{1}{12^{\frac{4}{5}}}. \tag{5.7}$$

Since the value of σ was negative, Kalisch and Nguyen (2010) stated that the eKdV equation will only have solitary wave solutions with positive amplitude.

In the solitary wave solution 5.4, all the variables depended on the phase speed c. Due to further calculations, I sought a solution where the only variable was A. Rewriting the relationship between c and the amplitude A gave

$$c = -\frac{1}{6\times 12^{\frac{4}{5}}}A^2 + \frac{1}{3}A.$$

Since v, b and K were dependent on c, they were rewritten such that they also depended on A:

$$v = -\frac{1}{24}A^2 + \frac{1}{2^{\frac{2}{5}}3^{\frac{1}{5}}}A + 2^{\frac{1}{5}}3^{\frac{3}{5}}.$$

$$b = \frac{-A}{A - 2 \times 12^{\frac{4}{5}}} \qquad \text{and} \qquad K = \sqrt{\frac{1}{12}A - \frac{1}{24 \times 12^{\frac{4}{5}}}A^2}.$$

By substituting all the coefficients and variables back into the equation, the exact solitary wave solution of the eKdV equation 5.2 was found to be

$$\eta_{exact} = \frac{\frac{2^{\frac{2}{5}}}{3^{\frac{4}{5}}}A}{\frac{-A}{A-2\times12^{\frac{4}{5}}} + \left(1 + \frac{A}{A-2\times12^{\frac{4}{5}}}\right)\cosh^2\left[\sqrt{\frac{1}{12}A - \frac{1}{24\times12^{\frac{4}{5}}}A^2}\left(2^{\frac{1}{5}}3^{\frac{3}{5}}x - \left(-\frac{1}{24}A^2 + \frac{1}{2^{\frac{2}{5}}3^{\frac{1}{5}}}A + 2^{\frac{1}{5}}3^{\frac{3}{5}}\right)t\right)\right]}. \tag{5.8}$$

In this solution, A represented a variable and not the amplitude of the solitary wave.

5.3 The maximum height of the solitary wave

In the previous section, the exact form of the solitary wave solution of the eKdV equation was given. Here, the derivation of the maximum analytical height of the solitary wave, by use of the conductive breaking criterion, will be presented. As explained in chapter 2, the conductive breaking criterion implies that the wave breaks if the horizontal particle velocity at the top of the leading wave exceeds the wave's local phase speed.

The horizontal particle velocity for the eKdV equation was found by substituting the horizontal component

$$\tilde{w} = \tilde{\eta} - \frac{1}{4}\alpha\tilde{\eta}^2 + \frac{1}{3}\beta\tilde{\eta}_{\tilde{x}\tilde{x}} + \frac{1}{8}\alpha^2\tilde{\eta}^3,$$

into the equation for the horizontal velocity, equation 2.39, which yielded

$$\tilde{\varphi}_x = \tilde{\eta} - \frac{1}{4}\alpha\tilde{\eta}^2 + \frac{1}{8}\alpha^2\tilde{\eta}^3 + \beta\left(\frac{1}{3} - \frac{\tilde{Y}^2}{2}\right)\tilde{\eta}_{xx}.$$

By reinserting the dimensional numbers, the dimensional horizontal velocity equation was

$$\varphi_x = \frac{g}{c_0}\eta - \frac{1}{4}\frac{g}{c_0 h_0}\eta^2 + \frac{1}{8}\frac{g}{c_0 h_0^2}\eta^3 + c_0 h_0\left(\frac{1}{3} - \frac{Y^2}{2h_0^2}\right)\eta_{xx}.$$

The variables were scaled by 2.47 and the horizontal particle velocity at the top of the leading wave for the eKdV equation with dimensions became

$$u = \eta - \frac{1}{4}\eta^2 + \frac{1}{8}\eta^3 + \left(\frac{1}{3} - \frac{(1+\eta)^2}{2}\right)\eta_{xx}.$$

The breaking criterion for the eKdV equation was then

$$\eta - \frac{1}{4}\eta^2 + \frac{1}{8}\eta^3 + \left(\frac{1}{3} - \frac{(1+\eta)\eta^2}{2}\right)\eta_{xx} \geq c_{\text{phase}}.$$

The breaking criterion was applied on the solitary wave given by equation 5.8. Hence, the second derivative of the solitary wave equation needed to be determined. The derivation presented further to find the maximum height of the solitary wave is given in terms of σ, ν, and λ for practical reasons, where the values are given as in 5.7. Due to the size of the expression, the part inside the cosh-term in the denominator of 5.4 was simplified to $\Psi(x,t)$ such that,

$$\Psi(x,t) = \sqrt{\frac{1}{24}\sigma A^2 + \frac{1}{12}A}\,(\mu x - \nu t).$$

The expression for the second derivative was obtained through regular derivation calculation, yielding the following result

$$\eta_{xx} = \frac{-2\lambda\mu^2\left(\frac{\sigma}{24}A^2 + \frac{1}{12}A\right)\left(1 + \frac{\sigma}{\sigma A+2}A\right)A\left[\sinh^2(\Psi) + \cosh^2(\Psi)\right]}{\left[-\frac{\sigma}{\sigma A+2}A + \left(1 + \frac{\sigma}{\sigma A+2}A\right)\cosh^2(\Psi)\right]^2} + \frac{8\lambda\mu^2\left(\frac{\sigma}{24}A^2 + \frac{1}{12}A\right)\left(1 + \frac{\sigma}{\sigma A+2}A\right)^2 A\left[\sinh^2(\Psi)\cosh^2(\Psi)\right]}{\left[-\frac{\sigma}{\sigma A+2}A + \left(1 + \frac{\sigma}{\sigma A+2}A\right)\cosh^2(\Psi)\right]^3}.$$

Since the shape of a solitary wave is constant, the wave will have the same height as the initial height for all time. Hence, the solitary wave was evaluated at $(x,t) = (0,0)$, i.e.

$$\eta = \lambda A, \qquad \text{and} \qquad \eta_{xx} = -2\lambda\mu^2\left(\frac{\sigma}{24}A^2 + \frac{1}{12}A\right)\left(1 + \frac{\sigma}{\sigma A+2}A\right)A.$$

The right-hand side of the breaking criterion was the phase speed of the solitary wave, which was equal to

$$c_{\text{phase}} = \frac{\nu}{\mu} = \frac{\sigma}{6\lambda\mu}A^2 + \frac{1}{3\lambda\mu}A + 1.$$

To find the maximum height of the solitary wave, the horizontal particle velocity was evaluated at the top of the solitary wave. The variable A was not the amplitude of the solitary wave since the amplitude of the solitary wave was λA. Hence, I substituted $H = \lambda A$ into the horizontal

particle velocity and the phase speed, such that H was the height of the wave. This gave the equation for the breaking criterion, i.e.

$$\eta - \frac{1}{4}H^2 + \frac{1}{8}H^3 + \left(\frac{1}{3} - \frac{(1+H)^2}{2}\right)\left(-2\mu^2\left(\frac{\sigma}{24\lambda^2}H^2 + \frac{1}{12\lambda}H\right)\left(1 + \frac{\sigma}{\sigma H + 2\lambda}H\right)H\right) \geq \frac{\sigma}{6\lambda^3\mu}H^2 + \frac{1}{3\lambda^2\mu} + 1.$$

The right-hand side was set equal to the left-hand side, and after rearranging the terms, the result was a sixth-order polynomial of the variable H:

$$P(H) = \frac{\sigma^2\mu^2}{12\lambda^2}H^6 + \left(\frac{2\sigma^2\mu^2 + 3\sigma\lambda\mu^2}{12\lambda^2}\right)H^5 + \left(\frac{2\sigma^2\mu^2 + 36\sigma\lambda\mu^2 + 12\lambda^2\mu^2 + 9\sigma\lambda^2}{72\lambda^2}\right)H^4 + \left(\frac{3\lambda^4\mu + 4\lambda^3\mu^3 + \sigma\lambda^2\mu^3 - 3\sigma\lambda^3\mu - 2\sigma}{12\lambda^3\mu}\right)H^3 + \left(\frac{-9\lambda^3\mu - 12\sigma + \lambda^2\mu^3 + 18\sigma\lambda^2\mu}{18\lambda^2\mu}\right)H^2 + \left(\frac{12\lambda^2\mu - 4 - 6\sigma\lambda\mu}{6\lambda\mu}\right)H - 2\lambda = 0.$$

The polynomial had six roots, where the correct root would give the maximum allowable height of the solitary wave. Since I sought a solitary wave with positive amplitude, the negative roots of P were excluded. The polynomial and its derivative are depicted in figure 5.2. The red graph shows the polynomial's derivative, which was always positive between 0 and 1, meaning that the polynomial increased in this interval. Since $P(0) < 0$ and $P(1) > 0$, there was only one root of P for $H \in [0,1]$. Using the bisection method, with an error smaller than $e-04$, the maximum height of the solitary wave solution of the eKdV equation was numerically approximated to be

$$H_{max} = 0.7079.$$

The maximum height of the solitary wave of the KdV equation was found to be 0.6879 (Brun & Kalisch, 2018). Hence, the maximum height of the KdV equation is lower than the maximum height of the solitary wave solution of the eKdV equation.

The eKdV equation would admit solutions with higher amplitude than the limit found here, but for natural waves, the breaking criterion was reached and the waves will break. Therefore, the waves simulated by the eKdV equation with amplitude higher than H_{max} would not describe an real surface wave. On the other hand, as Brun and Kalisch (2018) mentions, real waves with smaller amplitude than H_{max} may break before, and therefore, the wave simulation of the eKdV with lower amplitude will not necessarily describe an actual wave.

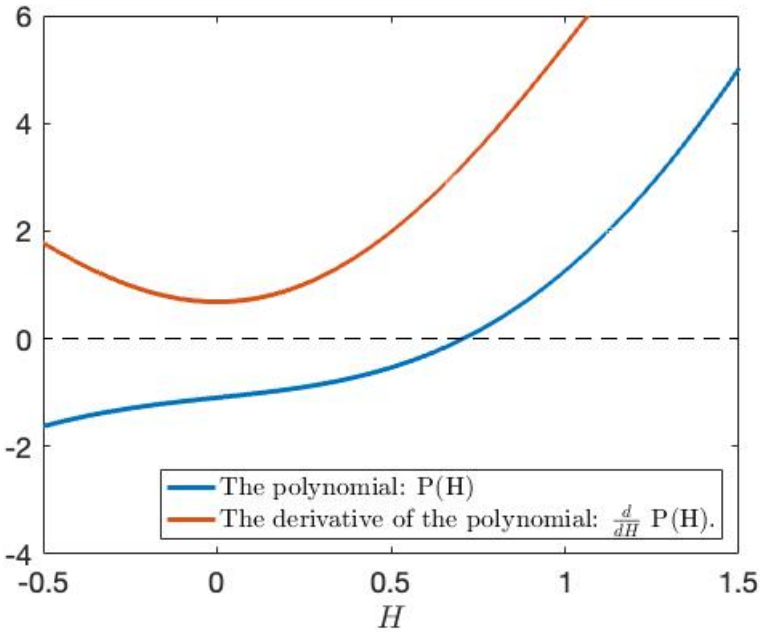

Figure 5.2: The blue graph is the polynomial of H, and the red graph is its derivative.

5.4 Code validation

Before determining the numerical breaking criterion of the undular bore, the numerical implementation of the eKdV equation had to be verified. With the boundary conditions presented in chapter 3, the boundary-value problem for the eKdV was

$$\begin{aligned} \eta_t + \eta_x + \frac{3}{2}\eta\eta_x - \frac{3}{8}\eta^2\eta_x + \frac{1}{6}\eta_{xxx} = 0,\ -h_0 < y < \eta, t > 0 \\ \eta(x,0) = \eta_0(x), \\ \eta(-l,t) = a_0, \\ \eta(l,t) = 0, \\ \eta_x(l,t) = 0. \end{aligned}$$

To make the problem usable to approximate solitary waves, an approximation for the free surface was made, $\eta = \xi + \eta_0$, such that homogeneous boundary conditions were achieved. When inserting this into the eKdV equation, the equation became

$$\xi_t = -\xi_x - \frac{3}{4}(\xi^2)_x - \frac{3}{2}(\xi\eta_0)_x + \frac{1}{8}(\xi^3)_x + \frac{3}{8}(\xi^2\eta_0 + \xi\eta_0^2) - \frac{1}{6}\xi_{xxx} + F,$$

where $F = -\eta_{0x} - \frac{3}{4}(\eta_0^2)_x + \frac{1}{8}(\eta_0^3)_x - \frac{1}{6}(\eta_0)_{xxx}$. The numerical scheme presented in chapter 3 was utilised to find a numerical approximation of the eKdV equation. The only change was the additional terms in the eKdV equation that had to be included in the numerical scheme. Since this term is non-linear, the Adams-Bashforth method was used to find the approximation. Hence, the difference equation to determine vector v, which consists of approximated solutions of ξ, was the following,

$$\begin{aligned}\frac{v^{n+1}-v^n}{\Delta t} &= \frac{3}{2}\left[-\frac{3}{2}D_1(v^n)^2 - \frac{3}{2}D_1(v^n\eta_0) + \frac{1}{8}D_1(v^n)^3 + \frac{3}{8}D_1((v^n)^2\eta_0 + v^n(\eta_0)^2)\right] \\ -\frac{1}{2}&\left[-\frac{3}{2}D_1(v^{n-1})^2 - \frac{3}{2}D_1(v^{n-1}\eta_0) + \frac{1}{8}D_1(v^{n-1})^3 + \frac{3}{8}D_1((v^{n-1})^2\eta_0 + v^{n-1}(\eta_0)^2)\right] \\ &+\frac{1}{2}\left[-D_1(v^{n+1}+v^n) - \frac{1}{6}D_3(v^{n+1}+v^n)\right] - F.\end{aligned}$$

The exact solitary wave solution of the eKdV equation presented in section 5.3 was used to test the implementation of the equation. Since this was the exact solution, I expected that the numerical approximation of the eKdV equation should converge towards it when the grid size was reduced. The initial condition of the solitary wave was

$$\eta_{exact} = \frac{\frac{2^{\frac{2}{5}}A}{3^{\frac{4}{5}}}}{\frac{-A}{A-2\times 12^{\frac{4}{5}}} + \left(1+\frac{A}{A-2\times 12^{\frac{4}{5}}}\right)\cosh^2\left[\sqrt{\frac{1}{12}A - \frac{1}{24\times 12^{\frac{4}{5}}}A^2}\left(2^{\frac{1}{5}}3^{\frac{3}{5}}x\right)\right]},$$

where A was set equal to 1.

First, the spatial convergence was tested. The time step was $\delta t = 0.001$, the length of the horizontal domain was $x \in [-50, 50]$ and the iteration was evaluated until the final time $T = 1$. The table 5.1 show the convergence results, where the L^2 norm was used to define the error between the exact solution and the numerical approximation.

Next, the temporal convergence was tested, shown in table 5.2. The spatial grid size was $\delta x = 0.01$ and the horizontal domain was the same. The implementation was run until a final time $T = 1$.

The tables 5.1 and 5.2 proves that the numerical approximation of the eKdV equation was converging towards the exact solitary wave solution with a second-order convergence of both time and space, showing that the scheme was accurate. To avoid the result being random, the convergence was also tested to a final time of $T = 7$ and $T = 10$, where both approximations had a second-order convergence. The value of A has also been tested for other values to ensure

Table 5.1: The spatial convergence rate of the numerical approximation of the eKdV equation.

δx	L^2-error	Convergence rate $\left(\frac{\log \frac{e_1}{e_2}}{\log \frac{\delta x_1}{\delta x_2}}\right)$
0.16	0.04570	-
0.08	0.01142	2.000
0.04	0.00285	2.004
0.02	0.00070	2.015
0.01	0.00017	2.061
0.005	0.00003	2.258

Table 5.2: The temporal convergence rate of the numerical approximation of the eKdV equation.

δt	L^2-error	Convergence rate $\left(\frac{\log \frac{e_1}{e_2}}{\log \frac{\delta t_1}{\delta t_2}}\right)$
2^{-2}	0.7564	-
2^{-3}	0.1872	2.014
2^{-4}	0.0439	2.091
2^{-5}	0.0108	2.014
2^{-6}	0.0026	2.048
2^{-7}	0.0006	2.243

that the value of A did not impact the result. Since the convergence was always second-order, I was confident that the implementation of the eKdV equation was correct. Therefore, the following results based on the eKdV implementation are reliable.

5.5 Numerical results on the breaking of undular bores

From section 5.3, the breaking criterion for the eKdV equation was presented and it was used to find the numerical result of the critical bore strength.

The breaking criterion was evaluated at each time step to find when the horizontal particle

velocity at the top of the leading wave exceeded the phase speed. Hence, the horizontal position of the top of the front wave was to be determined numerically. By defining the horizontal position of the leading wave as x_{front}, the value at the top of the wave was $\eta_{\text{front}} = \eta(x_{\text{front}}, t)$. A second-order finite difference scheme was used to calculate the second derivative. Hence, the numerical approximation of the horizontal velocity of the front wave was,

$$U^n_{\text{front}} = \eta^n_{\text{front}} - \frac{1}{4}(\eta^n_{\text{front}})^2 + \frac{1}{8}(\eta^n_{\text{front}})^3 + \left(\frac{1}{3} - \frac{(1+\eta^n_{\text{front}})^2}{2}\right)\frac{\eta^n_{\text{front}+1} + 2\eta^n_{\text{front}} + \eta^n_{\text{front}-1}}{\delta x^2}.$$

As for the KdV equation, the phase speed of the wave simulated by the eKdV equation was found using a finite-difference approximation. The horizontal particle velocity and the phase speed were approximated for different values of the bore strength to find the threshold for wave breaking. Since Favre (1935) discovered breaking with a bore strength of 0.281, this was the starting point. Figure 5.3 show the horizontal particle velocity and the local phase speed when the bore strength was 0.281. The horizontal particle velocity, colored in blue, was far from exceeding the phase velocity, colored in red. Hence, the wave was far from breaking.

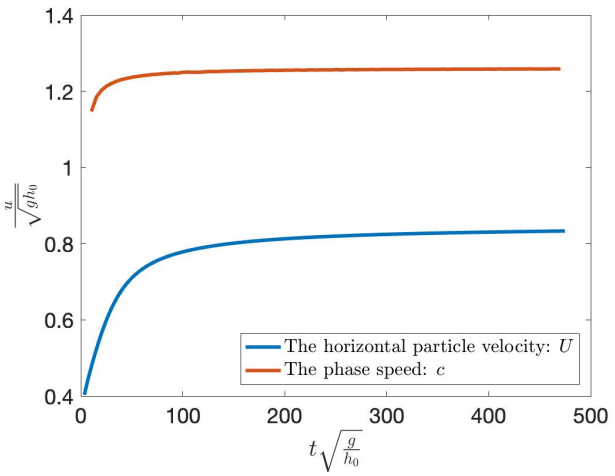

Figure 5.3: The red curve is the phase speed and the blue curve is the horizontal particle velocity. The bore strength was 0.281.

The wave did not break at the bore strength 0.281, it was, therefore, necessary to test higher values of the bore strength. To achieve this, increments of 0.001 was added to the bore strength until the breaking criterion was reached. With a bore strength of 0.363, figure 5.4 show that the horizontal particle velocity exceeded the phase speed. The red graph also show the oscillation of the phase speed, even when the mean value of 500 points was used.

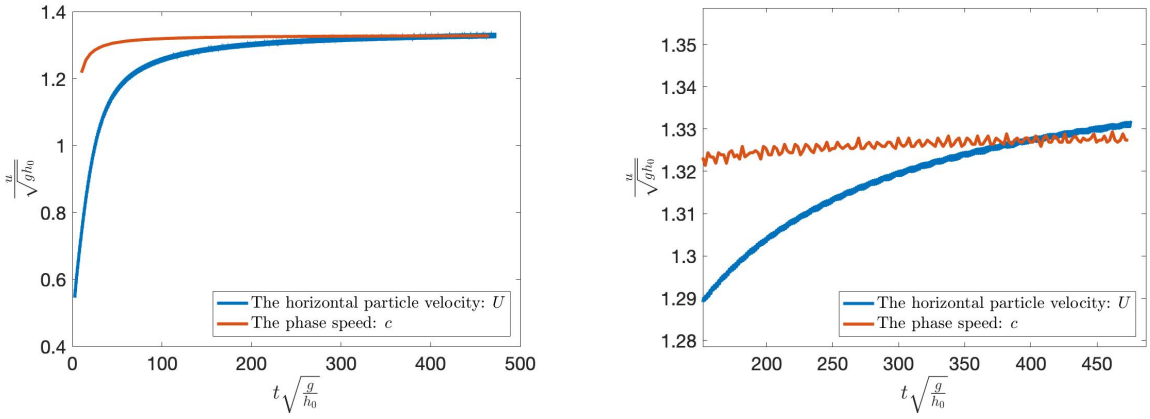

Figure 5.4: The horizontal particle velocity is coloured in blue and the phase velocity is coloured in red when the bore strength was 0.363. The right panel is a closer view of the left panel.

The conclusion was that a wave modelled by the eKdV equation would break with a bore strength of 0.363 when the bore was evaluated at 600 depths, making this the critical bore strength. However, figure 5.5 below illustrate the horizontal particle velocity and the phase speed with a bore strength of 0.362. The figure shows that the breaking criterion was almost reached, but the two graphs never crossed during the time evaluated. At the end, the two graphs are so close that it was assumed that the undular bore would break if it propagated a small distance further.

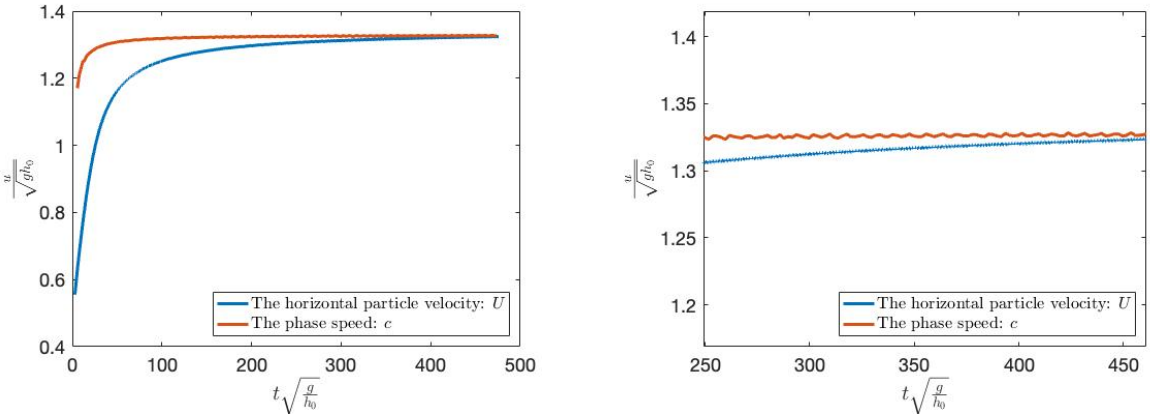

Figure 5.5: The horizontal particle velocity is colored in blue and the phase velocity is coloured in red when the bore strength was 0.362. The right panel is a closer view of the left panel.

To verify the result, the stability of the implementation was tested by decreasing the time grid when simulating the bore. With a time step of $\delta t = 0.001$, the result of the breaking criterion is shown in figure 5.6 with a bore strength of 0.362. The horizontal particle velocity never crossed the phase speed and the wave will not break here either. The conclusion was that the result was stable.

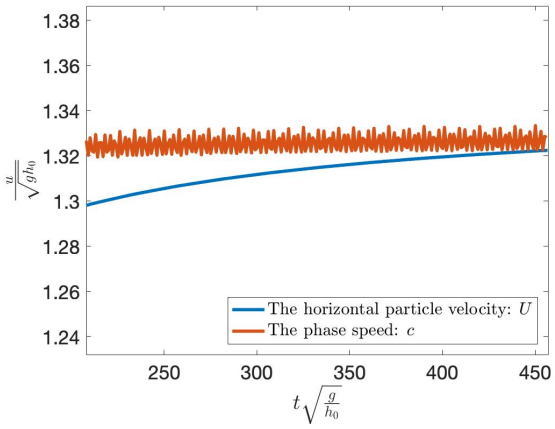

Figure 5.6: The horizontal particle velocity, coloured in blue, and the phase speed, coloured in red, with a bore strength of 0.362 and time grid $\delta t = 0.001$.

5.6 Discussion

The results conclude that the threshold for wave breaking modelled by the eKdV equation was for a bore strength of 0.363. The implementation of the undular bore with a smaller temporal grid strengthened the result by proving that it was not due to instabilities. Unfortunately, it did not improve the result of the KdV equation, where breaking was achieved for a bore strength of 0.353. However, the next chapter will present the study of the eeKdV equation where the next non-linear order was included.

Figure 5.5 indicates that the wave would break if the spatial domain were longer since the horizontal particle velocity was approaching close to the phase speed. Therefore, a smaller bore strength could cause the leading wave to break if it continued on an extended horizontal domain. However, as mentioned, this was not included in this study. Favre (1935) discovered that the front wave of the bore, when the bore strength was 0.281, reaches a height of 2.06 times the initial height of the wave before the wave broke. At 600 depths, the leading wave of the undular bore simulated by the eKdV equation reached a height of 1.97 times the initial height. Hence, to be a better approximation of Favre's experiment, the wave should have reached a higher height before it broke.

In section 5.3, the derivation of the maximum analytical height of the solitary wave solution of the eKdV equation was found to be 0.7079. The front wave of the numerical simulated undular bore with the critical bore strength 0.363 reached a height of 0.7183 at the endpoint of 600 depths. Hence, the numerical approximation of the undular bore was not far from the maximum analytical height of the solitary wave, but it was still higher. Therefore, ideally, the eKdV equation should be able to simulate the breaking of waves at a lower bore strength and

reach H_{max}, but this would demand an extended horizontal domain and reaching the analytical, critical height is assumable impossible. However, the result of the maximum analytical height somehow agrees with the study of Massel (1996), who found that the limiting wave height of a solitary wave was close to $0.78h_0$.

The max solitary wave solution of the KdV equation was found to be 0.6879 (Brun & Kalisch, 2018), which is lower than the maximum height of the eKdV equation. This explains why breaking of the undular bores simulated by the KdV equation happens at a lower bore strength than the eKdV equation.

6 Wave breaking modelled by the double extended KdV equation

The eKdV equation was not able to provide a better model of the experiment of Favre (1935) compared to the KdV equation. However, motivated by the same assumptions as for the eKdV equation, including the next order of the nonlinear terms might improve the approximation of the waves in the experiment of Favre (1935). Including α^3, the eeKdV equation is derived as an extension of the KdV equation. Therefore, like the KdV equation, the eeKdV equation is based on the Boussinesq equations, which balance the nonlinear terms and the dispersive term. The motivation and derivation of the eeKdV equation are based on the work of Norevik and Kalisch (2022), and the derivation is equal to the derivation made for the KdV equation based on the work of Whitham (1974). The derivation began by including the α^3 term in the $\tilde{w}$ equation:

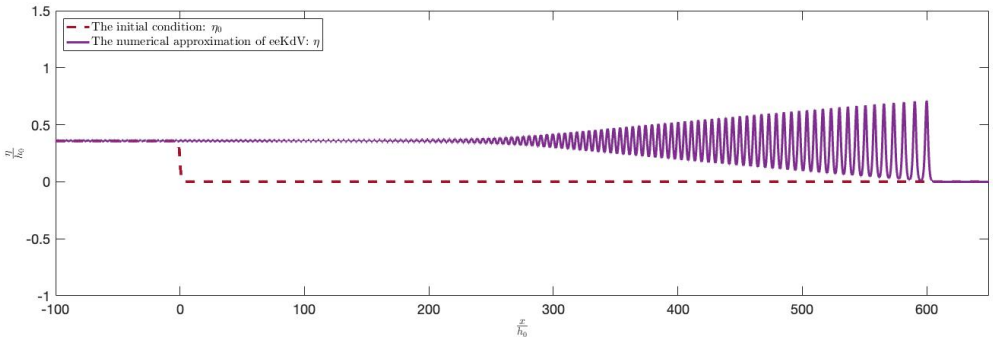

Figure 6.1: The wave was modelled by the eeKdV equation, where the bore strength was 0.353. The leading wave was at 600 depths with a height of 0.7112.

$$\tilde{w} = \tilde{\eta} + \alpha A(\tilde{\eta}) + \beta B(\tilde{\eta}) + \alpha^2 C(\tilde{\eta}) + \alpha^3 D(\tilde{\eta}) + O(\alpha^4, \alpha\beta, \beta^2). \tag{6.1}$$

The higher orders of α and β were assumed to be zero. The coefficients A, B, C and D were found by substituting 6.1 into the Boussinesq equations 2.38. The two equations were required to be equal such that

$$\begin{aligned}\alpha(A_x + 2\tilde{\eta}\tilde{\eta}_x) + \beta(B_x - \frac{1}{6}\tilde{\eta}_{xxx}) + \alpha^2(C_x + (A\tilde{\eta})_x) + \alpha^3(D_x + (C\tilde{\eta})_x) \\ = \alpha(A_t + \tilde{\eta}\tilde{\eta}_x) + \beta(B_t - \frac{1}{2}\tilde{\eta}_{xxt}) + \alpha^2(C_t + (A\tilde{\eta})_x) + \alpha^3(D_t + (C\tilde{\eta})_x + AA_x).\end{aligned}$$

The coefficients A, B and C were the same as for the eKdV equation, i.e.

$$A = -\frac{1}{4}\tilde{\eta}^2 \qquad B = \frac{1}{3}\tilde{\eta}_{\tilde{x}\tilde{x}} \qquad \text{and} \qquad C = \frac{1}{8}\tilde{\eta}^3. \tag{6.2}$$

The values were substituted back into the Boussinesq equations. The β terms were cancelling or the terms were assumed to be zero, such that the remaining part was

$$\alpha\frac{3}{2}\tilde{\eta}\,\tilde{\eta}_x - \alpha^2\frac{3}{8}\tilde{\eta}^2\tilde{\eta}_x + \alpha^3\left(D_x + \frac{1}{2}\tilde{\eta}^3\tilde{\eta}_x\right) = \alpha\left(-\frac{1}{2}\tilde{\eta}\,\tilde{\eta}_t + \tilde{\eta}\,\tilde{\eta}_x\right) + \alpha^2\left(\frac{3}{8}\tilde{\eta}^2\tilde{\eta}_t - \frac{3}{4}\tilde{\eta}^2\tilde{\eta}_x\right) + \alpha^3\left(D_t + \frac{1}{2}\tilde{\eta}^3\tilde{\eta}_x + \frac{1}{8}\tilde{\eta}^3\tilde{\eta}_x\right).$$

To determine the coefficient D, the next term in the derivation relation was included, which was the next term in the eKdV equation:

$$\tilde{\eta}_t = -\tilde{\eta}_x - \frac{3}{2}\alpha\tilde{\eta}\,\tilde{\eta}_x + \frac{3}{8}\alpha^2\tilde{\eta}^2\tilde{\eta}_x.$$

After inserting the derivation relation, the terms with α and α^2 cancel and the remaining part was

$$\alpha^3\left(2D_x + \frac{1}{2}\tilde{\eta}^3\tilde{\eta}_x + \frac{3}{16}\tilde{\eta}^3\eta_x + \frac{9}{16}\tilde{\eta}^3\tilde{\eta}_x - \frac{5}{8}\tilde{\eta}^3\tilde{\eta}_x\right) = 0 \qquad \rightarrow \qquad D = -\frac{5}{64}\tilde{\eta}^4.$$

Hence, the equation for $\tilde{w}$ became

$$\tilde{w} = \tilde{\eta} - \frac{1}{4}\alpha\tilde{\eta}^2 + \frac{1}{3}\beta\tilde{\eta}_{xxx} + \frac{1}{8}\alpha^2\tilde{\eta}^3 - \frac{5}{64}\alpha^3\tilde{\eta}^4.$$

This was inserted into the Boussinesq equations, and the requirement of the equations in the system to give identical equations was used such that the non-dimensional eeKdV equation became

$$\tilde{\eta}_t + \tilde{\eta}_x + \frac{3}{2}\alpha\tilde{\eta}\,\tilde{\eta}_x - \frac{3}{8}\alpha^2\tilde{\eta}^2\tilde{\eta}_x + \frac{3}{16}\alpha^3\tilde{\eta}^3\tilde{\eta}_x + \frac{1}{6}\beta\tilde{\eta}_{xxx} = 0.$$

The equation was then transformed back into dimensional variables by 2.32 and scaled by 2.47. The eeKdV equation with dimensional variables was

$$\eta_t + \eta_x + \frac{3}{2}\eta\,\eta_x + \frac{1}{6}\eta_{xxx} - \frac{3}{8}\eta^2\eta_x + \frac{3}{16}\eta^3\eta_x = 0.$$

6.1 Code validation

The exact solitary wave solution to the eeKdV is yet to be found, as we know. However, stated by Bona et al. (1996), the solution to the equation

$$\eta_t + \eta^P \eta_x + \varepsilon \eta_{xxx} = 0$$

is given by

$$\eta(x,t) = \Phi(x - ct) = A\,\mathrm{sech}^{\frac{2}{P}}\left(Kx - \omega t\right), \tag{6.3}$$

where

$$K = \sqrt{\frac{P^2 A^P}{2\varepsilon(P+1)(P+2)}} \qquad \text{and} \qquad \omega = \frac{2KA^P}{(P+1)(P+2)}.$$

Since it was already proven that the implementation of the eKdV equation had a second-order convergence, I only needed to test the convergence of the implementation of the additional term included in the eeKdV equation, $\frac{3}{16}\eta^3\eta_x$. Therefore, the exact solution 6.3 was used to find the convergence rate of the problem

$$\begin{aligned}
\eta_t + \eta^3\eta_x + \frac{1}{6}\eta_{xxx} = 0,\ -h_0 < y < \eta, t > 0 \\
\eta(x,0) \ = \eta_0(x), \\
\eta(-l,t) = a_0, \\
\eta(l,t) = 0, \\
\eta_x(l,t) = 0.
\end{aligned}$$

The exact solution to this problem, formed as a solitary wave, was then given by

$$\eta(x - ct) = \Phi(x,t) = A\,\mathrm{sech}^{\frac{2}{3}}\left(\sqrt{\frac{27A^3}{20}}\left(x - \frac{A^3}{10}t\right)\right),$$

where A was the given amplitude of the solitary wave. Also here, $\xi = \eta - \eta_0$ was used to achieve homogeneous boundary conditions, which resulted in the problem

$$\xi_t + \frac{1}{4}(\xi^4)_x + (\xi^3\eta_0)_x + \frac{3}{2}(\xi^2\eta_0^2)_x + (\xi\eta_0^3)_x + \frac{1}{6}\xi_{xxx} + F = 0,\ -h_0 < y < \eta, t > 0$$
$$\xi(x,0) = \eta_0(x),$$
$$\xi(-l,t) = 0,$$
$$\xi(l,t) = 0,$$
$$\xi_x(l,t) = 0,$$

where the forcing function was $F = -\frac{1}{4}(\eta_0^4)_x - \frac{1}{6}(\eta_0)_{xxx}$. As explained earlier, a Crank-Nicolson method was used to approximate the linear terms and Adams-Bashforth was used to approximate the nonlinear terms to find the evolution of the wave over time. With the approximation $v_j^n \approx \xi(x_j, t^n)$, the difference equation to determine vector v was then

$$\frac{v^{n+1} - v^n}{\delta t} = \frac{3}{2}D_1\left[-\frac{1}{4}(v^n)^4 - (v^n)^3\eta_0 - \frac{3}{2}(v^n)^2\eta_0^2 - v^n\eta_0^3\right]$$
$$-\frac{1}{2}D_1\left[\frac{1}{4}(v^{n-1})^4 - 4(v^{n-1})^3\eta_0 - 6(v^{n-1})^2\eta_0^2 - 4v^{n-1}\eta_0^3\right] - \left[\frac{1}{12}(v^n + v^{n-1})\right] - F.$$

Since this will produce solitary waves, the amplitude was constant and, therefore, chosen to be 1 when testing the convergence towards the exact solution. The discretisation errors and the convergence rate are shown in the table 6.1 below. The temporal grid size was $\delta t = 0.001$ and the wave was simulated to a final time $T = 1$.

Table 6.1: The spatial convergence rate of the numerical approximation of the eeKdV equation.

δx	L2-error	Convergence rate $\left(\frac{\log\frac{e_1}{e_2}}{\log\frac{\delta x_1}{\delta x_2}}\right)$
0.16	0.004000	-
0.08	0.000984	2.023
0.04	0.000245	2.006
0.02	0.000061	2.002
0.01	0.000015	2.001
0.005	0.000004	2.003

The discretisation error and the convergence rate for the time evaluation are shown in the table 6.2 below with a spatial grid size of $\delta x = 0.001$ and the final step size $T = 1$.

Table 6.2: The temporal convergence rate of the numerical approximation of the eeKdV equation.

δt	L^2-error	Convergence rate $\left(\frac{\log \frac{e_1}{e_2}}{\log \frac{\delta t_1}{\delta t_2}}\right)$
2^{-2}	0.001600	-
2^{-3}	0.000420	1.930
2^{-4}	0.000108	1.963
2^{-5}	0.000028	1.944
2^{-6}	0.000015	0.923
2^{-7}	0.000015	0

The tables 6.1 and 6.2 show that the approximation of the solitary wave was very close to a second-order convergence rate. Hence, by scaling the implementation of the additional term by $\frac{3}{16}$ and then adding the eKdV implementation, the conclusion was that the implementation of the eeKdV equation was accurate and valid.

6.2 The numerical convective wave breaking criterion for eeKdV

The full expression for the horizontal particle velocity was found by using the same procedure as was used for the KdV and the eKdV equation; the expression for $\tilde{w}$ was inserted into the equation for the non-dimensional horizontal particle velocity 2.39, i.e.

$$\tilde{\phi}_x = \tilde{\eta} - \frac{1}{4}\alpha\tilde{\eta}^2 + \frac{1}{8}\alpha^2\tilde{\eta}^3 - \frac{5}{64}\alpha^3\tilde{\eta}^4 + \beta(\frac{1}{3} - \frac{\tilde{Y}}{2})\tilde{\eta}_{xx}.$$

The equation was transformed back to dimensional variables using 2.32 and scaled by 2.47 to get the right scaling of the dimensions. The expression for the horizontal particle velocity with dimensional variables was evaluated at the top of the wave. It gave

$$u = \eta - \frac{1}{4}\eta^2 + \frac{1}{8}\eta^3 - \frac{5}{64}\eta^4 + \left(\frac{1}{3} - \frac{(1+\eta)^2}{2}\right)\eta_{xx}.$$

With x_{front} as the horizontal position of the front wave in the numerical simulation, such that $\eta_{\text{front}} = \eta(x_{\text{front}}, t)$ was the vertical position of the front wave, the horizontal particle velocity

at the top of the undular bore was given by

$$u = \eta_{\text{front}} - \frac{1}{4}\eta_{\text{front}}^2 + \frac{1}{8}\eta_{\text{front}}^3 - \frac{5}{64}\eta_{\text{front}}^4 + \left(\frac{1}{3} - \frac{(\eta_{1+\text{front}})^2}{2}\right)\eta_{\text{front}xx}.$$

When implementing the horizontal particle velocity, a central finite difference scheme approximates the second derivative of η_{front}.

$$u_j^n = \eta_j^n - \frac{1}{4}\left(\eta_j^n\right)^2 + \frac{1}{8}\left(\eta_j^n\right)^3 - \frac{5}{64}\left(\eta_j^n\right)^4 + \left(\frac{1}{3} - \frac{(n+1)^2}{2}\right)\left(\frac{\eta_{j-1}^n - 2\eta_j^n + \eta_{j+1}^n}{\delta x^2}\right)$$

The local phase speed was found by using the first-order finite difference scheme

$$c_n = \frac{x_{\text{front}}^n - x_{\text{front}}^{n-1}}{\delta t}.$$

6.3 Numerical results on the breaking of undular bores

The breaking criterion was first tested with the bore strength 0.281 to compare it to Favre's result. As the figure 6.2 show, the wave was far from breaking.

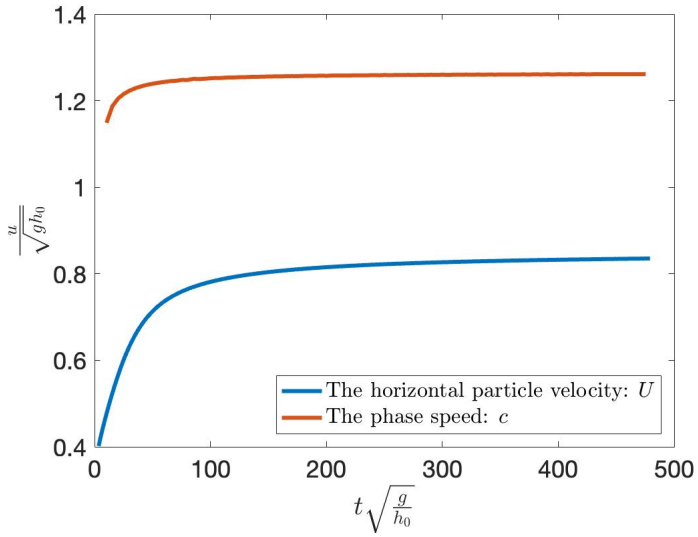

Figure 6.2: The horizontal particle velocity, coloured in blue, and the phase speed, coloured in red, with a bore strength of 0.281.

The horizontal particle velocity and the phase speed were then found for other values of the bore strength, where the bore strength was increased by 0.001 until the breaking criterion was satisfied. At a bore strength of 0.359, the horizontal particle velocity exceeded the phase speed,

as figure 6.3 below show. The maximum value of both velocities was found, concluding that the horizontal velocity was the highest. In figure 6.3, the mean values of both the horizontal particle

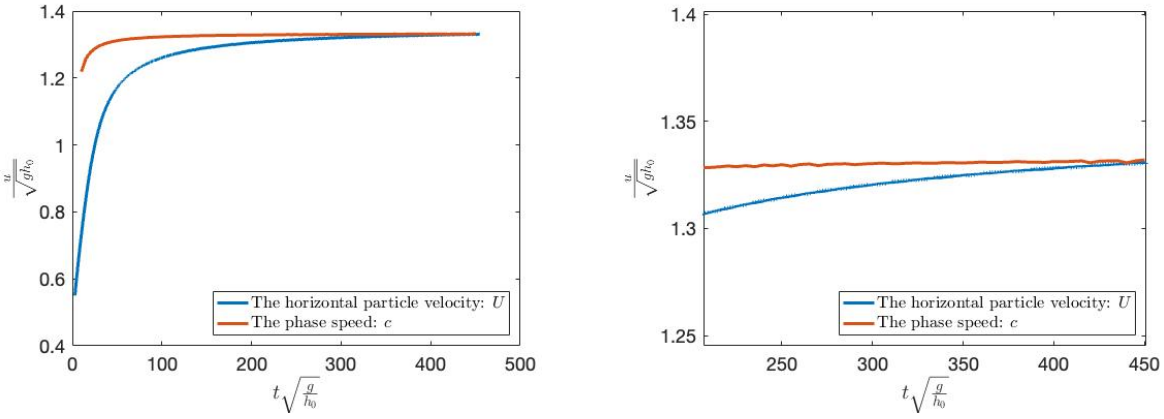

Figure 6.3: The horizontal particle velocity, coloured in blue, and the phase speed, coloured in red, with a bore strength of 0.359. The right panel is a closer view of the left panel.

velocity and the phase speed were used to provide a result possible to analyse. However, figure 6.4 depicts the two velocities with a bore strength of 0.358 without calculating the mean value of the horizontal particle velocity. The horizontal particle velocity was then represented by a thicker line, resulting in the horizontal velocity exceeding the phase speed. This show the challenge when evaluating if the wave breaks, indicating that this aspect must be considered when determining the threshold for wave breaking. Nevertheless, using the same definitions for breaking as for KdV and eKdV, the conclusion was that the wave breaks for bore strength of 0.359.

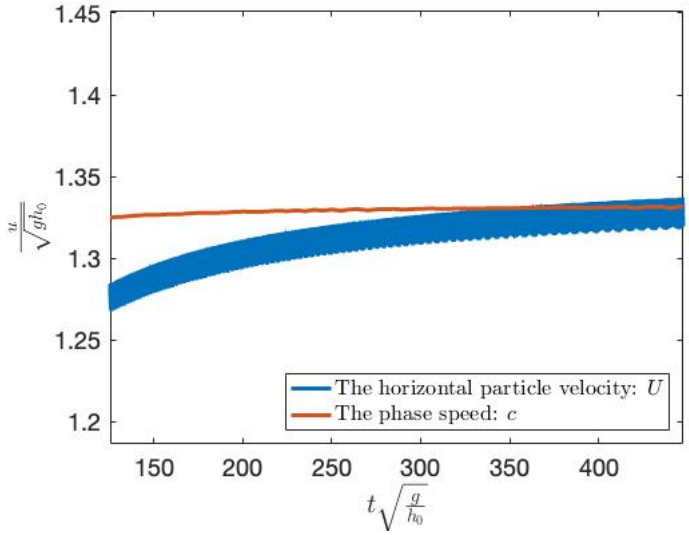

Figure 6.4: The horizontal particle velocity, coloured in blue, and the phase speed, coloured in red, with a bore strength of 0.358.

6.4 Discussion

The results show that the undular bore simulated by the eeKdV equation broke for a bore strength of 0.359. The result did not improve the approximation of wave breaking compared to the regular KdV equation, where breaking happened at 0.353. However, the wave breaking for the eeKdV equation occurred at a lower bore strength than the eKdV equation, which broke at 0.363. The conclusion so far was that the KdV equation was the most optimal approximation of undular bore breaking.

Even though the result of both eKdV and eeKdV were not quantitatively good, since the agreement with the experiment of Favre (1935) was lacking, using an equation with α^3 was closer to approximating Favre's experiment, then the equation including α^2. Consequently, utilising even higher-order equations may yield further improvements. On the other hand, when we compared the results to the KdV equation, it was hard to imagine that higher-order equations would improve it further.

Figure 6.5, on the next page, depicts an undular bore simulated by the KdV equation in 6.5a), the eKdV equation in 6.5b) and the eeKdV equation in 6.5c). The initial conditions of the undular bore were the same for all the simulations. The bore had an initial height of $a_0 = 0.3$, the wave's steepness was $k = 1$ and the bores were simulated until the final time $T = 450$. The height and position of the leading waves are presented in table 6.3 below.

Table 6.3: The height and the horizontal position of the leading wave for the numerical approximation of the KdV, the eKdV and the eeKdV equations at the final time T = 450.

Equation	Leading wave height	Leading wave position
KdV	0.5952	577.4
eKdV	0.5943	567.2
eeKdV	0.5949	569.0

Figure 6.6 show a plot where all the simulations of the undular bore are presented together, with the same initial conditions as before. It was evident that the undular bore simulated by the KdV equation propagated the fastest, followed by the wave simulated by the eeKdV equation and last the wave simulated by the eKdV equation. This show that the KdV equation had the highest phase speed and reached a larger height earlier, which was consistent with my result. Since the leading wave reached a higher amplitude faster, the wave would break earlier. On the other hand, a higher phase speed makes the conductive breaking criterion harder to achieve. But, the

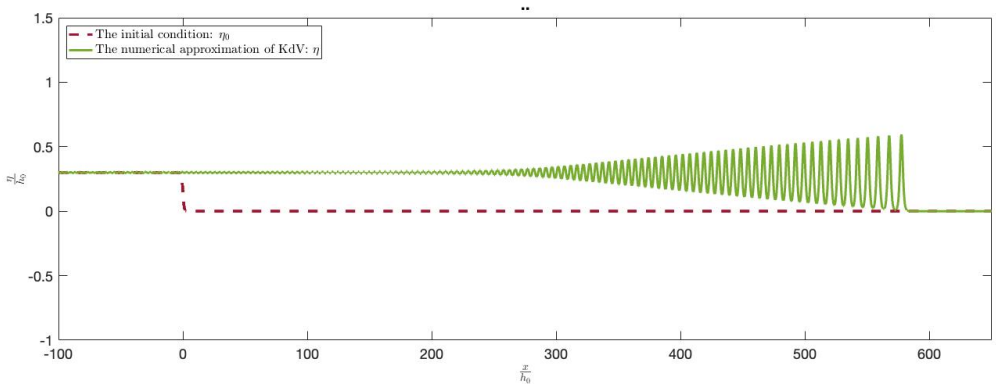

(a)

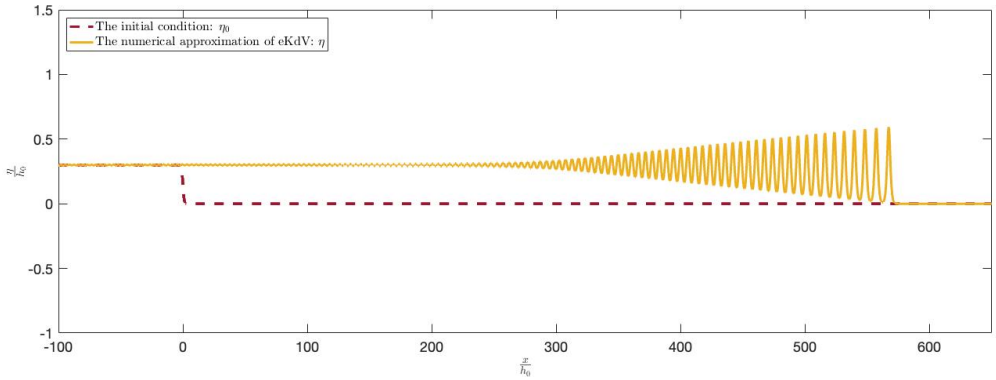

(b)

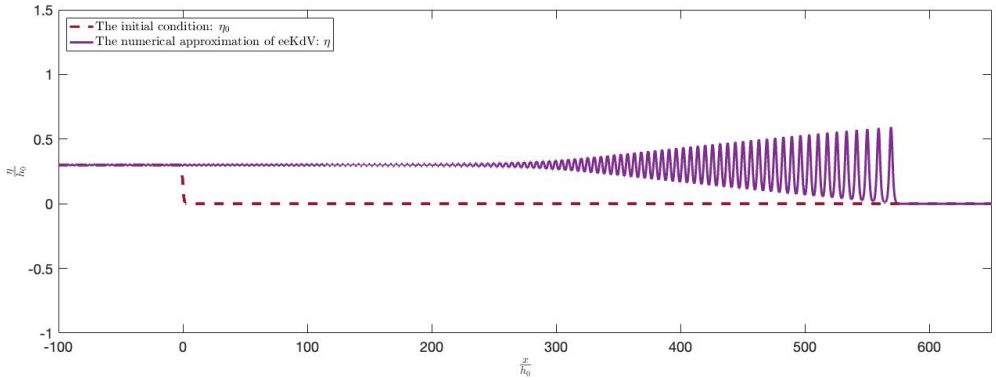

(c)

Figure 6.5: A simulation of the undular bore where all initial values were equal, and the bore propagated until it reached 600 depths. The bore was simulated by a) the KdV equation, b) the eKdV equation and c) the eeKdV equation.

results from chapter 4 prove that the horizontal particle velocity at the top of the front wave for the KdV equation was higher at lower bore strength than the horizontal particle velocity at the top of the front wave for the eKdV equation and the eeKdV equation. For the corresponding critical bore strength, figure 4.2 showed that the horizontal particle velocity with the KdV equation reached approximately $1.35\sqrt{\frac{h_0}{g}}$, while figure 5.4 showed that the horizontal particle velocity reached $1.33\sqrt{\frac{h_0}{g}}$ with the eKdV equation and figure 6.3 showed that the horizontal

particle velocity reached approximately $1.33\sqrt{\frac{h_0}{g}}$ with the eeKdV equation.

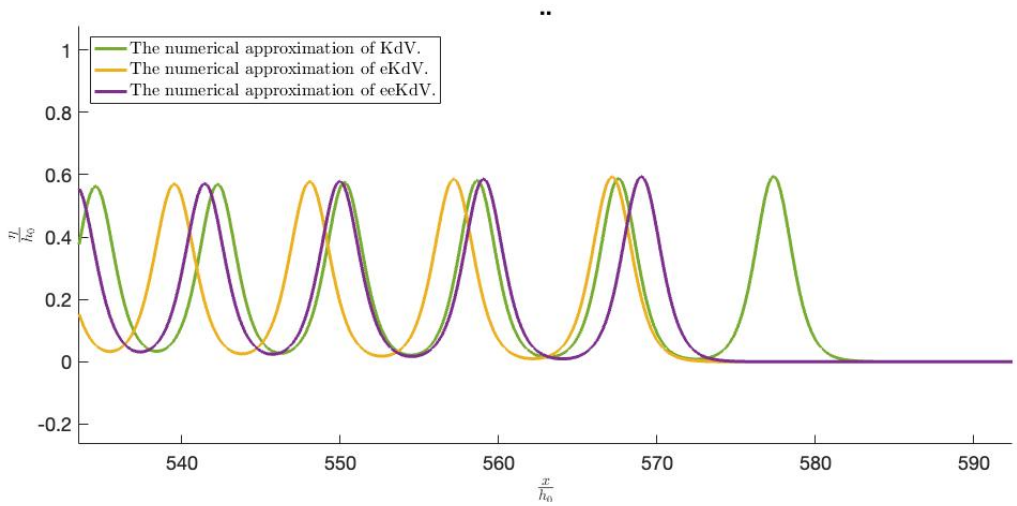

Figure 6.6: A closer view of an undular bore approximated by KdV, eKdV, and eeKdV. The green graph show the approximation of the KdV equation, the yellow by eKdV, and the purple by eeKdV. Here, $\delta t = 0.01$ and T = 450.

The same undular bores were simulated with temporal grid size $\delta t = 0.005$ when testing the stability of the implementation, shown in figure 6.7. The undular bore simulated by the KdV, the eKdV and the eeKdV equation had no difference in the horizontal position compared to figure 6.6 where $\delta t = 0.01$. Therefore, this strongly implied that the implementation was stable. Especially when we use higher-order non-linear equations, the phase errors associated with the numerical implementations can grow large when simulating waves over an extended period. However, the results indicated that this was not the case here.

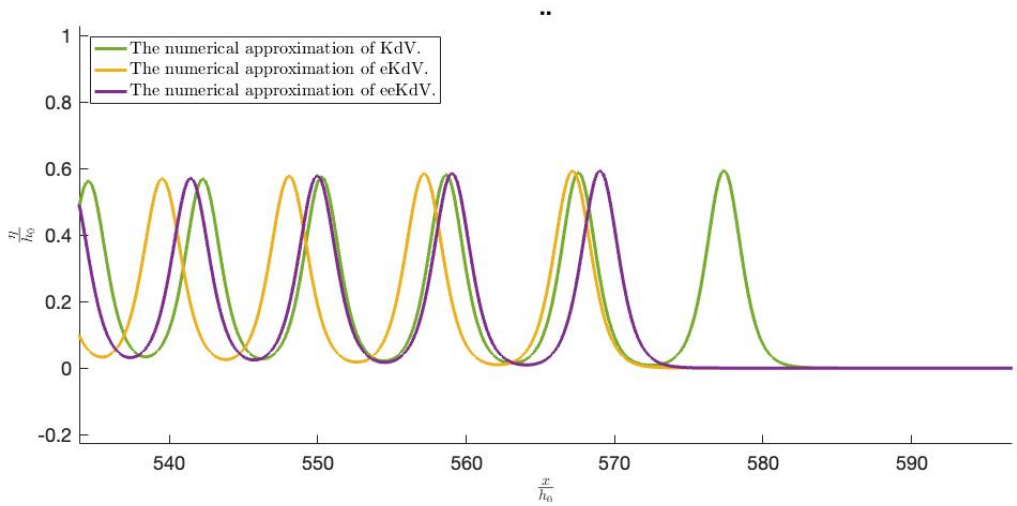

Figure 6.7: A closer view of an undular bore approximated by KdV, eKdV, and eeKdV. The green graph show the approximation of the KdV equation, the yellow by eKdV, and the purple by eeKdV. Here, $\delta t = 0.005$ and T = 450.

Favre (1935) discovered that the undular bore with the critical bore strength reached a height of 2.07 time the initial height above the undisturbed water depth. With the corresponding critical bore strength the KdV equation reached a height 1.981 times the initial height, the eKdV equation reached a height of 1.979 times the initial height and the eeKdV equation reached a height of 1.981 times the initial height. Notably, the KdV and eeKdV equations exhibited the same ratio at the breaking point, accurate to three decimal places. These results indicate that all the equations, ideally, should have the potential to reach higher heights before the leading wave breaks. However, the equations do not include all the physical considerations involved in the experiment of Favre (1935) and therefore the equations are not entirely ideal.

There can be many reasons for the lack of improved results; one might be that the equations considered here do not include damping. The energy across a bore was discussed in chapter 2. As mentioned, Rayleigh proposed that the energy was not conserved, and equation 2.26 show that energy was decreasing (Whitham, 1974). Thus, across a bore, there should have been a dissipation of energy, but the KdV equation does not consider this. Sturtevant (1965) discussed energy damping for a weak undular bore. The author explained that Benjamin and Lighthill proved that a steady train of undular cnoidal waves travelling into water with uniform flow was possible only if there was a change at the front in either mass, momentum, or energy. If not, the only viable solution was the solitary wave. The conclusion was that some turbulence must lead to dissipation at the front of the weak bore. Sturtevant (1965) then did an experiment demonstrating the damping in the boundary layer at the bottom of the channel. The author concluded that the energy flow was more significant behind the undular bore than in front of it. On the other hand, Ali and Kalisch (2010), who studied bores in shallow water, used a higher order dispersion equation and established that the energy loss was then accounted for; it vanished in the oscillations developing behind the bore front. Hence, it would be interesting to see if the result established so far could be improved by considering the energy loss for an undular bore by either considering a damping boundary layer or by including a higher-order dispersive term.

Another reason might be that the equations are based on the theory of an irrotational flow and omit vorticity. This was evaluated for the eKdV equation and is presented in the next chapter.

7 Wave breaking modelled by eKdV with background shear flow

Da Silva and Peregrine (1988) explains how shear can have a dominant effect on shallow water waves and that currents cause shear at the bottom of the sea for natural waves. Further, the authors argue that solutions of waves with constant shear flow for shallow water are a good representation because, for shallow water, the disturbance of the vorticity is less important than the non-zero mean vorticity. Considering the experiment of Favre (1935), when the water is pumped into the water tank, it is assumable to imagine that the forces from the water are stronger at the bottom than at the top since the water is pumped in at the bottom. A constant background shear is included in the eKdV equation to investigate wave breaking and if this improves the approximation of the experiments of Favre (1935). The following calculations are based on the theory of Senthilkumar and Kalisch (2019) and Yaosong et al. (1994).

7.1 Derivation of eKdV with constant background shear flow

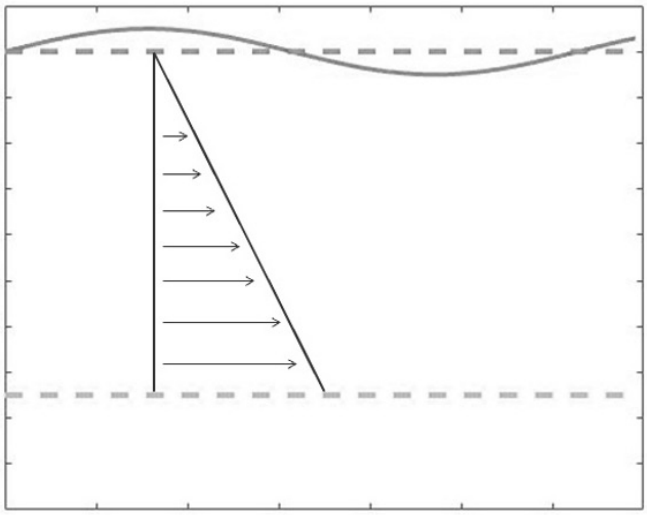

Figure 7.1: An illustration of the background shear flow $U = y\Gamma$. Here Γ is negative.

The background current is shown in Figure 7.1. It was a constant shear flow, such that the velocity components became

$$u = \varphi_x + \Gamma y,$$

$$v = \varphi_y.$$

Γ was the constant vorticity and at the bottom it was assumed that $u_0 = 0$ without loss of generality.

To derive the eKdV equation with included vorticity, the derivation started with the inviscid Navier Stokes equation where the dynamic assumption $p = p_0$ was already assumed:

$$\nabla\varphi_t + \nabla\frac{1}{2}|\bar{u}|^2 + g\bar{j} = \bar{u} \times \bar{\omega}$$

The argument was that since the left side was a gradient, the right side had to also be a gradient. Hence, a potential function G had to exist such that

$$\nabla G = \bar{u} \times \bar{\omega}.$$

To find the function G, it was convenient to use three dimensions. Hence, I used the vector (x_1, x_2, y), where x_1 represented the previous value of x, x_2 denoted the component orthogonal to the other variables and y represented the previous y. This gave the velocity vector $\bar{u} = (u_1, u_2, v) = (\phi_x + \Gamma y, 0, \phi_y)$. Deriving the cross product $\bar{\omega} = \nabla \times \bar{u}$, resulted in

$$\bar{\omega} = \begin{bmatrix} 0 & \Gamma & 0 \end{bmatrix}.$$

Then,

$$\bar{u} \times \bar{\omega} = \begin{bmatrix} -\Gamma v & 0 & \Gamma u_1 \end{bmatrix} = \begin{bmatrix} -\Gamma\varphi_y & 0 & \Gamma\varphi_x + \Gamma^2 y \end{bmatrix}.$$

Since the component in the x_2 direction was equal to zero, we could go back to the original two dimensions, i.e.

$$\nabla G = \bar{u} \times \bar{\omega} = \begin{bmatrix} -\Gamma\varphi_y & \Gamma\varphi_x + \Gamma^2 y \end{bmatrix}.$$

The equation

$$G = \Gamma \int_{-h_0}^{y} \varphi_x dy + \frac{\Gamma^2}{2} y^2$$

will satisfy ∇G and this was proved by finding the elements in $\nabla G = (G_x, G_y)$. The first element was

$$G_x = \Gamma \int_{-h_0}^{y} \varphi_{xx} dy,$$

and using the Laplace equation 2.7, it became

$$G_x = -\Gamma \int_{-h_0}^{y} \varphi_{yy} dy = -\Gamma\varphi_y.$$

The second element in the gradient was

$$G_y = \Gamma\varphi_x + \Gamma^2 y.$$

The fundamental theorem of calculus was used to solve the integral of both equations. As we can see, the derivative components of G are equal to the components in ∇G. Hence, the Navier-Stokes equation could be written as a gradient, i.e.

$$\nabla\left(\varphi_t + \frac{1}{2}|\bar{u}|^2 + gy - G\right) = 0 \tag{7.1}$$

The non-dimensionalization 2.32 was utilised to derive the problem for shallow water waves with a shear flow and the corresponding boundary conditions. From chapter 2 it was shown that the Laplace equation had to be satisfied for water waves and the non-dimensional form yielded

$$\beta\tilde{\varphi}_{\tilde{x}\tilde{x}} + \tilde{\varphi}_{\tilde{y}\tilde{y}} = 0, \qquad -1 < \tilde{y} < \alpha\tilde{\eta}.$$

The boundary condition at the bottom was a no through flow condition, such that the non-dimensional boundary condition was

$$\tilde{\varphi}_{\tilde{y}} = 0, \qquad \tilde{y} = -1.$$

At the top of the wave, the kinematic boundary conditions for the free surface had to be derived. From chapter 2, this was found to be

$$\eta_t + u\eta_x = \varphi_x, \qquad y = \eta.$$

The velocity components was substituted into the equation, resulting in,

$$\eta_t + (\varphi_x + \Gamma y)\,\eta_x = \varphi_x.$$

Using the non-dimensionalization 2.32, the non-dimensional kinematic condition at the free surface became,

$$\tilde{\eta}_{\tilde{t}} + \left(\alpha\tilde{\varphi}_{\tilde{x}} + \alpha\tilde{\Gamma}\tilde{\eta}\right)\tilde{\eta}_{\tilde{x}} = \frac{1}{\beta}\tilde{\varphi}_{\tilde{y}}, \qquad \tilde{y} = \alpha\tilde{\eta}.$$

As mentioned, the dynamic boundary condition at the free surface comes from the pressure in the air and water to be equal, such that $p = p_0$, which was already included earlier in the derivation. Hence, integrating over 7.1 and assume an infinitesimal fluid parcel, the Navier-

Stokes equation became

$$\varphi_t + \frac{1}{2}u^2 + \frac{1}{2}v^2 + gy - G = 0.$$

Substituting the horizontal particle velocity into the equation gave

$$\varphi_t + \frac{1}{2}(\varphi_x + \Gamma y)^2 + \frac{1}{2}v^2 + gy - G = 0.$$

Scaling the variables, such that they are dimensionless, resulted in the dynamical boundary condition in non-dimensional form,

$$\tilde{\varphi}_{\tilde{t}} + \tilde{\eta} + \frac{1}{2}\alpha\left(\tilde{\varphi}_{\tilde{x}} + \frac{1}{\alpha}\tilde{\Gamma}(\alpha\eta)\right) + \frac{\alpha}{2\beta}(\tilde{\varphi}_{\tilde{y}})^2 - \frac{\tilde{G}}{ag} = 0, \qquad \tilde{y} = \alpha\tilde{\eta}.$$

Due to the shallow water, the vertical components could be separated from the horizontal components, and the velocity potential was expanded in an asymptotic series. Hence, it was assumed a solution on the form

$$\tilde{\varphi} = \sum_{n=0}^{\infty}(1+\tilde{y})^n \tilde{f}(x,t)_n.$$

The derivation was the same as was shown for equation 2.31 in section 2.4. With the use of the Laplace equation and the boundary condition at the bottom $\phi_x = 0$ for y=0 the odd terms of $\tilde{f}$ vanished, and the first terms in the asymptotic expansion were

$$\tilde{\varphi} = \tilde{f} - \frac{\beta}{2}(1+\tilde{y})^2 \tilde{f}_{\tilde{x}\tilde{x}} + \frac{\beta^2}{24}(1+\tilde{y})^4 \tilde{f}_{\tilde{x}\tilde{x}\tilde{x}\tilde{x}} + O\left(B^3\right) \tag{7.2}$$

The non-dimensional equation for G were found to be

$$\tilde{G} = ag\tilde{\Gamma}\int_{-1}^{\alpha\tilde{\eta}} \tilde{\varphi}_{\tilde{x}} d\tilde{y} + gh_0\frac{\tilde{\Gamma}^2}{2}\tilde{y}.$$

Inserting the asymptotic expansion of $\tilde{\varphi}$ gave the integral

$$\int_{-1}^{\alpha\tilde{\eta}} \tilde{\varphi}_{\tilde{x}} d\tilde{y} = (1+\alpha\tilde{\eta})\tilde{f} - \frac{\beta}{6}(1+\alpha\tilde{\eta})^3 \tilde{f}_{\tilde{x}\tilde{x}} + \frac{\beta^2}{120}(1+\alpha\tilde{\eta})^5 \tilde{f}_{\tilde{x}\tilde{x}\tilde{x}\tilde{x}} + O\left(\beta^3\right),$$

such that

$$\tilde{G} = ag\tilde{\Gamma}\left((1+\alpha\tilde{\eta})\tilde{f}_x - \frac{\beta}{6}(1+\alpha\tilde{\eta})^3 \tilde{f}_{\tilde{x}\tilde{x}\tilde{x}} + \frac{\beta^2}{120}(1+\alpha\tilde{\eta})^5 \tilde{f}_{\tilde{x}\tilde{x}\tilde{x}\tilde{x}\tilde{x}}\right) + gh_0\frac{\tilde{\Gamma}^2}{2}\tilde{y} + O\left(\beta^3\right).$$

The equation for $\tilde{G}$ was used in the dynamic boundary condition, where the expression was divided by ag, therefore this was considered at this point. Also, the evaluation at the top of the

wave was considered, such that $\tilde{y} = \alpha\tilde{\eta}$. The first terms in the series were then

$$\frac{\tilde{G}}{ag} = \tilde{\Gamma}(1+\alpha\tilde{\eta})\tilde{f}_{\tilde{x}} - \beta\frac{\tilde{\Gamma}(1+\alpha\tilde{\eta})^3}{6}\tilde{f}_{\tilde{x}\tilde{x}\tilde{x}} + \beta^2\frac{\tilde{\Gamma}(1+\alpha\tilde{\eta})^5}{120}\tilde{f}_{\tilde{x}\tilde{x}\tilde{x}\tilde{x}\tilde{x}} + \alpha\frac{\tilde{\Gamma}^2}{2}\tilde{\eta}^2 + O\left(\beta^3\right).$$

The asymptotic expansion for the velocity potential was substituted into the kinematic boundary condition at surface, yielding

$$\tilde{\eta}_{\tilde{t}} + \left(\alpha\left(\tilde{f} - \beta\frac{(1+\tilde{y})^2}{2}\tilde{f}_{\tilde{x}\tilde{x}} + \cdots\right)_{\tilde{x}} + \alpha\tilde{\Gamma}\tilde{\eta}\right)\tilde{\eta}_{\tilde{x}} =$$
$$\frac{1}{\beta}\left(\tilde{f} - \beta\frac{(1+\tilde{y})^2}{2}\tilde{f}_{\tilde{x}\tilde{x}} + \beta^2\frac{(1+\tilde{y})^4}{24}\tilde{f}_{\tilde{x}\tilde{x}\tilde{x}\tilde{x}}\cdots\right)_{\tilde{y}} + O\left(\alpha^3, \alpha\beta, \beta^2\right), \qquad \tilde{y} = \alpha\tilde{\eta}.$$

Using that $\tilde{w} = \tilde{f}_{\tilde{x}}$ and assuming that $O\left(\alpha^3, \alpha\beta, \beta^2\right)$ terms were equal to zero, the kinematic boundary condition became

$$\tilde{\eta}_{\tilde{t}} + \tilde{w}_{\tilde{x}} + \alpha\tilde{\Gamma}\tilde{\eta}\,\tilde{\eta}_{\tilde{x}} + \alpha\left(\tilde{w}\tilde{\eta}\right)_{\tilde{x}} - \frac{\beta}{6}\tilde{w}_{\tilde{x}\tilde{x}\tilde{x}} = 0, \qquad \tilde{y} = \alpha\tilde{\eta}.$$

The dynamic boundary condition was found by inserting the asymptotic expansion for the velocity potential and the equation of G into the non-dimensional dynamical boundary condition.

$$\left(\tilde{f} - \beta\frac{(1+\alpha\tilde{\eta})^2}{2}\tilde{f}_{\tilde{x}\tilde{x}}\right)_{\tilde{t}} + \tilde{\eta} + \frac{\alpha}{2}\left(\tilde{f}_{\tilde{x}} - \beta\frac{(1+\alpha\tilde{\eta})^2}{2}\tilde{f}_{\tilde{x}\tilde{x}\tilde{x}} + \frac{1}{\alpha}\tilde{\Gamma}(\alpha\tilde{\eta})\right)^2 + \frac{\alpha}{2\beta}\left(-\beta\left(1+\alpha\tilde{\eta}\right)\tilde{f}_{\tilde{x}\tilde{x}}\right)^2$$
$$-\left(\tilde{\Gamma}(1+\alpha\tilde{\eta})\tilde{f}_{\tilde{x}} - \beta\frac{\tilde{\Gamma}(1+\alpha\tilde{\eta})^3}{6}\tilde{f}_{\tilde{x}\tilde{x}\tilde{x}} + \beta^2\frac{\tilde{\Gamma}(1+\alpha\tilde{\eta})^5}{120}\tilde{f}_{\tilde{x}\tilde{x}\tilde{x}\tilde{x}\tilde{x}} + \alpha\frac{\tilde{\Gamma}^2}{2}\tilde{\eta}^2\right) = 0.$$

Assuming that $O\left(\alpha^3, \alpha\beta, \beta^2\right)$ was zero, and differentiate the equation with respect to x, resulted in the dynamical boundary condition at the top of the wave

$$\tilde{w}_{\tilde{t}} + \tilde{\eta}_{\tilde{x}} + \alpha\tilde{w}\tilde{w}_{\tilde{x}} - \tilde{\Gamma}\tilde{w}_{\tilde{x}} - \frac{\beta}{2}\tilde{w}_{\tilde{x}\tilde{x}\tilde{t}} + \frac{\beta}{6}\tilde{\Gamma}\tilde{w}_{\tilde{x}\tilde{x}\tilde{x}} = 0, \qquad \tilde{y} = \alpha\tilde{\eta}.$$

Hence, to sum up, the Boussinesq system with constant background vorticity was derived and it was found to be

$$\begin{aligned}\tilde{\eta}_{\tilde{t}} + \tilde{w}_{\tilde{x}} + \alpha\tilde{\Gamma}\tilde{\eta}\,\tilde{\eta}_{\tilde{x}} + \alpha\left(\tilde{w}\tilde{\eta}\right)_{\tilde{x}} - \frac{\beta}{6}\tilde{w}_{\tilde{x}\tilde{x}\tilde{x}} = 0,\\ \tilde{w}_{\tilde{t}} + \tilde{\eta}_{\tilde{x}} + \alpha\tilde{w}\tilde{w}_{\tilde{x}} - \tilde{\Gamma}\tilde{w}_{\tilde{x}} - \frac{\beta}{2}\tilde{w}_{\tilde{x}\tilde{x}\tilde{t}} + \frac{\beta}{6}\tilde{\Gamma}\tilde{w}_{\tilde{x}\tilde{x}\tilde{x}} = 0.\end{aligned} \tag{7.3}$$

By neglecting the orders of $O(\alpha,\beta)$ the Boussinesq equations became

$$\tilde{\eta}_{\tilde{t}} + \tilde{w}_{\tilde{x}} = 0,$$
$$\tilde{w}_{\tilde{t}} + \tilde{\eta}_{\tilde{x}} - \tilde{\Gamma}\tilde{w}_{\tilde{x}} = 0.$$

This can be written as the system

$$\begin{bmatrix} \tilde{\eta} \\ \tilde{w} \end{bmatrix}_{\tilde{t}} + \begin{bmatrix} 0 & 1 \\ 1 & -\tilde{\Gamma} \end{bmatrix} \begin{bmatrix} \tilde{\eta} \\ \tilde{w} \end{bmatrix}_{\tilde{x}} = \begin{bmatrix} 0 \\ 0 \end{bmatrix}. \tag{7.4}$$

I used the diagonalisation method, as it was utilised in section 2.5, to find the solution of the system. The eigenvalues of the system were calculated by the use of the characteristic equation, $\det(A-\lambda I)=0$, where λ were the eigenvalues.

$$\det(A-\lambda I) = \det\left(\begin{bmatrix} -\lambda & 1 \\ 1 & -\lambda-\tilde{\Gamma} \end{bmatrix}\right) = \lambda^2 + \Gamma\lambda - 1 = 0.$$

Hence, the eigenvalues were $\lambda_1 = \frac{\tilde{\Gamma}}{2} + \sqrt{\frac{\tilde{\Gamma}^2}{4}+1}$ and $\lambda_2 = \frac{\tilde{\Gamma}}{2} - \sqrt{\frac{\tilde{\Gamma}^2}{4}+1}$. The eigenvalues are the characteristics of the system, therefore we denoted $\tilde{c}_+$ the positive eigenvalue and $\tilde{c}_-$ the negative one. Using $A\bar{v} = \lambda\bar{v}$, the corresponding eigenvectors $\bar{v}$ were following

$$\bar{v}_1 = \begin{bmatrix} 1 \\ \tilde{c}_+ \end{bmatrix} \text{ and } \bar{v}_2 = \begin{bmatrix} \tilde{c}_+ \\ -1 \end{bmatrix}.$$

This was found by using that $\tilde{c}_+^2 + \tilde{c}_+\tilde{\Gamma} = 1$ and $\tilde{c}_+ + \tilde{c}_- + \tilde{\Gamma} = 0$. The diagonalised system yielded

$$A = \frac{1}{1+\tilde{c}_+} \begin{bmatrix} 1 & \tilde{c}_+^2 \\ \tilde{c}_+ & -1 \end{bmatrix} \begin{bmatrix} \tilde{c}_+^2 & 0 \\ 0 & \tilde{c}_+ \end{bmatrix} \begin{bmatrix} 1 & \tilde{c}_+ \\ \tilde{c}_+ & -1 \end{bmatrix}.$$

The variables r and s were then introduced, such that $(r,s) = P^{-1}(r,s)$. Where

$$P^{-1} = \frac{1}{1+\tilde{c}_+^2} \begin{bmatrix} 1 & \tilde{c}_+ \\ \tilde{c}_+ & -1 \end{bmatrix}.$$

r and s were substituted into system 7.4, which yielded the result

$$\begin{bmatrix} r_t \\ s_t \end{bmatrix} + \begin{bmatrix} \tilde{c}_+ & 0 \\ 0 & \tilde{c}_- \end{bmatrix} \begin{bmatrix} r_x \\ s_x \end{bmatrix} = \begin{bmatrix} 0 \\ 0 \end{bmatrix},$$

and this had the solution

$$r = r_0(x - \tilde{c}_+ t)$$
$$s = s_0(x - \tilde{c}_- t).$$

Since $r = \frac{1}{1+\tilde{c}^2_+}(\tilde{\eta} + \tilde{c}_+ \tilde{w})$ and $s = \frac{1}{1+\tilde{c}^2_-}(\tilde{c}_+ \tilde{\eta} - \tilde{w})$, the constants were found and the results were

$$r = \frac{1}{1+\tilde{c}^2_+}\left[\tilde{\eta}_0(x - \tilde{c}_+ t) + \tilde{c}_+ \tilde{w}_0(x - \tilde{c}_+ t)\right],$$
$$s = \frac{1}{1+\tilde{c}^2_+}\left[\tilde{c}_+ \tilde{\eta}_0(x - \tilde{c}_- t) - \tilde{w}_0(x - \tilde{c}_- t)\right].$$

Since $(r,s) = P^{(-1)}(\tilde{\eta}, \tilde{w})$, multiplying both sides with the matrix P gives the solution, of η and $\tilde{w}$, which was

$$\tilde{\eta} = \frac{1}{1+\tilde{c}^2_+}\left[\tilde{\eta}_0(x - \tilde{c}_+ t) + \tilde{c}_+ \tilde{w}_0(x - \tilde{c}_+ t) + \tilde{c}^2_+ \tilde{\eta}_0(x - \tilde{c}_- t) - \tilde{c}_+ \tilde{w}_0(x - \tilde{c}_- t)\right],$$
$$\tilde{w} = \frac{1}{1+\tilde{c}^2_+}\left[\tilde{c}_+ \tilde{\eta}_0(x - \tilde{c}_+ t) + \tilde{c}^2_+ \tilde{w}_0(x - \tilde{c}_+ t) - \tilde{c}_+ \tilde{\eta}_0(x - \tilde{c}_- t) + \tilde{w}_0(x - \tilde{c}_- t)\right].$$

The unidirectional eKdV equation was derived from the Boussinesq system by considering a wave moving to the right. Then $\tilde{w} = \tilde{c}_+ \tilde{\eta}$ and from this I sought a solution of the form

$$\tilde{w} = \tilde{c}_+ \tilde{\eta} + \alpha A + \beta B + \alpha^2 D + O\left(\alpha^3, \alpha\beta, \beta^2\right).$$

To not confuse the coefficient corresponding to α^2 with the characteristic value $\tilde{c}_+$, the coefficient was denoted D (in stead of C). With the assumption that $O\left(\alpha^3, \alpha\beta, \beta^2\right)$ were equal to zero, the equation was substituted into the boundary conditions 7.3. Ordering the terms by α, β

and α^2 yielded

$$\begin{aligned}
&\tilde{\eta}_{\tilde{t}}+\tilde{c}_+\tilde{\eta}_{\tilde{x}}+\alpha\left(A_{\tilde{x}}+\tilde{\Gamma}\tilde{\eta}\,\tilde{\eta}_{\tilde{x}}+2\tilde{c}_+\tilde{\eta}\,\tilde{\eta}_{\tilde{x}}\right)+\beta\left(B_{\tilde{x}}-\frac{1}{6}\tilde{c}_+\tilde{\eta}_{\tilde{x}\tilde{x}\tilde{x}}\right)\\
&\qquad+\alpha^2\left(D_{\tilde{x}}+(A\tilde{\eta})_{\tilde{x}}\right)=0,\\
&\tilde{c}_+\tilde{\eta}_{\tilde{t}}+\tilde{\eta}_{\tilde{x}}-\tilde{\Gamma}\tilde{c}_+\tilde{\eta}_{\tilde{x}}+\alpha\left(A_{\tilde{t}}+\tilde{c}_+^2\tilde{\eta}\,\tilde{\eta}_{\tilde{x}}-\tilde{\Gamma}A_{\tilde{x}}\right)+\beta\left(B_{\tilde{t}}-\tilde{\Gamma}B_{\tilde{x}}-\frac{1}{2}\tilde{c}_+\tilde{\eta}_{\tilde{x}\tilde{x}\tilde{t}}+\frac{1}{6}\tilde{\Gamma}\tilde{c}_+\tilde{\eta}_{\tilde{x}\tilde{x}\tilde{x}}\right)\\
&\qquad+\alpha^2\left(D_{\tilde{t}}+\tilde{c}_+(A\tilde{\eta})_{\tilde{x}}-\tilde{\Gamma}D_{\tilde{x}}\right)=0.
\end{aligned}$$

The first equation was multiplied by $\tilde{c}_+$ and in the second equation the terms $\tilde{\eta}_{\tilde{x}}-\tilde{\Gamma}\tilde{c}_+\tilde{\eta}_{\tilde{x}}=\tilde{c}_+^2\tilde{\eta}_{\tilde{x}}$, such that

$$\begin{aligned}
&\tilde{c}_+\tilde{\eta}_{\tilde{t}}+\tilde{c}_+^2\tilde{\eta}_{\tilde{x}}+\alpha\left(\tilde{c}_+A_{\tilde{x}}+\tilde{c}_+\tilde{\Gamma}\tilde{\eta}\,\tilde{\eta}_{\tilde{x}}+2\tilde{c}_+^2\tilde{\eta}\,\tilde{\eta}_{\tilde{x}}\right)+\beta\left(\tilde{c}_+B_{\tilde{x}}-\frac{1}{6}\tilde{c}_+^2\tilde{\eta}_{\tilde{x}\tilde{x}\tilde{x}}\right)\\
&\qquad+\alpha^2\left(\tilde{c}_+D_{\tilde{x}}+\tilde{c}_+(A\tilde{\eta})_{\tilde{x}}\right)=0,\\
&\tilde{c}_+\tilde{\eta}_{\tilde{t}}+\tilde{c}_+^2\tilde{\eta}_{\tilde{x}}+\alpha\left(A_{\tilde{t}}+\tilde{c}_+^2\tilde{\eta}\,\tilde{\eta}_{\tilde{x}}-\tilde{\Gamma}A_{\tilde{x}}\right)+\beta\left(B_{\tilde{t}}-\tilde{\Gamma}B_{\tilde{x}}-\frac{1}{2}\tilde{c}_+\tilde{\eta}_{\tilde{x}\tilde{x}\tilde{t}}+\frac{1}{6}\tilde{\Gamma}\tilde{c}_+\tilde{\eta}_{\tilde{x}\tilde{x}\tilde{x}}\right)\\
&\qquad+\alpha^2\left(D_{\tilde{t}}+\tilde{c}_+(A\tilde{\eta})_{\tilde{x}}-\tilde{\Gamma}D_{\tilde{x}}\right)=0.
\end{aligned}\tag{7.5}$$

By setting the equations equal to each other the coefficients A and B were found by using $\tilde{\eta}_t=-\tilde{c}_+\tilde{\eta}_{\tilde{x}}$, i.e.

$$A=\frac{-1}{2\left(2\tilde{c}_++\tilde{\Gamma}\right)}\tilde{\eta}^2 \qquad \text{and} \qquad B=\frac{1+3\tilde{c}_+^2}{3\left(2\tilde{c}_++\tilde{\Gamma}\right)}\tilde{\eta}_{\tilde{x}\tilde{x}}.$$

Inserting the values for A and B back into one of the equations in 7.5, and ignoring the terms with α^2, resulted in the KdV equation with background shear flow

$$\tilde{\eta}_++\tilde{c}_+^2\tilde{\eta}_{\tilde{x}}+\alpha\frac{\tilde{c}_+\left(3+\tilde{\Gamma}^2\right)}{\left(1+\tilde{c}_+^2\right)}\tilde{\eta}\,\tilde{\eta}_{\tilde{x}}+\beta\frac{\tilde{c}_+^3}{6\left(1+\tilde{c}_+^2\right)}\tilde{\eta}_{\tilde{x}\tilde{x}\tilde{x}}=0.$$

To derive the coefficient D, the coefficient A and B were inserted back into the 7.5 and the three first terms in the KdV equation with background shear was used as the derivation relation

$$\tilde{\eta}_+=-\tilde{c}_+^2\tilde{\eta}_{\tilde{x}}-\alpha\frac{\tilde{c}_+\left(3+\tilde{\Gamma}^2\right)}{\left(1+\tilde{c}_+^2\right)}\tilde{\eta}\,\tilde{\eta}_{\tilde{x}},$$

resulting in

$$D=\frac{\tilde{c}_+\left(3+\tilde{\Gamma}^2\right)}{3\left(2\tilde{c}_++\tilde{\Gamma}\right)^2\left(\tilde{c}_+^2+1\right)}\tilde{\eta}^3.$$

The equation for $\tilde{w}$ was then

$$\tilde{w} = \tilde{c}_+\tilde{\eta} + \alpha\frac{-1}{2\left(2\tilde{c}_+ + \tilde{\Gamma}\right)} + \beta\frac{1+3\tilde{c}_+^2}{6\left(2\tilde{c}_+ + \tilde{\Gamma}\right)} + \alpha^2\frac{\tilde{c}_+\left(3+\tilde{\Gamma}^2\right)}{3\left(2\tilde{c}_+ + \tilde{\Gamma}\right)^2\left(\tilde{c}_+^2+1\right)}\tilde{\eta}^3. \tag{7.6}$$

Substituting all the coefficients back into one of the equations in 7.5 gave the non-dimensionalized eKdV equation with constant vorticity,

$$\tilde{\eta}_{\tilde{t}} + \tilde{c}\tilde{\eta}_{\tilde{x}} + \alpha\left(\frac{\tilde{c}_+\left(3+\tilde{\Gamma}^2\right)}{1+\tilde{c}_+^2}\right)\tilde{\eta}\,\tilde{\eta}_{\tilde{x}} + \beta\left(\frac{\tilde{c}_+^3}{3\left(1+\tilde{c}_+^2\right)}\right)\tilde{\eta}_{\tilde{x}\tilde{x}\tilde{x}} + \alpha^2\left(\frac{2\tilde{\Gamma}^2\tilde{c}_+ - 6\tilde{c}_+^3 - 3\tilde{\Gamma}\tilde{c}_+^2 - 3\tilde{\Gamma}}{2\left(2\tilde{c}_+ + \tilde{\Gamma}\right)^2\left(c_+^2+1\right)}\right)\tilde{\eta}^2\tilde{\eta}_{\tilde{x}} = 0$$

The dimensional variables were substituted back with 2.32 and scaled by 2.47 to have h_0 as the spatial unit and $\frac{h_0}{g}$ as a unit of time. Hence, the eKdV equation with constant vorticity was found to be

$$\eta_t + c_+\eta_x + \left(\frac{c_+\left(3+\Gamma^2\right)}{c_+^2+1}\right)\eta\,\eta_x + \left(\frac{c_+^3}{3\left(c_+^3+1\right)}\right)\eta_{xxx} + \left(\frac{2\Gamma^2c_+ - 6c_+^3 - 3\Gamma c_+^2 - 3\Gamma}{2\left(2c_+ + \Gamma\right)^2\left(c_+^2+1\right)}\right)\eta^2\eta_x = 0, \tag{7.7}$$

with the corresponding equation for w,

$$w = c_+\eta + \frac{-1}{2\left(2c_+ + \Gamma\right)}\eta^2 + \frac{1+3c_+^2}{6\left(2c_+ + \Gamma\right)}\eta_{xx} + \frac{c_+\left(3+\Gamma^2\right)}{3\left(2c++\Gamma\right)^2\left(c_+^2+1\right)}\eta^3. \tag{7.8}$$

7.2 The maximum height of the solitary wave

The procedure to determine the solitary wave solution of the eKdV equation outlined in section 5.2 was utilised to find the solitary wave solution of the eKdV equation with constant background shear flow. It is presented here. Stated byKalisch and Nguyen (2010), the solitary wave solution of the non-dimensional eKdV equation

$$\tilde{\eta}_t + \tilde{\eta}\,\tilde{\eta}_x + \sigma\tilde{\eta}^2\tilde{\eta}_x + \tilde{\eta}_{xxx} = 0, \tag{7.9}$$

is on the form

$$\tilde{\eta}\left(x-ct\right) = \Phi\left(\xi\right) = \frac{A}{b+(1-b)\cosh^2\left(K\xi\right)}, \tag{7.10}$$

where

$$A = \frac{-1 \pm \sqrt{1+6c\sigma}}{\sigma}, \qquad K = \frac{\sqrt{c}}{2} \qquad \text{and} \qquad b = -\frac{\sigma A^2}{6c}. \tag{7.11}$$

Hence, all the variables depend on the phase speed c, which had to be given as an initial value of the wave. Setting 7.10 into 7.9 yielded

$$-c\Phi' + \Phi\Phi' + \sigma\Phi^2\Phi' + \Phi''' = 0, \tag{7.12}$$

where $\Phi' = \frac{\partial \Phi}{\partial \xi}$. It was assumed that the solution was of the form $\eta = \lambda\Phi(\mu x - \nu t)$, where Φ was the solitary solution 7.10. The variables λ, μ, and ν were determined by inserting the assumed solution into the eKdV equation with constant background vorticity, equation 7.7, and scaling the solution such that it satisfied 7.12. Hence, the following system of equations had to be solved

$$\begin{aligned}
\lambda\left(-\nu + c_+\mu\right) &= -c, \\
\lambda^2\mu\left(\frac{c_+\left(3+\Gamma^2\right)}{c_+^2+1}\right) &= 1, \\
\lambda\mu^3\left(\frac{c_+^3}{3\left(c_+^3+1\right)}\right) &= 1
\end{aligned}$$

and

$$\lambda^3\mu\left(\frac{2\Gamma^2 c_+ - 6c_+^3 - 3\Gamma c_+^2 - 3\Gamma}{2\left(2c_+ + \Gamma\right)^2\left(c_+^2+1\right)}\right) = \sigma.$$

The variables b and K could be made solely dependent on the amplitude by first express c in terms of the amplitude. This was done by use of the expression for A in 7.11, i.e.

$$c = \frac{1}{6}\sigma A^2 + \frac{1}{3}A.$$

Following, the values of b and K became

$$b = -\frac{\sigma}{A\sigma + 2}A \qquad \text{and} \qquad K = \frac{\sqrt{\frac{1}{6}\sigma A^2 + \frac{1}{3}A}}{2}.$$

Solving the system of equation and inserting the equations for b, K and c into the solution, the solitary wave solution of the eKdV equation with constant background vorticity was

$$\eta(x,t) = \frac{\lambda A}{-\frac{\sigma}{\sigma A+2}A + \left(1-\frac{\sigma}{\sigma A+2}A\right)\cosh^2\left[\frac{\sqrt{\frac{\sigma}{6}A^2+\frac{1}{3}A}}{2}(\mu x+\nu t)\right]} \tag{7.13}$$

where

$$\mu = \frac{9^{\frac{1}{5}}\left(3+\Gamma^2\right)^{\frac{1}{5}}\left(c_+^2+1\right)^{\frac{1}{5}}}{c_+}, \tag{7.14}$$

$$\lambda = \frac{\left(c_+^2+1\right)^{\frac{2}{5}}}{3^{\frac{1}{5}}\left(3+\Gamma^2\right)^{\frac{3}{5}}}, \tag{7.15}$$

$$\nu = \frac{3^{\frac{1}{5}}\left(3+\Gamma^2\right)^{\frac{3}{5}}}{\left(c_+^2+1\right)^{\frac{2}{5}}}\left(\frac{1}{6}\sigma A+\frac{1}{3}A\right)+9^{\frac{1}{5}}\left(3+\Gamma^2\right)^{\frac{1}{5}}\left(c_+^2+1\right)^{\frac{1}{5}}, \tag{7.16}$$

and

$$\sigma = \frac{\left(2\Gamma^2 c_+ - 6c_+^3 - 3\Gamma c_+^2 - 3\Gamma\right)\left(c_+^2+1\right)^{\frac{2}{5}}}{2\times 3^{\frac{1}{5}}c_+\left(2c_++\Gamma^2\right)\left(3+\Gamma\right)^{\frac{8}{5}}}. \tag{7.17}$$

Having determined the solitary wave solution for the eKdV equation with vorticity, it could be used to derive the corresponding breaking criterion. This involved deriving the non-dimensional velocity potential φ by substituting equation 7.6 into equation 7.2 and then differentiating the non-dimensional velocity potential with respect to x, yielded

$$\tilde{\varphi}_{\tilde{x}} = \tilde{c}_+\tilde{\eta} + \alpha\frac{-1}{2\left(2\tilde{c}_++\tilde{\Gamma}\right)}\tilde{\eta}^2 + \alpha^2\frac{\tilde{c}_+\left(3+\tilde{\Gamma}^2\right)}{3\left(2\tilde{c}_++\tilde{\Gamma}\right)^2\left(\tilde{c}_+^2+1\right)}\tilde{\eta}^3 + \beta\left(\frac{1+3\tilde{c}_+^2}{6\left(2\tilde{c}_++\tilde{\Gamma}\right)} - \frac{(1+\eta)^2}{2}\tilde{c}_+\right)\tilde{\eta}_{xx}.$$

The dimensional variables were inserted back into the equation to find the velocity potential with dimensions using 2.32 and then scaled by 2.47. The velocity potential was then used to find the horizontal particle velocity, given by $u = \varphi_x + y\Gamma$, i.e.

$$u = c_+\eta + \frac{-1}{2\left(2c_++\Gamma\right)}\eta^2 + \frac{c_+\left(3+\Gamma^2\right)}{3\left(2c_++\Gamma\right)^2\left(c_+^2+1\right)}\eta^3 + \left(\frac{1+3c_+^2}{6\left(2c_+\Gamma\right)} - \frac{(1+y)^2}{2}c_+\right)\eta_{xx} + \Gamma y.$$

From the solitary wave expression, the phase velocity was given by

$$c = \frac{\nu}{\mu} = \frac{1}{\lambda^2\mu}\left(\frac{1}{6\lambda}\sigma H^2 + \frac{1}{3}H\right) + c_+.$$

Hence, the breaking criterion for the eKdV equation with constant background vorticity was as

follow

$$c_+\eta+\frac{-1}{2\left(2c_++\Gamma\right)}\eta^2+\frac{c_+\left(3+\Gamma^2\right)}{3\left(2c_++\Gamma\right)^2\left(c_+^2+1\right)}\eta^3+\left(\frac{1+3c_+^2}{6\left(2c_+\Gamma\right)}-\frac{(1+y)^2}{2}c_+\right)\eta_{xx}+\Gamma y \geq \frac{1}{\lambda^2\mu}\left(\frac{1}{6\lambda}\sigma H^2+\frac{1}{3}H\right)+c_+. \quad (7.18)$$

Using standard differential methods, the second order derivative of the solitary wave solution 7.20 became

$$\eta_{xx}=\frac{-2\lambda\mu^2\left(\frac{\sigma}{24}A^2+\frac{1}{12}A\right)\left(1+\frac{\sigma}{\sigma A+2}A\right)A\left[\sinh^2(\Psi)+\cosh^2(\Psi)\right]}{\left[-\frac{\sigma}{\sigma A+2}A+\left(1+\frac{\sigma}{\sigma A+2}A\right)\cosh^2(\Psi)\right]^2} + \frac{8\lambda\mu^2\left(\frac{\sigma}{24}A^2+\frac{1}{12}A\right)\left(1+\frac{\sigma}{\sigma A+2}A\right)^2A\left[\sinh^2(\Psi)\cosh^2(\Psi)\right]}{\left[-\frac{\sigma}{\sigma A+2}A+\left(1+\frac{\sigma}{\sigma A+2}A\right)\cosh^2(\Psi)\right]^3},$$

Since the solitary wave remains its shape for all time, the wave was evaluated at $(x,t)=(0,0)$, such that

$$\eta=\lambda A \qquad \text{and} \qquad \eta_{xx}=-2\lambda\mu^2\left(\frac{\sigma}{24}A^2+\frac{1}{12}A\right)\left(1+\frac{\sigma}{\sigma A+1}A\right)A.$$

To find the maximum allowable height of the solitary wave, it was necessary to evaluate the horizontal particle velocity and the phase speed at the top of the wave, such that $\lambda A=H$, where H was the height of the wave. Substituting the expressions for η and η_{xx} into the breaking criterion, yielded

$$c_+H+\frac{-1}{2\left(2c_++\Gamma\right)}H^2+\frac{c_+\left(3+\Gamma^2\right)}{3\left(2c_++\Gamma\right)^2\left(c_+^2+1\right)}H^3- \left(\frac{1+3c_+^2}{6\left(2c_+\Gamma\right)}-\frac{(1+H)^2}{2}c_+\right)\left(-2\mu^2\left(\frac{\sigma}{24\lambda^2}H^2+\frac{1}{12\lambda}H\right)\left(\lambda+\frac{\sigma}{\sigma H+\lambda}H\right)H\right)+\Gamma y \geq \frac{1}{\lambda^2\mu}\left(\frac{1}{6\lambda}\sigma H^2+\frac{1}{3}H\right)+c_+. \quad (7.19)$$

Setting the horizontal particle velocity equal to the phase speed and rearranging the terms, a

6th-order polynomial of H was obtained.

$$
\begin{aligned}
P(H) = {} & \frac{\sigma^2\mu^2 c_+}{12\lambda^2}H^6 + \left(\frac{3\sigma\lambda\mu^2 c_+ + 2\sigma^2\mu^2 c_+}{12\lambda^2}\right)H^5 \\
& + \left(\frac{2\lambda^2\mu^2 c_+ + 6\sigma\lambda\mu^2 c_+ - 2\left(\frac{1+3c_+^2}{6(2c_+\Gamma)} - \frac{c_+}{2}\right)\sigma^2\mu^2 + 12\left(\frac{c_+\left(3+\Gamma^2\right)}{3(2c_+\Gamma)^2\left(c_+^2+1\right)}\right)\lambda^2\sigma}{12\lambda^2}\right)H^4 \\
& + \left(\frac{12\left(\frac{c_+\left(3+\Gamma^2\right)}{3(2c_+\Gamma)^2\left(c_+^2+1\right)}\right)\lambda^4\mu + 2\lambda^3\mu^3 c_+ - 3\left(\frac{1+3c_+^2}{6(2c_+\Gamma)} - \frac{c_+}{2}\right)\sigma\lambda^2\mu^3 + 6\left(\frac{-1}{2(2c_+\Gamma)}\right)\sigma\lambda^3\mu - \sigma^2}{6\lambda^3\mu}\right)H^3 \\
& + \left(\frac{12\left(\frac{-1}{2(2c_+\Gamma)}\right)\lambda^3\mu - 4\sigma - 2\left(\frac{1+3c_+^2}{6(2c_+\Gamma)} - \frac{c_+}{2}\right)\lambda^2\mu^3 + 6\sigma\lambda^2\mu c_+ + 6\Gamma\sigma\lambda^2\mu}{6\lambda^2\mu}\right)H^2 \\
& + \left(\frac{6\lambda^2\mu c_+ - 2 + 6\Gamma\lambda^2\mu - 3\sigma\lambda\mu c_+}{3\lambda\mu}\right)H - 2\lambda c_+ = 0.
\end{aligned}
$$

Bjørnestad et al. (2021) made numerical simulation of the KdV equation with constant shear to model a bore front. The height and the wavelength of the first five waves after the bore front were compared to those behind the bore front in experiments of Favre (1935). Discrete values of the vorticity ranging from -0.4 to 0.4 were tested, and the relative error between Favre's experiment and the numerical approximation was derived for each value of the vorticity. Based on the lowest relative error, they discovered that $\Gamma = -0.2213$ was the best estimate of the vorticity in Favre's experiment. In the article, the authors have defined the background shear flow such that the circulation was headed in the opposite direction to how the background shear flow was defined in this study. Due to this, Γ had to be positive to achieve the same vorticity. Therefore, $\Gamma = 0.2213$ was substituted into the polynomial of H. The polynomial and its derivative were implemented numerically and the result was shown in figure 7.2. The red graph is the derivative of the polynomial $P(H)$ and it was positive between 0 and 1, meaning that the polynomial increases between these values. Since $P(0) < 0$ and $P(1) > 0$, the polynomial had to have a root between 0 and 1. Using the bisection method, a numerical approximation of the root was found. Hence, the maximum height for the solitary wave solution of the eKdV equation with constant background vorticity was approximated to be

$$H_{max} = 0.6215.$$

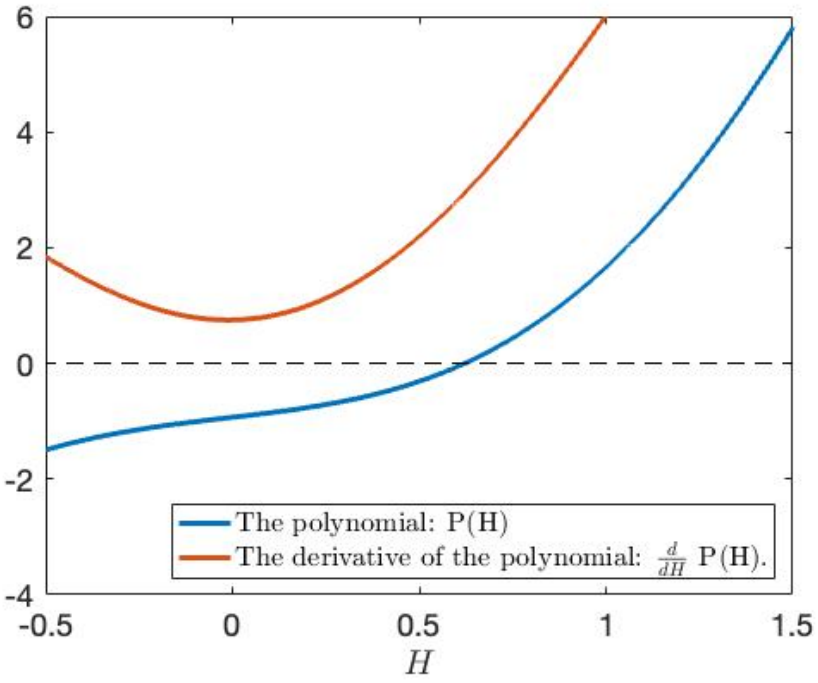

Figure 7.2: The polynomial $P(h)$ is the blue graph and its derivative is the red graph.

The maximum height of the solitary wave solution of the KdV equation was 0.6879 and the solitary wave solution of the eKdV equation was found to be 0.7079, hence the result of adding a shear flow to the eKdV equation was a solitary wave with much lower maximum height than both the KdV equation and the eKdV equation.

Additionally, the maximum height of the solitary wave was investigated for various vorticity values in the eKdV equation with constant background vorticity. Using the numerical bisection method, a numerical approximation of the roots of polynomial P was found by inserting different values of $\Gamma \in [-0.4, 0.4]$. With the argument given in the previous paragraph, the maximum height of the solitary wave corresponding to each vorticity was found, and the graph representing the points is depicted in figure 7.3 below. As the vorticity approaches zero and beyond, the maximum wave height decreased. This behaviour aligns with using positive vorticity when approximating Favre's experiment since a solution with minimal wave height was wanted.

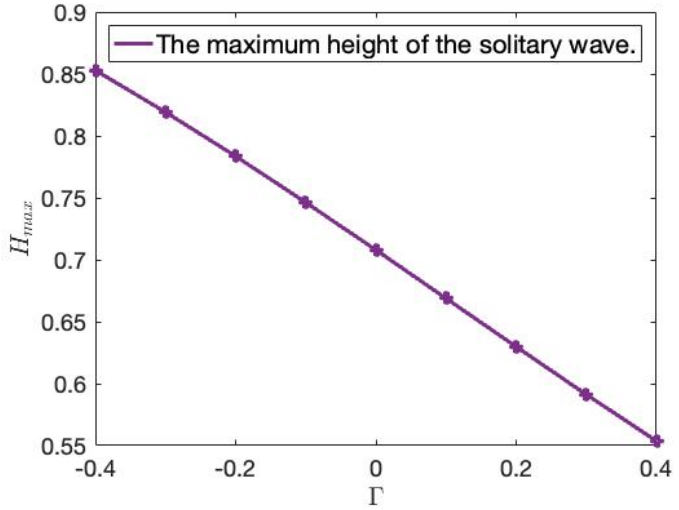

Figure 7.3: The graph show the maximum height of the solitary wave for various values of the vorticity ranging from $\Gamma \in [-0.4, 0.4]$.

7.3 Code validation

I aimed to make a numerical implementation of the eKdV equation with constant background shear such that the breaking criterion could be defined and the critical bore strength found. The numerical method presented in chapter 3 was utilised for this. Hence, together with finite difference spatial operators, the linear terms were approximated by the Crank-Nicolson method and the non-linear methods were approximated by the Adams-Bashforth method. The auxiliary function $\xi(x,t) = \eta(x,t) - \eta_0(x)$ was defined to incorporate homogeneous boundary conditions and with the discretisation $v_j^n \approx \xi(x_i, t^n)$, the scheme became

$$\begin{aligned}
\frac{v^{n+1}-v^n}{\delta t} &= \frac{3}{2}D_1\left[-\frac{1}{2}\left(\frac{c_+\left(3+\Gamma^2\right)}{c_+^2+1}\right)\left((v^n)^2+2v^n\eta_0\right)\right] \\
&+\frac{3}{2}D_1\left[-\frac{1}{3}\left(\frac{2\Gamma^2c_+-6c_+^3-3\Gamma c_+^2-3\Gamma}{2\left(2c_++\Gamma\right)^2\left(c_+^2+1\right)}\right)\left((v^n)^3+3\left(v^n\right)^2\eta_0+3v^n\eta_0^2\right)\right] \\
&-\frac{1}{2}D_1\left[-\frac{1}{2}\left(\frac{c_+\left(3+\Gamma^2\right)}{c_+^2+1}\right)\left(\left(v^{n-1}\right)^2+2v^{n-1}\eta_0\right)\right] \\
&-\frac{1}{2}D_1\left[-\frac{1}{3}\left(\frac{2\Gamma^2c_+-6c_+^3-3\Gamma c_+^2-3\Gamma}{2\left(2c_++\Gamma\right)^2\left(c_+^2+1\right)}\right)\left(\left(v^{n-1}\right)^3+3\left(v^{n-1}\right)^2\eta_0+3v^{n-1}\eta_0^2\right)\right] \\
&+\frac{1}{2}\left[-c_+D_1\left(v^{n+1}+v^n\right)-\left(\frac{c_+^3}{3\left(c_+^3+1\right)}\right)D_3\left(v^{n+1}+v^n\right)\right]-F,
\end{aligned}$$

where

$$F = c_+ (\eta_0)_x + \frac{1}{2}\left(\frac{c_+\left(3+\Gamma^2\right)}{c_+^2+1}\right)\left(\eta_0^2\right)_x + \frac{1}{3}\left(\frac{2\Gamma^2 c_+ - 6c_+^3 - 3\Gamma c_+^2 - 3\Gamma}{2\left(2c_+ + \Gamma\right)^2\left(c_+^2+1\right)}\right)\left(\eta_0^3\right)_x + \left(\frac{c_+^3}{3\left(c_+^3+1\right)}\right)(\eta_0)_{xxx}.$$

The previous numerical analysis using the hybrid Crank-Nicolson/Adams-Bashforth method proves that we should expect a second-order convergence of the approximation toward the exact solution. The exact solitary wave solution found in the section 7.2 was tested towards the numerical implementation of the wave, where the initial value was

$$\eta(x,t) = \frac{\lambda A}{-\frac{\sigma}{\sigma A+2}A + \left(1 + -\frac{\sigma}{\sigma A+2}A\right)\cosh^2\left[\frac{\sqrt{\frac{\sigma}{6}A^2+\frac{1}{3}A}}{2}\mu x\right]}, \tag{7.20}$$

where the values of λ , μ and σ were given by 7.14, 7.15, 7.16 and 7.17, and $A = 1$ when testing the convergence of the solution. When calculating the error between the approximation and the exact solution, the L^2-norm was used. The spatial convergence was tested for $\delta t = 0.001$ until the final time $T = 1$, shown in table 7.1.

Table 7.1: The spatial convergence of the numerical approximation of the eKdV equation with $\Gamma = 0.2213$.

δx	L^2-norm	Convergence rate
0.16	0.0517	-
0.08	0.0129	2.00279
0.04	0.0032	2.01123
0.02	7.9624e-04	2.00687
0.01	1.9143e-04	2.05654

The temporal convergence was tested for $\delta x = 0.01$ to final time $T = 1$. It is shown in table 7.2.

Table 7.2: The temporal convergence of the numerical approximation of the eKdV equation with $\Gamma = 0.2213$.

δx	L^2-norm	Convergence rate
2^{-2}	0.81540	-
2^{-3}	0.20420	1.99753
2^{-4}	0.04640	2.13779
2^{-5}	0.01140	2.02509
2^{-6}	0.00270	2.07800
2^{-7}	0.00057	2.24392

The result presented in the tables show that the implementation of the solitary wave solution of eKdV equation with constant background vorticity converges toward the exact solitary wave with a second order convergence, as expected. Hence, we can be confident that the result based on the implementation is correct.

7.4 Numerical results on the breaking of undular bores

The scheme derived in the previous section was used to simulate an undular bore propagating from left to right. The breaking criterion at each time evaluation was derived by calculating the horizontal particle velocity at the top of the front wave and comparing it to the approximation of the local phase speed. With different values of the bore strength, the breaking criterion was tested. The simulation started with $\alpha = 0.281$ as in the experiment of Favre (1935), and an increment of 0.001 was added to the bore strength until the horizontal velocity exceeded the phase speed. The implementation was made such that when the wave reached a distance of 610 h_0, the simulation ended.

Figure 7.4 displays the result of the horizontal particle velocity and the phase speed with bore strength 0.318. The figure 7.4b provides a closer view of 7.4a, and in both figures, the mean value of every 10th value of the horizontal particle velocity is shown, with the result that the horizontal particle velocity never exceeded the phase speed. In figure 7.4c the horizontal particle velocity without the use of the mean value is depicted. At the very end, a small part at the

top of the horizontal particle velocity exceeds the phase speed, indicating that the wave might be breaking.

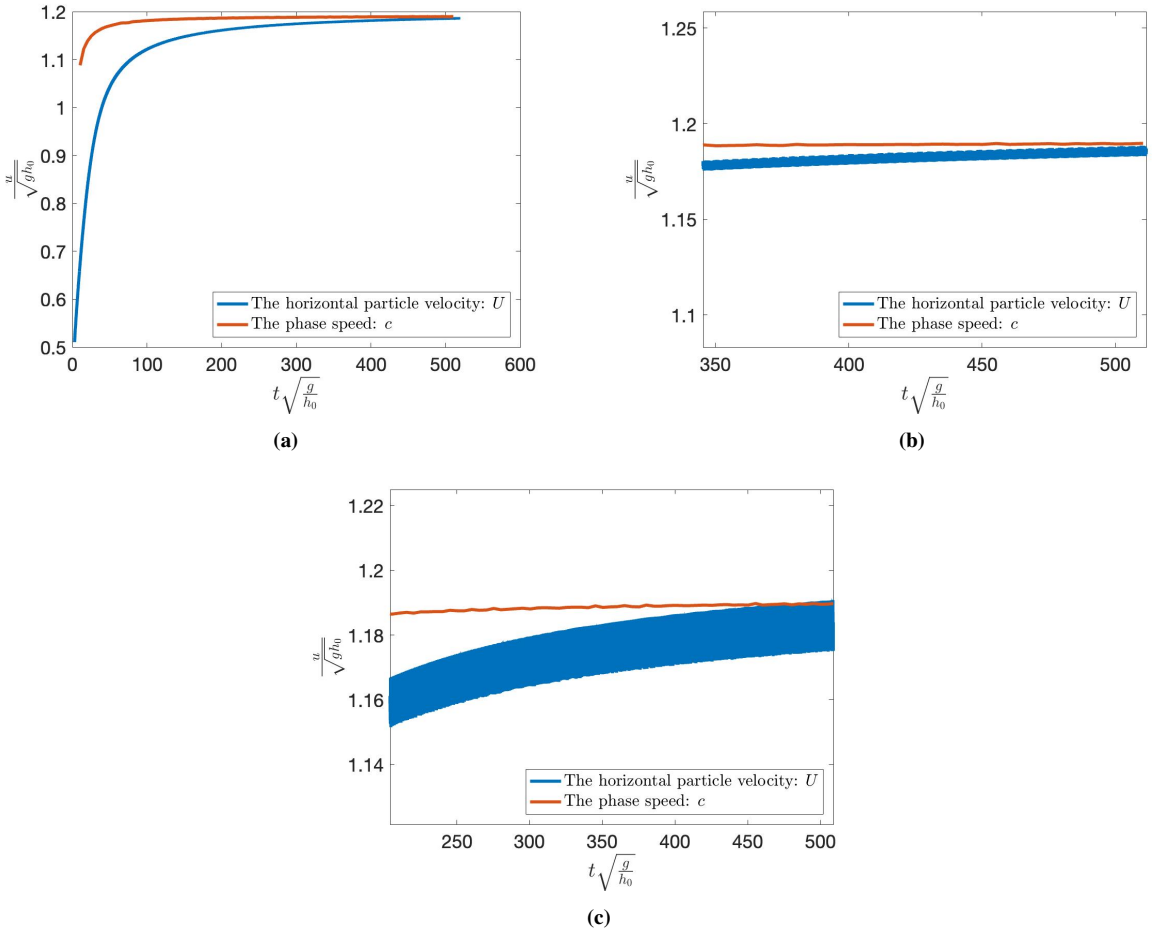

Figure 7.4: The horizontal particle velocity coloured in blue and the phase velocity is coloured in red when the bore strength is 0.318. b) is a closer view of panel a).

The horizontal particle velocity at the top of the front wave and the phase speed are depicted in figure 7.5 with the bore strength 0.319. The mean value of each 10th value of the horizontal particle velocity was presented. The result show that the breaking criterion was satisfied and that the wave was breaking.

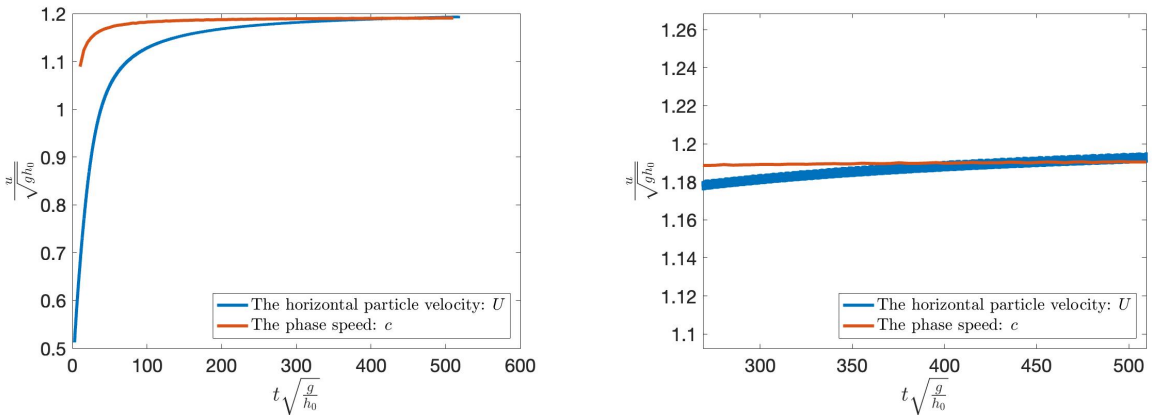

Figure 7.5: The horizontal particle velocity coloured in blue and the phase velocity is coloured in red when the bore strength was 0.319. The right panel is a closer view of the left panel.

7.5 Discussion

For the numerical simulation of an undular bore with the eKdV with constant background vorticity, the results show that the breaking criterion was satisfied at a bore strength of 0.319. Figure 7.4 indicated that the wave could break at the bore strength 0.318, but since this was not satisfied in 7.4b, I stated that the critical bore strength was 0.319. This result was closer to the experimental result of Favre (1935) than the eKdV equation without shear flow. Thus, including constant background vorticity in the eKdV equation was an improvement. However, it did not exceeded the result of Bjørnestad et al. (2021) when a constant background vorticity was added to the KdV-equation. Neither a higher-order non-linear equation with shear flow did improve the KdV equation with included vorticity.

The maximum analytical height of the solitary wave was calculated to be $H_{\max} = 0.6215$. This means that waves simulated by the eKdV equation with constant background vorticity with higher amplitude than $H_{\max}$ do not describe actual surface waves, even though the equation can simulate waves with higher amplitude. The height of the numerically simulated undular, with the bore strength 0.319, was found to be 0.6315. Thus, the analytical $H_{\max}$ was smaller than the height of the simulated leading wave with the critical bore strength. Hence, the numerical undular bore breaking do not fulfill this prediction during the domain determined in this study, which was not assumable either.

An interesting comparison was the different bores simulated by different vorticity values, shown in figure 7.6. The waves had the same initial conditions where $a_0 = 0.3$, $k = 1$ and the final time was $T = 450$. They are shown in figure 7.6. In a), coloured in yellow, is the eKdV equation with $\Gamma = 0$, in b) $\Gamma = 0.2213$ and in c) $\Gamma = -0.2213$.

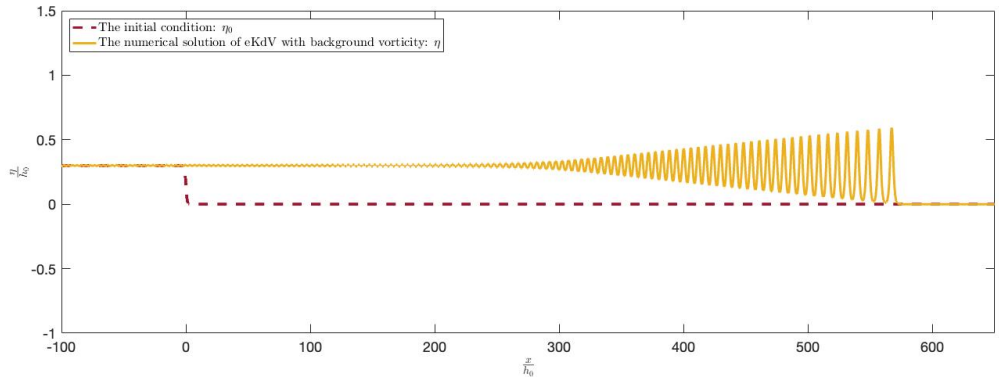

(a)

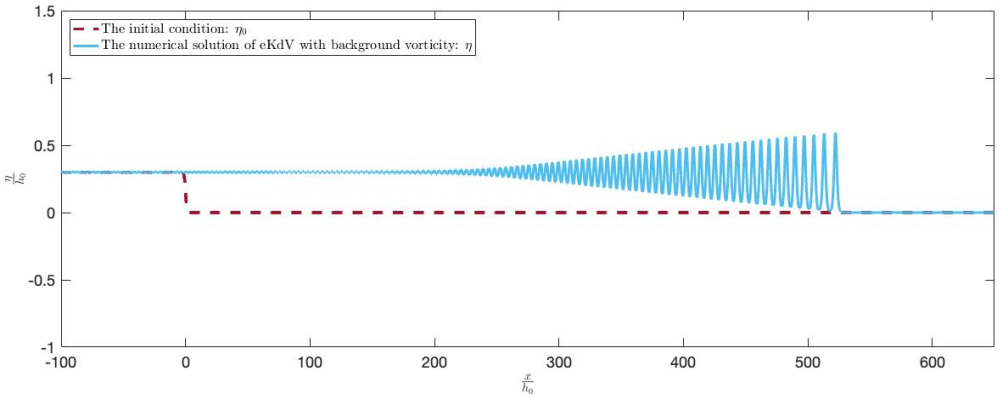

(b)

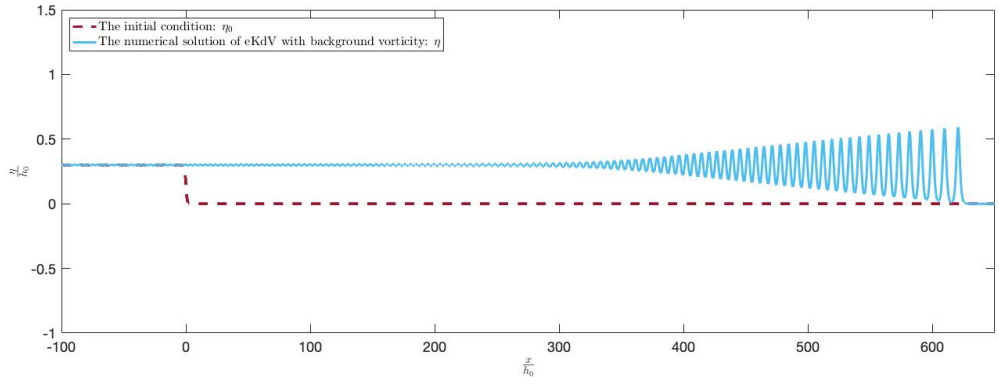

(c)

Figure 7.6: Comparing the undular bore simulated by the eKdV equation for different values of vorticity. a) $\Gamma = 0$, b) $\Gamma = 0.2213$ and c) $\Gamma = -0.2213$.

The leading waves' height and horizontal position are presented in table 7.3. Clearly, the bore with negative vorticity propagated much faster than the two other waves. However, it had not gained a higher front wave. Figure 7.3 show that the maximum allowable height of the solitary wave with $\Gamma = -0.2213$ was numerically approximated to 0.7911, which indicated that if the numerical undular bore in Figure 7.6c was a real, natural wave, it would be far from breaking. Further, the simulation of the eKdV equation with $\Gamma = -0.2213$ show that

the horizontal velocity for $\alpha = 0.3$ had a much lower horizontal particle velocity at the top of the front wave and it never exceeded 0.8319, while the phase speed reached 1.4, which was a quite big difference. Russel (1844) showed that waves with higher amplitude propagate faster. However, the shear flow have affected the phase speed, and therefore, a wave with a smaller amplitude propagated faster. The wave with the lowest critical bore strength was the central bore with $\Gamma = 0.2213$ and, as depicted in figure 7.6, it had a much lower phase speed, but higher leading wave.

Table 7.3: The height and the horizontal position of the leading wave for the numerical approximation of the eKdV with different vorticity values at the final time T = 450.

Vorticity Γ	Leading wave height	Leading wave position
0	0.5934	567.2
0.2213	0.5942	522.2
- 0.2213	0.5929	620.5

Figure 7.7 show the eKdV equation with $\Gamma = 0.2213$ where the undular bore was implemented with $\delta t = 0.005$. To check the stability of the implementation of the eKdV equation with vorticity, the wave was simulated with half the temporal grid size. The position of the leading waves was the same as when using grid size $\delta t = 0.01$. Hence there were no phase errors affecting the phase speed of the wave.

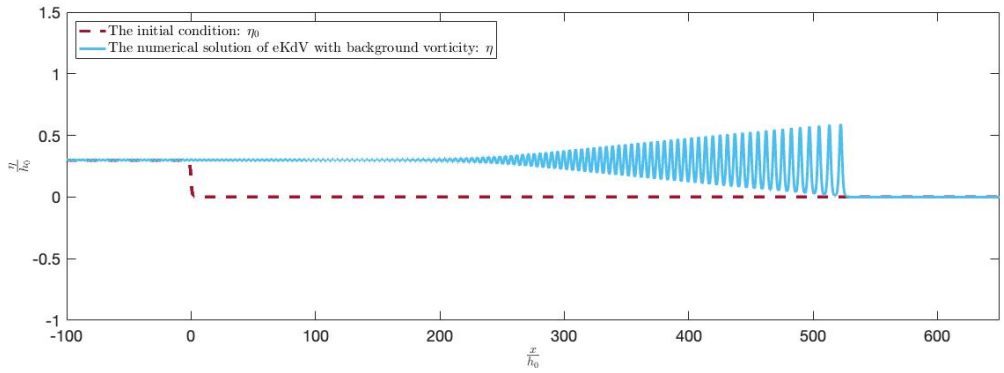

Figure 7.7: An undular bore simulated by the eKdV equation with background vorticity $\Gamma = 0.2213$ and with temporal grid size 0.005

.

The results derived for the eKdV equation with constant background shear are qualitatively good. Still, they are quantitatively inconclusive, meaning that they do not agree so well with

the experiments of Favre. Other actions could be made to improve the quantitative result. Wilkinson and Banner (1977) did an experiment where the bore was created by a weir that was moved through a wave tank, resulting in bores that were different from the bores formed in Favre's experiment. The authors discovered that the waves were breaking with a bore strength of 1.38, higher than the critical bore strength found by Favre. Hatland and Kalisch (2019) used the Boussinesq system to simulate the undular bores made in the experiment of Wilkinson and Banner (1977) and then used the conductive breaking criterion to find the critical bore strength. The numerical result gave a critical bore strength within an error of 2% from the result of Wilkinson and Banner (1977) . When the wire moves through the tank, it generates an undular bore due to the upstream flow caused by the wire and the flow was assumed to be inviscid. The numerical result was quite close to the actual result from the experiment of Wilkinson and Banner (1977) , giving a much better outcome than the result achieved in this report.

Further, the article of Hatland and Kalisch (2019) demonstrated that the bore strength was a suitable parameter to determine breaking when a wire created the wave. Senthilkumar and Kalisch (2019) stated that the breaking criterion is a good indicator for breaking in some practical situations, usually for shallow water, but it might be less correct in other situations. It is therefore worth mentioning that this might have influenced the lack of agreement with the experiment of Favre. Further Senthilkumar and Kalisch (2019) mentioned that the error in deriving the breaking criterion is often due to the difficulty of determining the phase speed. We have discussed for the KdV equation in chapter 4, that the phase speed was wildly oscillating, and therefore the determination of it was an approximation that might lack from the real phase speed. However, as mentioned before, Favre's experiment was made physically and therefore determining the phase speed was hard there as well. Still, most likely, the lack of good results was not due to the phase speed.

Another question is how the vorticity actually influenced the experiment of Favre (1935), and further, what directions were the circulations? Due to the length of Favre's wave tank, the forces coming from the inflow might not influence the water waves when they reach the end of the wave tank. Even though the inflow creates a shear flow, the flow might evolve into other types of flows influencing the waves at the breaking point.

8 Conclusion

The purpose of the report has been to find a good approximation of Favre's experiment on the breaking of undular bores by use of higher order KdV equations. Starting with the KdV equation, an equation that balances the nonlinearity with the dispersive effects, two extensions of the nonlinear part have been made with the motivation that the equation will better simulate the waves in Favre's experiment when adding higher non-linearity. However, the bores simulated by the eKdV and the eeKdV equations did not break for a smaller bore strength than the bore strength already established for the KdV equation by Brun and Kalisch (2018).

Assuming a constant background shear to the eKdV equation gave a lower critical bore strength, indicating that the vorticity was important in the approximation. However, the addition of a background shear flow to the KdV equation derived by Bjørnestad et al. (2021) resulted in an undular bore with an even lower threshold for breaking. Hence, even with a background shear flow, did a higher-order non-linear KdV equation improve the approximation of the waves in Favre (1935) experiment. Figure 8.1 show the analysed equations' bore strengths and the previous results.

This report has also derived the maximum height of the solitary wave solutions for the eKdV with and without background shear flow. Since the eeKdV solitary wave solution has yet to be found, it has not been included. The maximum height of the eKdV equation with the constant shear flow was lower than the maximum height of the solitary wave solution of the KdV and the eKdV equations, which predicted that the waves would break at a lower height. Senthilkumar and Kalisch (2019) derived the maximum height of the solitary wave solution of the KdV equation with a constant background shear flow and got a lower critical height than the eKdV with constant background shear flow. This conclusion is supported by the result of Bjørnestad et al. (2021). Adding a background shear flow to the KdV equation resulted in breaking for a lower bore strength than the eKdV equation.

There have been other factors discussed that might have improved the result. Since the equations based on the KdV equation do not involve damping, this was discussed, based on the work of Sturtevant (1965). Also, Ali and Kalisch (2010) added higher-order dispersion to an equation to include the lack of energy. Further, Hatland and Kalisch (2019) derived the equation with a base where the undular bore was created by a wire that moved through the tank. This indicates that the lack of results could also be qualitative. Hence, the equations might estimate this experiment better. This would be interesting for further work.

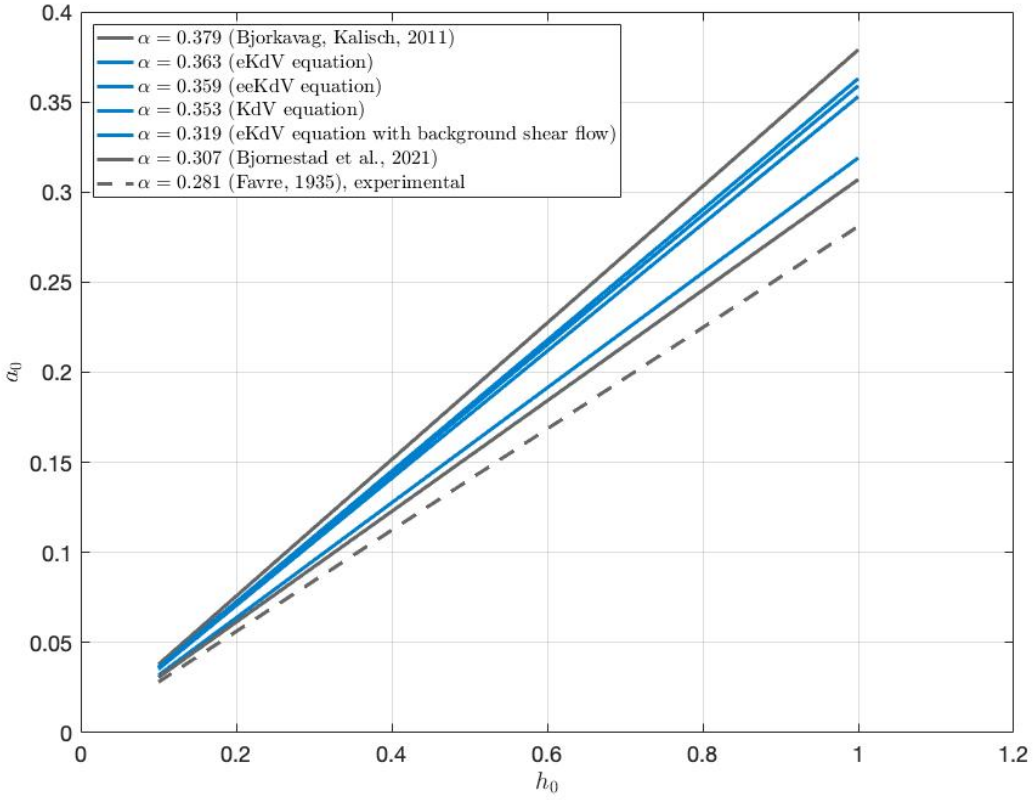

Figure 8.1: The relationship between the initial height of the wave above the undisturbed water and the undisturbed water height is shown for the different equations and Favre's experimental result.

In the end, it is important to remember that even though Favre made a qualitatively good experiment, the experiment was carried out outdoors. Therefore, other physical effects may influence the result. In contrast, the equations used in this report are idealised and do not consider all this.

Bibliography

Aavatsmark, I. (2004). Bevarelsesmetoder for hyperbolske differensialligninger.

Ali, A., & Kalisch, H. (2010). Energy balance for undular bores. *Comptes Rendus Mécanique*, *338*(2), 67–70. https://doi.org/10.1016/j.crme.2010.02.003

Benney, D. (1966). Long waves on liquid films. *Journal of Mathematics and Physics*, *45*(1-4), 150–155. https://doi.org/https://doi.org/10.1002/sapm1966451150

Bjørkavåg, M., & Kalisch, H. (2011). Wave breaking in Boussinesq models for undular bores. *Physics Letters A*, *375*(14), 1570–1578. https://doi.org/10.1016/j.physleta.2011.02.060

Bjørnestad, M., Kalisch, H., Abid, M., Kharif, C., & Brun, M. (2021). Wave breaking in undular bores with shear flows. *Water Waves*, *3*, 473–490. https://doi.org/10.1007/s42286-020-00046-6

Bona, J., Shu, M., Sun, & Zhang, B. (2003). A nonhomogeneous boundary-value problem for the Korteweg–de Vries equation posed on a finite domain. *Communications in Partial Differential Equations*, *28*, 1391–1436. https://doi.org/10.1081/PDE-120024373

Bona, J., Dougalis, V., Karakashian, 0., & McKinney, W. (1996). The effect of dissipation on solutions of the generalized Korteweg-de Vries equation. *Journal of Computational and Applied Mathematics*, *74*(1-2), 127–153. https://doi.org/10.1016/0377-0427(96)00021-0

Brun, M. K., & Kalisch, H. (2018). Convective wave breaking in the KdV equation. *Analysis and Mathematical Physics*, *8*(1), 57–75. https://doi.org/10.1007/s13324-017-0163-y

Da Silva, A. F. T., & Peregrine, D. H. (1988). Steep, steady surface waves on water of finite depth with constant vorticity. *Journal of Fluid Mechanics*, *195*, 281–302. https://doi.org/10.1017/S0022112088002423

Drazin, P., & Johnson, R. (1998). *Solitons: And introduction* [Digital print:2002]. Cambridge University Press.

Favre, H. (1935). *Ondes de translation*. Dunod.

Filippini, A. G., Arpaia, L., Bonneton, P., & Ricchiuto, M. (2019). Modeling analysis of tidal bore formation in convergent estuaries. *European Journal of Mechanics-B/Fluids*, *73*, 55–68.

Gavrilyuk, S. L., Makarenko, N., & Sukhinin, S. (2017). *Waves in continuous media*. Birkhäuser.

Hatland, S. D., & Kalisch, H. (2019). Wave breaking in undular bores generated by a moving weir. *Physics of Fluids*, *31*(3). https://doi.org/10.1063/1.5085861

Iserles, A. (2000). *A first course in the numerical analysis of differential equation*. Cambrigde University Press. (Original work published 1996)

Johnson, R. (1997). *A modern introduction to the mathematical theory of water waves.* Cambridge University Press.

Kalisch, H., & Nguyen, N. T. (2010). On the stability of internal waves. *Journal of Physics A: Mathematical and Theoretical*, *43*(49). https://doi.org/10.1088/1751-8113/43/49/495205

Kundu, P. K., Cohen, I. M., & Dowling, D. R. (2016). *Fluid mechanics* (Sixth edition). Academic Press.

Lee, R. C., C.Y.; Beardsley. (1974). The generation of long nonlinear internal waves in a weakly stratified shear flow. *J. Geophys. Res.*, *79*(3), 453–462. https://doi.org/https://doi.org/10.1029/JC079i003p00453

Lin, C., Kao, M.-J., Wong, W.-Y., Shao, Y.-P., Hu, C.-F., Yuan, J.-M., & Raikar, R. V. (2019). Effect of leading waves on velocity distribution of undular bore traveling over sloping bottom. *European Journal of Mechanics-B/Fluids*, *73*, 75–99.

Lubin, P., & Chanson, H. (2017). Are breaking waves, bores, surges and jumps the same flow? *Environmental Fluid Mechanics*, *17*, 47–77.

Massel, S. (1996). On the largest wave height in water of constant depth. *Ocean Engineering*, *23*(7), 553–573. https://doi.org/https://doi.org/10.1016/0029-8018(95)00049-6

Norevik, A. M., & Kalisch, H. (2022). On the formulation of energy conservation on the eeKdV equation. [accepted 2023]. *Applied Numerical Mathematics*.

Russel, J. (1844). *Report on waves.*

Senthilkumar, A., & Kalisch, H. (2019). Wave breaking in the KdV equation on a flow with constant vorticity. *European Journal of Mechanics - B/Fluids*, *73*, 48–54. https://doi.org/https://doi.org/10.1016/j.euromechflu.2017.12.006

Skogestad, J. O., & Kalisch, H. (2009). A boundary value problem for the KdV equation: Comparison of finite-difference and Chebyshev methods. *Mathematics and Computers in Simulation*, *80*(1), 151–163. https://doi.org/https://doi.org/10.1016/j.matcom.2009.06.009

Sturtevant, B. (1965). Implications of experiments on the weak undular bore (6th ed.). *The Physics of Fluids*, *8*, 1052–1055. https://doi.org/10.1063/1.1761354

Whitham, G. B. (1974). *Linear and nonlinear waves*. John Wiley & Sons.

Wilkinson, D., & Banner, M. (1977). Undular bores (6th). *Australian Hydraulics and Fluid Mechanics Conference*.

Wong, W.-Y., Bjørnestad, M., Lin, C., Kao, M.-J., Kalisch, H., Guyenne, P., Roeber, V., & Yuan, J.-M. (2019). Internal flow properties in a capillary bore. *Physics of fluids*, *31*(11), 113602.

Yaosong, C., Guocan, L., & Tao, J. (1994). Non-linear water waves on shearing flows. *Acta Mechanica Sinica*, *10*, 97–102. https://doi.org/10.1007/BF02486579